# NAVAL POSTGRADUATE SCHOOL
# MONTEREY, CALIFORNIA


DTIC
ELECTE
JAN 11 1996
F

# THESIS

**REPETITIVE TROPICAL CYCLOGENESIS DURING TCM-93**

by

Michael S. Kalafsky

June, 1995

Thesis Co-Advisors: R. L. Elsberry
P. A. Harr

**Approved for public release; distribution is unlimited.**

19960103 205

# REPORT DOCUMENTATION PAGE

Form Approved OMB No. 0704-0188

Public reporting burden for this collection of information is estimated to average 1 hour per response, including the time for reviewing instruction, searching existing data sources, gathering and maintaining the data needed, and completing and reviewing the collection of information. Send comments regarding this burden estimate or any other aspect of this collection of information, including suggestions for reducing this burden, to Washington Headquarters Services, Directorate for Information Operations and Reports, 1215 Jefferson Davis Highway, Suite 1204, Arlington, VA 22202-4302, and to the Office of Management and Budget, Paperwork Reduction Project (0704-0188) Washington DC 20503.

| 1. AGENCY USE ONLY *(Leave blank)* | 2. REPORT DATE June 1995 | 3. REPORT TYPE AND DATES COVERED Master's Thesis |
|---|---|---|

4. TITLE AND SUBTITLE Repetitve Tropical Cyclogenesis During TCM-93

5. FUNDING NUMBERS

6. AUTHOR(S) Michael S. Kalafsky

7. PERFORMING ORGANIZATION NAME(S) AND ADDRESS(ES)
Naval Postgraduate School
Monterey CA 93943-5000

8. PERFORMING ORGANIZATION REPORT NUMBER

9. SPONSORING/MONITORING AGENCY NAME(S) AND ADDRESS(ES)

10. SPONSORING/MONITORING AGENCY REPORT NUMBER

11. SUPPLEMENTARY NOTES The views expressed in this thesis are those of the author and do not reflect the official policy or position of the Department of Defense or the U.S. Government.

12a. DISTRIBUTION/AVAILABILITY STATEMENT
Approved for public release; distribution is unlimited.

12b. DISTRIBUTION CODE

13. ABSTRACT *(maximum 200 words)*

The small Tropical Storm (TS) Ofelia developed in the wake of Typhoon (TY) Nathan, and just prior to the development of TY Percy, during a small field experiment called Tropical Cyclone Motion (TCM-93) that was conducted in the western North Pacific from 20 July 1993 to 12 August 1993. Two Aircraft Observing Periods, AOP-1A and AOP-1B, provided flight-level winds and Omega Dropwinsonde (ODW) data in a region of north-oriented confluent flow between the monsoon gyre and the subtropical ridge on the two days prior to the formation of TS Ofelia. The ODW data and the flight-level winds are used in a multiquadric interpolation technique to define the mesoscale structure on a 100 km grid. A mid-tropospheric mesoscale cyclonic circulation with a horizontal scale of about 400 km is documented during AOP-1A and AOP-1B. The mesoscale cyclonic circulation extended between 700 mb and 400 mb during AOP-1A and then extended down to the surface in AOP-1B. Visible imagery on the day following AOP-1B indicates a vortex of tightly curved low-level cumulus clouds that then developed deep convection that subsequently led to the formation of TS Ofelia. This is considered to be the best data set of the pre-existing environmental structure in which a "midget" typhoon forms.

| 14. SUBJECT TERMS Tropical Cyclone, Mesoscale Convective System | | | 15. NUMBER OF PAGES 107 |
|---|---|---|---|
| | | | 16. PRICE CODE |
| 17. SECURITY CLASSIFICATION OF REPORT Unclassified | 18. SECURITY CLASSIFICATION OF THIS PAGE Unclassified | 19. SECURITY CLASSIFICATION OF ABSTRACT Unclassified | 20. LIMITATION OF ABSTRACT UL |

NSN 7540-01-280-5500

Standard Form 298 (Rev. 2-89)
Prescribed by ANSI Std. 239-18 298-102

**Approved for public release; distribution is unlimited**

# REPETITIVE TROPICAL CYCLOGENESIS DURING TCM-93

Michael S. Kalafsky
Lieutenant, United States Navy
B.S., United States Naval Academy, 1989

Submitted in partial fulfillment
of the requirements for the degree of

**MASTER OF SCIENCE IN METEOROLOGY AND PHYSICAL OCEANOGRAPHY**

from the

**NAVAL POSTGRADUATE SCHOOL**
**June 1995**

Author: _____
Michael S. Kalafsky

Approved by: _____
R. L. Elsberry, Thesis Co-Advisor

_____
P. A. Harr, Thesis Co-Advisor

_____
Robert L. Haney, Chairman
Department of Meteorology

## ABSTRACT

The small Tropical Storm (TS) Ofelia developed in the wake of Typhoon (TY) Nathan, and just prior to the development of TY Percy, during a small field experiment called Tropical Cyclone Motion (TCM-93) that was conducted in the western North Pacific from 20 July 1993 to 12 August 1993. Two Aircraft Observing Periods, AOP-1A and AOP-1B, provided flight-level winds and Omega Dropwinsonde (ODW) data in a region of north-oriented confluent flow between the monsoon gyre and the subtropical ridge on the two days prior to the formation of TS Ofelia. The ODW data and the flight-level winds are used in a multiquadric interpolation technique to define the mesoscale structure on a 100 km grid. A mid-tropospheric mesoscale cyclonic circulation with a horizontal scale of about 400 km is documented during AOP-1A and AOP-1B. The mesoscale cyclonic circulation extended between 700 mb and 400 mb during AOP-1A and then extended down to the surface in AOP-1B. Visible imagery on the day following AOP-1B indicates a vortex of tightly curved low-level cumulus clouds that then developed deep convection that subsequently led to the formation of TS Ofelia. This is considered to be the best data set of the pre-existing environmental structure in which a "midget" typhoon forms.

Accesion For
NTIS CRA&I ☒
DTIC TAB ☐
Unannounced ☐
Justification
By
Distribution /
Availability Codes
Dist | Avail and / or Special
A-1

## TABLE OF CONTENTS

## LIST OF FIGURES

## LIST OF TABLES

## ACKNOWLEDGMENTS

The sponsorship of the Office of Naval Research Marine Meteorology Program and the Naval Postgraduate School Direct Research Fund made TCM-93 possible. The aircraft operations for TCM-93 were provided by the 815th Weather Squadron based at Keesler Air Force Base. The participation of Dr. Hugh Willoughby as chief aircraft scientist is also gratefully acknowledged.

I would like to thank Dr. Russell L. Elsberry for his encouragement, guidance, and support throughout the preparation of this thesis. He helped to make this thesis a rewarding experience. I would also like to thank Dr. Pat Harr for providing me with the data and the computer knowledge to complete this research. This thesis would not have been possible without his help. Most importantly, I want to thank my wife Michelle, my son Michael, and my daughter Melissa for their love, understanding, and support throughout my time at the Naval Postgraduate School.

# I. INTRODUCTION

More tropical cyclones form over the western North Pacific than any other basin in the world. An average of 26 tropical cyclones reach tropical storm strength each year in the western North Pacific with approximately two-thirds of these storms becoming mature tropical cyclones (Frank 1987). The reasons for the large number of tropical storm occurrences in this region are the large areas of very warm water and the upper-level easterly flow overlying low-level easterlies (minimum vertical wind shear). The warm waters of this region, which can have temperatures exceeding 30°C from July to October, lie west of the Tropical Upper Tropospheric Trough (TUTT) and near the entrance region of the upper tropospheric tropical easterly jet. The TUTT and the upper tropospheric tropical easterly jet may contribute to the broad region of upper-level divergence, which is thought to be favorable for tropical cyclone genesis (Frank 1987).

Most cyclones form in the shear zones between monsoonal (usually cross-equatorial) westerlies and the trade easterlies. In the western North Pacific, approximately 80% of all tropical disturbances form in the monsoon trough while approximately 10% form from waves in the easterlies in conjunction with upper-level cold lows, or in the baroclinic zones of intruding midlatitude troughs (Frank 1987).

Understanding the causes of tropical cyclogenesis is imperative to increase the accuracy and reliability of forecasts for military and civilian users. Although large numbers of tropical cyclones occur in the western North Pacific, determining the cause of these storm formations is difficult due to the lack of observations in this region. Satellite imagery is useful in determining the large-scale flow surrounding tropical cyclones. However, the triggering mechanism of tropical cyclogenesis may be linked to mesoscale phenomena. Forecasting experience and research with numerical models suggest that tropical cyclones do not arise spontaneously but are triggered by disturbances of independent dynamical origin (Emanuel 1993). By examining mesoscale features and their effect on tropical cyclogenesis, a better understanding of

the causes of tropical cyclogenesis may be developed.

The role of the Mesoscale Convective System (MCS) in the genesis of tropical cyclones has been studied extensively in recent years. These convective storm systems were initially compared to midlatitude mesoscale convective complexes (MCCs), which have been studied extensively by researchers in the United States. The more generic label of MCSs has been given to the convective systems in the tropics because they do not satisfy the specific horizontal dimensions, durations, or ellipticity requirements of the midlatitude MCC (Harr et al. 1993). Although many documented similarities exist between midlatitude MCCs and tropical MCSs, the lack of data over the eastern and western Pacific regions has hindered the ability of researchers to identify accurately the structure and causes of tropical MCSs.

Occurrences of midlatitude MCCs over the United States have given researchers the opportunity to study the mesoscale structure and possible causes of these midlatitude convective storms. Long-lived MCCs have been shown to produce the bulk of the warm-season rainfall over much of the midwestern United States (Miller and Fritsch 1991). Basic components of a midlatitude MCC include a leading squall line, which includes regions of mesoscale updrafts and downdrafts, and a trailing region of stratiform precipitation (Smull and Houze 1985). These basic components are similar to those found in tropical squall systems (Zipser 1977; Houze 1977).

Studies of tropical MCSs were initially based on the assumed similarity of tropical MCSs to midlatitude MCCs. Miller and Fritsch (1991) conducted a climatological study of MCCs from 1983 to 1985 over the western Pacific region using full-disc, enhanced IR, and visible imagery from the Japanese Geostationary Meteorological Satellite (GMS). The results of this study indicate that MCSs that also meet the MCC criteria do occur in the western Pacific region and display many of the same characteristics as midlatitude MCCs found in the Americas, e. g., the life cycle, duration, seasonal distribution, and size distribution of the cold cloud-shield areas. However, many tropical MCSs have minimum cloud-top temperatures that are much less than the MCC criteria, and other horizontal area and duration specifications may

be more appropriate. Recent aircraft missions into MCSs in the tropical eastern North Pacific have shown that these systems have convective organization similar to midlatitude MCCs (Emanuel 1993).

Models of midlatitude MCCs have been proposed to apply to the mesoscale structure of tropical MCSs (Zehr 1992). Much of the attention has been focused on the mid-troposphere mesoscale cyclonic circulations produced by certain MCSs. Midlatitude MCCs frequently produce mesoscale vortices that sometimes persist for several days. These mesoscale convectively generated vortices (MCVs) appear to be qualitatively similar to those observed with pre-tropical storm disturbances (Zehr 1992). Inertially stable, warm-core MCVs associated with midlatitude MCCs have their strongest cyclonic circulation at mid-levels (450-700 mb), but may extend downward to near the surface.

Frank and Chen (1991) and Frank (1992) have numerically simulated MCV formation in the stratiform rain region. They propose that a mesoscale vortex forms due to the organized ascent and latent heat release in the stratiform area behind a deep convection line. The rotational motion associated with the MCS may also be attributed to the stretching of the vortex in the vertical due to the evaporative cooling associated with rainfall below the stratiform cloud. Rotational motion is proposed to be favored when the Rossby radius of deformation is reduced from values exceeding 1000 km to magnitudes of the radius of the stratiform rain cloud (~125 km). When these special conditions occur, the latent heat release is more efficient at increasing the temperatures and the rotational winds than a similar amount of heating in a cluster of individual clouds in an unsaturated environment. This means the vortex could be developed on the time scale of a diurnal cycle of deep convection. In the Frank and Chen model, the spinup of the mesoscale vortex took only 12 hours rather than days.

Raymond and Jiang (1990) and Hertenstein and Schubert (1991) suggest that MCVs in the stratiform rain region are convectively produced potential vorticity anomalies where the horizontal scale of the diabatic forcing is comparable or larger than the Rossby radius of deformation. Cross-sections through the mesoscale vortex center of a midlatitude MCC have a positive potential vorticity anomaly at mid-levels

and a well defined minimum directly above (Fritsch et al. 1994).

Raymond and Jiang (1990) also propose that the longevity of the mesoscale vortex may be due to low-level inflow that provides a continual source of water vapor that ascends over the raised isentropic surfaces associated with the evaporatively cooled downdraft region that is below the mid-level positive potential vorticity anomaly. In the midlatitude MCC study of Fritsch et al. (1994), low-level isentropic surfaces slope upward from the rear of the potential vorticity anomaly into the vortex center. Thus, relatively fast-moving low-level southwesterly flow overtaking the slow-moving vortex from the rear ascended as it approached the vortex center (Fritsch et al. 1994). Since these MCC studies were entirely over land, surface fluxes from a warm ocean did not contribute to the growth of the vortices.

One different aspect of the tropical maritime MCS versus the observations and models of the MCS over land in the midlatitudes is the likely magnitude of the isentropic lifting at low levels (Elsberry et al. 1992). In the midlatitudes, the rain-induced cooling below the high cloud bases can lead to strong downdrafts. Over land, this cold air may be little modified by surface fluxes, and strong, cold highs may persist. In the tropics, the cloud bases of the convective clouds are lower and the low-level rain cooling is smaller. However, saturated mesoscale downdrafts adjacent to the convective clouds do reach the ground and spread forward to form the lifting mechanism in tropical squall lines. The mesoscale downdrafts below the trailing stratiform rain region probably have too little rain-cooling to create substantial cold pools with significant isentropic slopes as in the midlatitudes (Elsberry et al. 1992). However, the high equivalent potential temperature ($\theta_E$) values of tropical air do not require as much vertical lifting to trigger convection.

The role of the MCV in the genesis of tropical cyclones is not yet understood. Zehr (1992) proposed that a low-level environmental surge is necessary to embed a mesoscale vortex in an active MCS for the tropical cyclogenesis process to proceed. Results from the Tropical Experiment in Mexico (TEXMEX) suggest that the formation of a cold-core mesoscale cyclone in the middle troposphere, and then subsequent moistening of the core, may be a necessary precursor to tropical cyclone

development (Emanuel 1993). Understanding the role of the MCS and associated mesovortices in the genesis of tropical cyclones requires additional measurements and studies to be conducted.

A small field experiment called Tropical Cyclone Motion (TCM-93) was conducted in the western North Pacific from 20 July 1993 to 12 August 1993 (Harr et al. 1993). This experiment was a sequel to a similar experiment conducted the previous summer called TCM-92. The purpose of TCM-93 was to provide *in situ* measurements and observations of tropical MCSs using an Air Force Reserve WC-130 instrumented aircraft from the 815th Weather Squadron. Seven aircraft missions were conducted in which flight-level and omega dropwinsonde (ODW) data were collected. Two Aircraft Observing Periods (AOPs), AOP-1A and AOP-1B, were of particular interest in this study. AOP-1A was conducted from 0311 UTC 23 July 1993 to 0934 UTC 23 July 1993, while AOP-1B was conducted from 0206 UTC 24 July 1993 to 1204 UTC 24 July 1993.

Over the week-long period from 19 July 1993 to 27 July 1993, repeated tropical cyclogenesis (Typhoon Nathan, Tropical Storm Ofelia, and Typhoon Percy) occurred along the eastern edge of the monsoon gyre circulation (Harr et al. 1993). In addition to each formation being similar, each tropical cyclone followed a similar north-oriented track toward landfall over southern Japan. During this period, the large-scale monsoon circulation over the western North Pacific was similar to the large cyclonic gyres discussed by Lander (1994) that have diameters on the order of 2000 km and a life span of a week or more. Lower-level circulations were such that persistent deep convection was continually being forced in a region of confluence between the gyre to the west and a large subtropical ridge to the east. At 200 mb, subsidence under an intense cell within the TUTT contributed to the strengthening and westward extension of the subtropical ridge. Each successive tropical cyclogenesis occurred to the west of the previous formation as the entire system of TUTT cell, subtropical ridge, and monsoon gyre moved westward over the subtropical western North Pacific.

The foci of this study are: (i) the structure of the circulations that contributed

to the forcing of the persistent convection along the eastern edge of the monsoon gyre; and (ii) the mesoscale structure of the region of deep convection that subsequently resulted in the formation of Tropical Storm Ofelia. First, rawinsonde observations from Guam, Palau, Chuuk, Pohnpei, and Yap will be used to document the structure of the large-scale flow surrounding the MCS in the confluent flow region between the subtropical ridge and the monsoon gyre. The hypothesis is that the moist southwesterly flow around the southern portion of the gyre was subjected to large-scale lifting as it was undercut by the easterly winds along the southern portion of the subtropical ridge. This confluence between the two large-scale circulations contributed to the maintenance of a large region of persistent deep convection throughout the period of westward migration of both large-scale circulations. Repeated tropical cyclogenesis occurred in this region of persistent deep convection.

Second, a multiquadric interpolation technique will be used to blend the ODW data and aircraft flight-level winds from AOP-1A and AOP-1B into background fields from archived Fleet Numerical Meteorology and Oceanography Center (FNMOC) global analyses. These ODWs are an essential component in documenting the structure of the MCS. Thermodynamic and dynamic structures are analyzed directly from the dropwinsondes and from gridded analysis fields. The structure and evolution of the long-lived MCSs along the eastern portion of the monsoon gyre will be identified and related to the eventual formation of Tropical Storm Ofelia.

# II. METHODOLOGY

## A. DATA

The aircraft missions for AOP-1A and AOP-1B were designed relative to a fix of the approximate MCS center based on Geostationary Meteorological Satellite (GMS) enhanced infrared (IR) or visible satellite imagery at the beginning of each mission. The majority of time for each mission was spent investigating the target MCS. The flight durations of AOP-1A and AOP-1B were 6.5 h and 10 h respectively and a total of 35 Omega Dropwinsondes (ODWs) were deployed (Tables 1 and 2). Because the WC-130 ODW processing system permitted the collection of data from two sondes simultaneously, the ODW spacing ranged between 110 and 280 km. The spacing was slightly less at lower flight levels and slightly more at higher flight levels. The ODWs reported winds, heights, temperatures, and relative humidity at both mandatory and significant levels (Harr et al. 1993).

For AOP-1A, the primary focus of the mission was to determine the structure of the MCS after two successive diurnal convection maximum periods (Harr et al. 1993). The flight began at 0245 UTC 23 July 1993 and the WC-130 ascended to 500 mb and proceeded north-northwest to enter the MCS from the east (Fig. 1). An alpha pattern centered at 16°N, 141.5°E was completed at 500 mb and then another alpha pattern rotated by 45° was completed at 400 mb. This alpha pattern terminated to the southeast of the MCS and the aircraft returned to Guam (Harr et al. 1993). A total of 18 ODWs was deployed for AOP-1A (Table 1).

The flight plan for AOP-1B (Fig. 2) was similar to AOP-1A of the previous day. The WC-130 took off from Guam at 0225 UTC 24 July 1993. The flight was centered on a persistent area of convection at 17°N, 141°E within the main confluent monsoon flow south of TS Nathan. As Nathan moved north-northwest and intensified, a convective area about 5° lat. south of Nathan appeared to connect Nathan with the monsoon trough cloudiness. The mission began at 850 mb with an east-to-west leg along 17°N to locate the center. A return track at 700 mb eastward along 17°N

| Drop No. | Launch Time (UTC/hhmm) | Location (°N,°E) | Launch Height (m) | Sea-level Pressure | Remarks |
|---|---|---|---|---|---|
| 1 | 0325 | 16.0,144.0 | 5856.8 | 1004.4 | |
| 2 | 0340 | 16.0,142.6 | 5848.6 | 1000.4 | |
| 3 | 0354 | 16.0,141.5 | 5845.5 | 1000.6 | |
| 4 | 0409 | 16.0,140.2 | 3168.4 | 5844.0 | |
| 5 | 0423 | 16.0,139.1 | 5842.7 | 1003.2 | |
| 6 | 0506 | 18.5,141.5 | 5836.3 | 1001.3 | No winds, failed at 868 mb |
| 7 | 0512 | 18.1,141.5 | 5839.4 | 1001.6 | |
| 8 | 0522 | 17.3,141.5 | 5836.6 | 1001.8 | |
| 9 | 0550 | 14.8,141.5 | 5837.4 | 1000.5 | |
| 10 | 0605 | 13.5,141.5 | 5842.9 | 1002.9 | |
| 11 | 0630 | 14.0,140.0 | 7564.1 | 997.3 | |
| 12 | 0644 | 15.0,140.7 | 7558..8 | 995.2 | |
| 13 | 0713 | 17.0,142.2 | 7561.0 | 991.2 | |
| 14 | 0731 | 18.0,143.0 | 8052.2 | 994.1 | |
| 15 | 0751 | 18.0,141.2 | 8069.3 | 994.6 | |
| 16 | 0818 | 16.3,141.5 | 7558.8 | 992.9 | |
| 17 | 0831 | 15.5,142.1 | 7561.4 | 995.2 | |
| 18 | 0857 | 14.6,143.3 | 7561.4 | 995.4 | |

Table 1. Summary of ODWs for AOP-1A from 0311 UTC 23 July 1993 to 0934 UTC 23 July 1993.

| Drop No. | Launch Time (UTC/hhmm) | Location (°N,°E) | Launch Height (m) | Sea-level Pressure | Remarks |
|---|---|---|---|---|---|
| 1 | 0442 | 17.0,138.3 | 3156.3 | 1004.2 | |
| 2 | 0502 | 17.0,139.7 | 3164.8 | 1004.3 | |
| 3 | 0522 | 17.0,141.0 | 3158.1 | 1006.6 | |
| 4 | 0543 | 17.0,142.3 | 3168.4 | 1008.4 | |
| 5 | 0603 | 17.0,143.7 | 3183.6 | 1009.6 | |
| 6 | 0700 | 19.2,141.0 | 3159.7 | 1004.7 | |
| 7 | 0717 | 18.3,141.0 | 3173.5 | 1007.1 | |
| 8 | 0800 | 15.8,141.0 | 3193.2 | 1008.0 | |
| 9 | 0822 | 14.5,141.0 | 3217.1 | 1009.2 | |
| 10 | 0842 | 14.8,139.8 | 5884.0 | 996.7 | Failed at 756 mb |
| 11 | 0901 | 16,1,140.5 | 5846.1 | 996.8 | |
| 12 | 0935 | 18.3,141.8 | 5887.5 | 1000.4 | |
| 13 | 0950 | 19.2,142.3 | 5884.7 | 1002.7 | |
| 14 | 1023 | 19.1,139.8 | 5833.7 | 998.9 | |
| 15 | 1043 | 18.1,140.4 | 5855.2 | 999.6 | |
| 16 | 1102 | 17.0,141.0 | 5848.2 | 1001.0 | |
| 17 | 1118 | 16.2,141.5 | 5820.0 | 1000.8 | |

Table 2. Summary of ODWs for AOP-1B from 0206 UTC 24 July 1993 to 1204 UTC 24 July 1993.

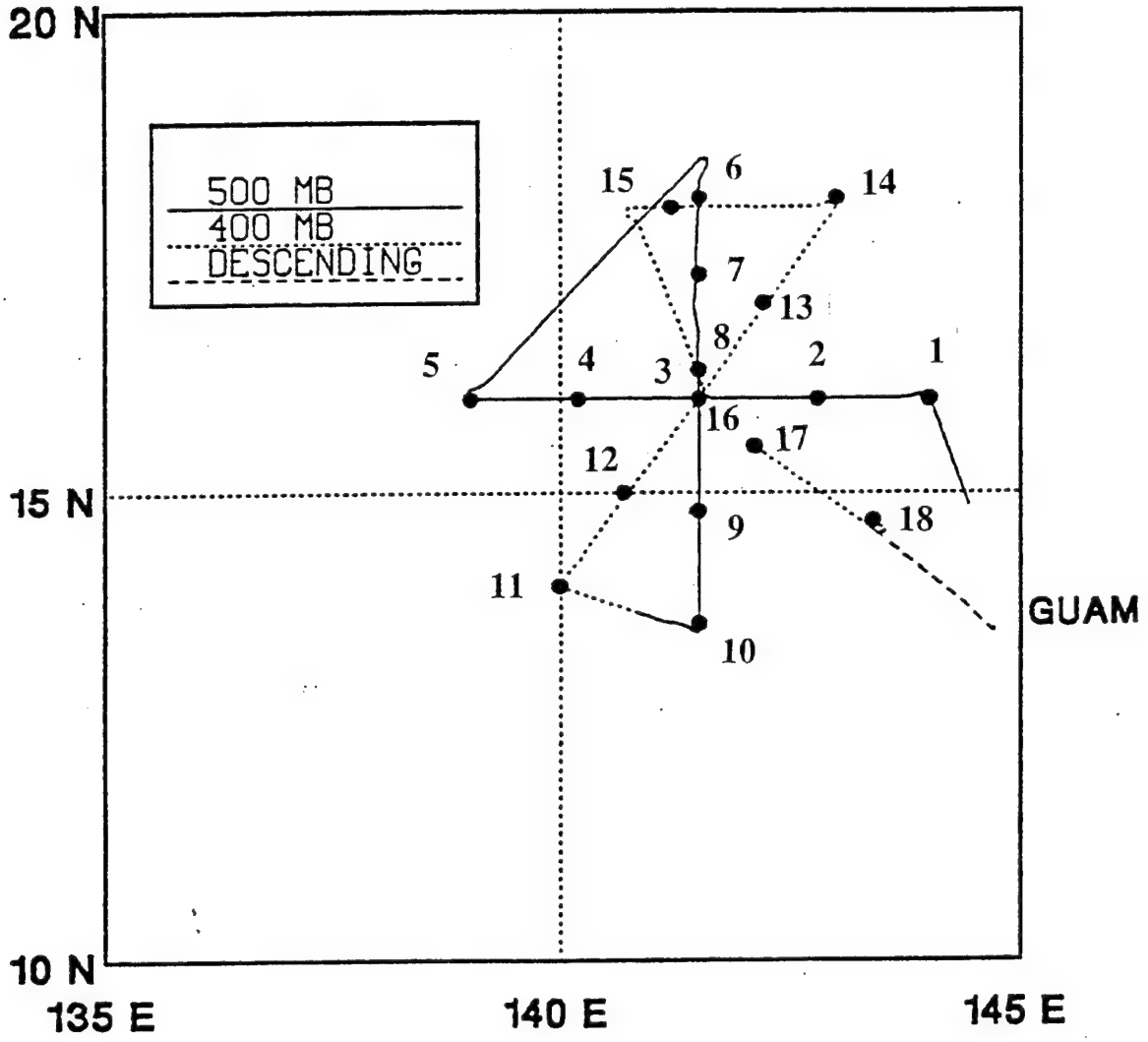


Figure 1. Flight track (altitudes indicated in the inset) and ODW locations for AOP-1A.

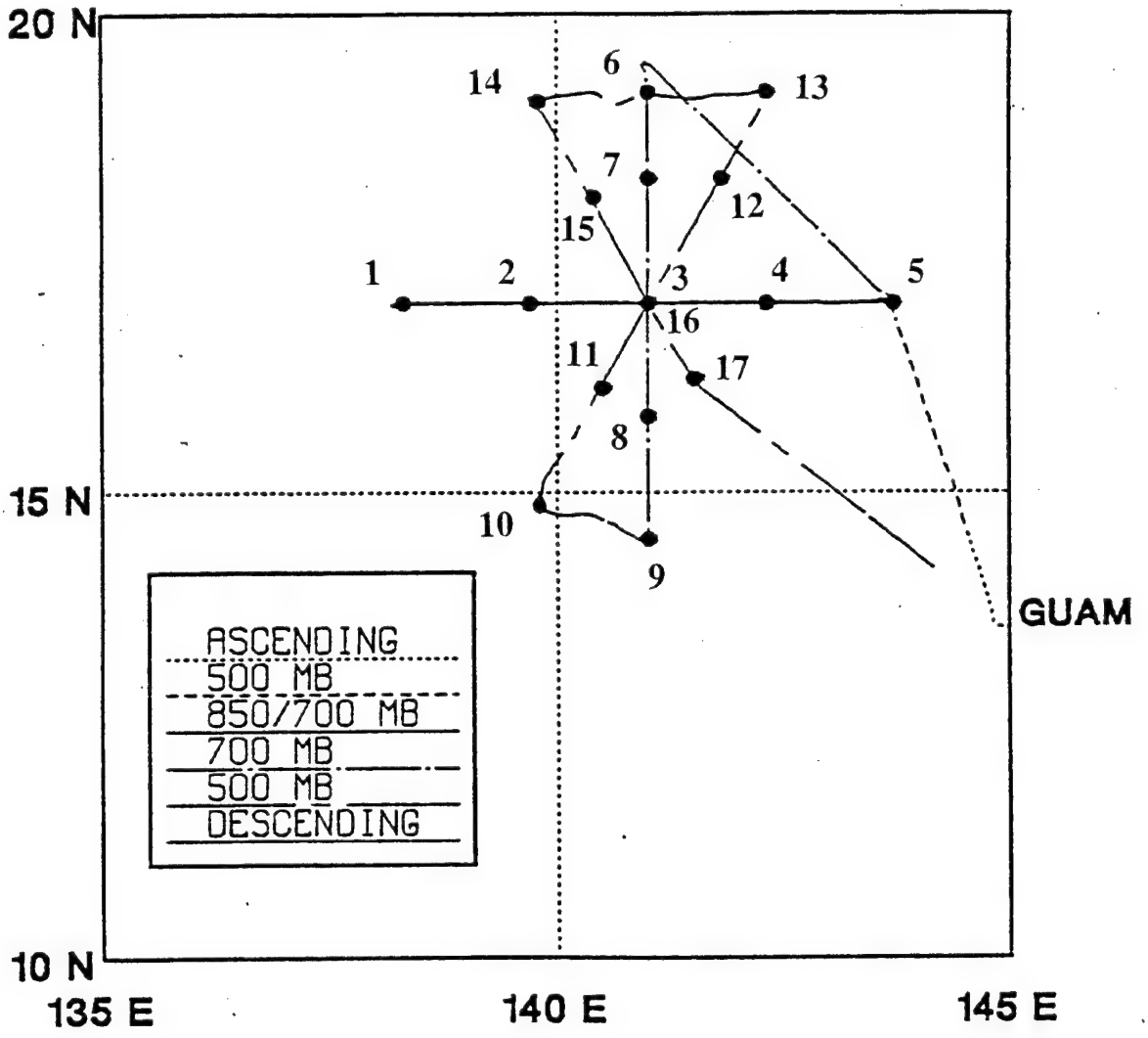


Figure 2. Flight track (altitudes given in inset) and ODW locations for AOP-1B. The east-west leg was flown at both 850 and 700 mb.

began an alpha pattern that was completed by a north-to-south leg terminating near 14.5°N, 141.5°E. After ascending to 500 mb, an alpha pattern rotated 45° from the 700 mb pattern was completed (Harr et al. 1993). A total of 17 ODWs was deployed during AOP-1B (Table 2).

Rawinsonde observations from Guam, Palau, Chuuk, Pohnpei, and Yap were obtained from the Automated Weather Network at the Joint Typhoon Warning Center (JTWC) on Guam. Mandatory and significant level rawinsonde data were interpolated to 50 mb levels beginning at 950 mb. Relevant satellite cloud-tracked wind data at 200 mb were also obtained for inclusion in the final data set. Additional data included standard synoptic station data and analyzed fields from the Fleet Numerical Meteorology and Oceanography Center (FNMOC). All observations are positioned in a storm-relative reference frame that is centered at 0600 UTC 23 July 1993 for AOP-1A and 0800 UTC 24 July 1993 for AOP-1B. The rawinsonde observations, ODW data, cloud-tracked winds, and the aircraft flight-level winds from AOP-1A and AOP-1B are first converted to *increments* relative to the background fields from archived FNMOC global analyses interpolated to the observation points.

## B. ANALYSIS PROCEDURES

A two-dimensional, single-variable, multiquadric interpolation technique proposed by Nuss and Titley (1994) is used to interpolate these increments to a regular grid. The multiquadric interpolation method uses hyperboloid radial basis functions to fit scattered data to a uniform grid. Multiquadric interpolation produces excellent analyses that retain small-scale features resolved by the observations in any subregion of the domain. Nuss and Titley (1994) have shown that multiquadric interpolation is more accurate than the Barnes (1973) or Cressman (1959) schemes for an analytical function. The accuracy of multiquadric interpolation has also been compared to the Barnes scheme using a data set from the Experiment on Rapidly Intensifying Cyclones over the Atlantic (ERICA), which was designed to study extratropical cyclones over the ocean (Nuss and Titley 1994). In the analysis of this data set, the Barnes scheme had boundary problems and had difficulty with data-void regions of the domain. Data-

void regions can be fixed by increasing the smoothing length scale to retain scales that are larger than the data-void region. However, increasing the smoothing length scale prevents the retention of smaller-scale structure in regions where the observations may support it.

Multiquadric interpolation seems to provide a plausible analysis in data-void regions and does not appear to have boundary problems if observations are available near the boundary around the domain that helps to constrain the analysis at the boundary. When observations are a large distance from the boundary, the multiquadric scheme has a tendency to continue the gradient defined by the nearest observations. The multiquadric scheme smoothly analyzes the scales represented by the observations in a particular region of the domain while not producing undesired results in the data-void regions. Consequently, data-sparse regions retain only large-scale features, while data-dense regions have small-scale features present in the data, which are retained for a given value of smoothing or filtering (Nuss and Titley 1994). Because the method is computationally very efficient and well-behaved in the data-void regions, the multiquadric technique is recommended for local analysis of meteorological fields (Nuss and Titley 1994).

Franke (1982) found multiquadric interpolation to be as accurate as statistical interpolation. A first-guess or background field can be incorporated into the scheme if desired. The background fields for the TCM-93 data set are extracted from the real-time analyses produced by the Navy Operational Global Atmospheric Prediction System (NOGAPS) at FNMOC. The analyses from NOGAPS are used to provide the larger scale environment of the detailed observations in the TCM-93 region. Increment values equal to zero are specified outside the region of real observations to constrain the analyses from the boundary problems discussed above. The multiquadric analyses are constructed on a 1° lat./long. grid, which is consistent with the 100 km average spacing between dropwindsonde observations (Harr et al. 1993). The horizontal domain of the multiquadric grid is from the equator to 30°N and 130°-160°E. In the vertical, the multiquadric analyses are constructed at 50 mb intervals from 950 mb to 100 mb. The NOGAPS analyses, which are on a 2.5° lat./long. grid,

are interpolated using B-splines to the 1 degree multiquadric grid. After the multiquadric interpolation was performed on increment values, the interpolated values at the gridpoints are added to the background field to give the total field. In the data-void regions (where zero increments are specified), the multiquadric analysis will simply return the background field. This procedure allows the NOGAPS fields to be assimilated into the multiquadric analysis over portions of the domain that do not contain any TCM-93 observations (Harr and Elsberry 1995).

The multiquadric analyses are limited by the distribution of the data. The maximum flight levels attained during TCM-93 by the WC-130 for AOP-1A and AOP-1B were 400 mb and 500 mb respectively. Consequently, the true vertical extent of atmospheric phenomena in the upper troposphere is unknown due to the lack of dropwindsonde or flight-level data above these levels. The rawinsonde observations from the surrounding island stations provide valuable information concerning the large-scale flow surrounding the target MCSs for each observing period. In addition, the rawinsondes provide critical observations for ensuring vertical consistency above the levels not observed by the WC-130. The addition of several cloud-track wind observations at 200 mb, which were not included in the original NOGAPS analysis, also helped to validate the upper-level analyses. As indicated above, the multiquadric analysis in the data-void regions surrounding the target MCSs for AOP-1A and AOP-1B are constrained to return to the NOGAPS background fields.

# III. AIRCRAFT OBSERVING PERIOD (AOP) SUMMARIES

## A. DESCRIPTION OF THE LARGE-SCALE CIRCULATION OVER THE TROPICAL WESTERN NORTH PACIFIC DURING TCM-93

The following description of the large-scale circulation is based on the field experiment summary by Harr et al. (1993). The tracks of three tropical cyclones that occurred during TCM-93 (Fig. 3) reflect the large-scale circulation patterns that occurred during AOP-1A and AOP-1B and subsequent periods. During the period from 20 July to 31 July 1993, TY Nathan, TS Ofelia, and TY Percy followed north-oriented tracks around a low-level monsoon gyre. At the start of TCM-93, the monsoon gyre was well-defined and centered near 15°N, 140°E (Fig. 4). TY Nathan had tracked around the eastern edge of the gyre under the influence of a strong northward steering flow that existed between the monsoon gyre and the large subtropical anticyclone located to the northeast. Notice the axis of the north-oriented, confluent flow near 145°E between the monsoon gyre and the subtropical anticyclone. The intense convective activity within this north-oriented, confluent flow became the subject of AOP-1A and AOP-1B. As TY Nathan moved between the gyre and the subtropical anticyclone, the anticyclone began to build to the southwest and connect with a near-equatorial anticyclonic circulation near 5°N, 145°E (Fig. 4). At 200 mb (Fig. 5), an intense Tropical Upper Tropospheric Trough (TUTT) cell was centered near 15°N, 155°E, which was immediately east of the 700 mb ridge axis that extended southwestward from the subtropical anticyclone center.

Over the following ten days, the strength of the subtropical anticyclone extension to the southwest increased as it moved westward, which displaced the monsoon gyre westward. Thus, the axis of the north-oriented confluent flow between the monsoon gyre and the expanding subtropical ridge was steadily shifted westward. The expansion of the subtropical anticyclone to the west and southwest occurred in conjunction with a westward movement of the large 200 mb TUTT cell (Fig. 5). As TY Nathan moved northward, the southwest-to-northeast oriented anticyclonic

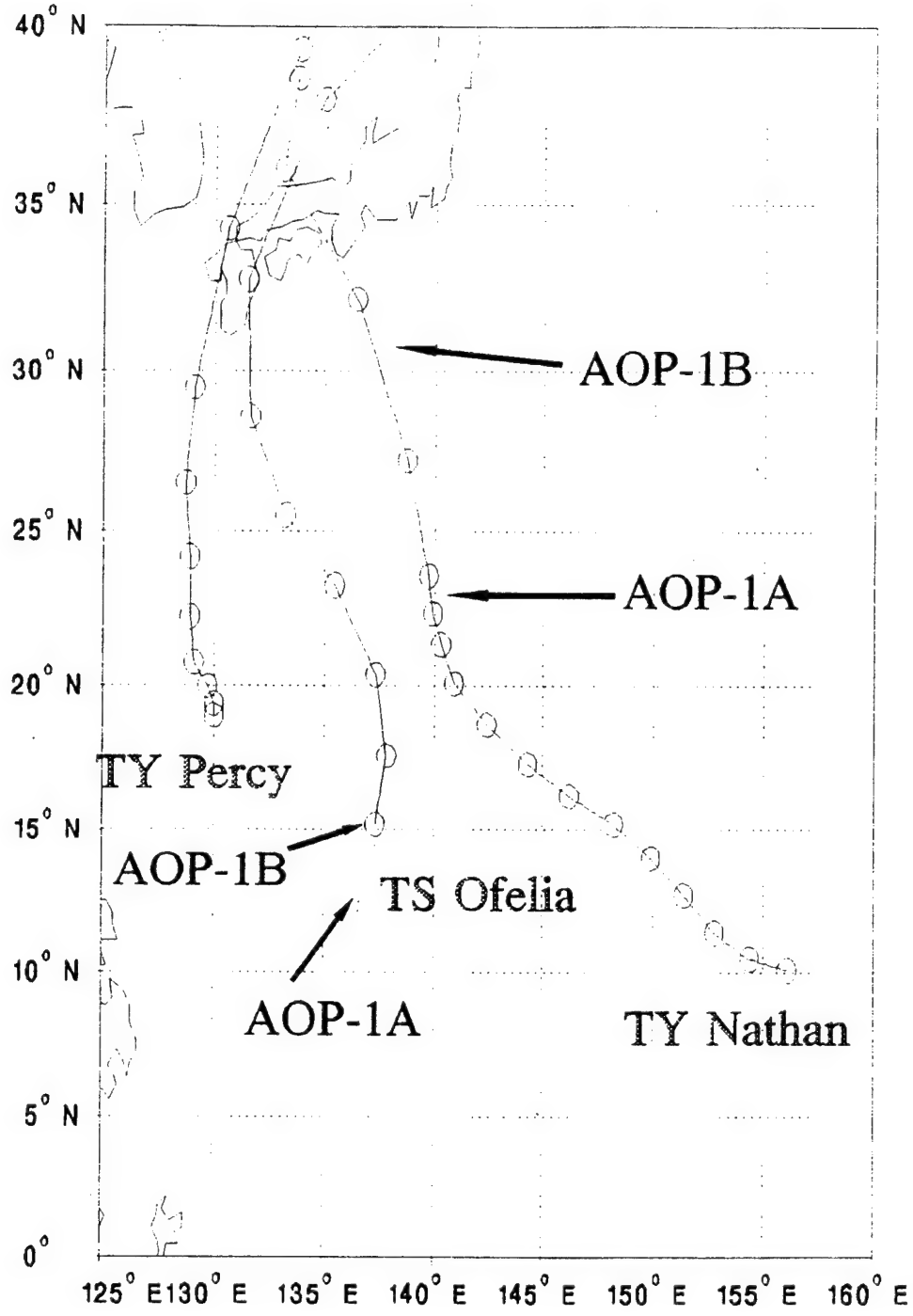


Figure 3. Tracks of tropical cyclones that occurred between 17 July 1993 and 31 July 1993.

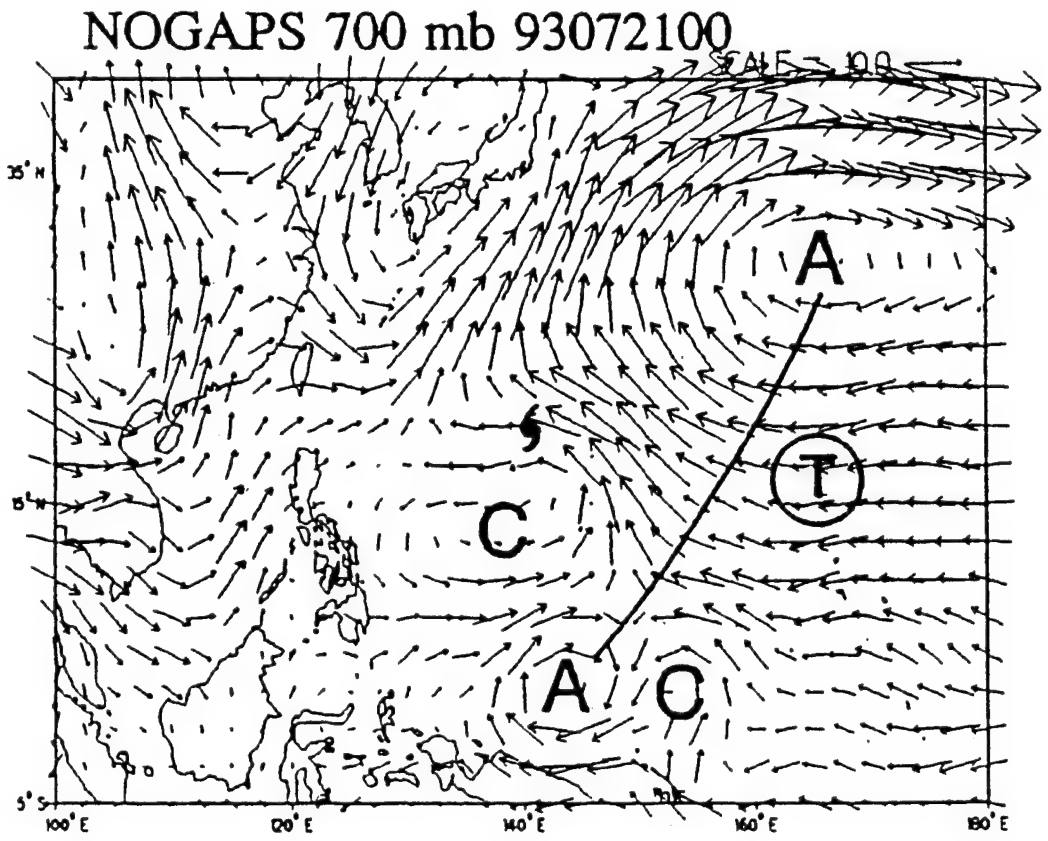


Figure 4. NOGAPS analysis of the 700 mb winds for 0000 UTC 21 July 1993 with positions of key cyclonic (C) and anticyclonic (A) circulations. The positions of Nathan (TY symbol) and the upper-tropospheric trough center (circle T) are also shown (Harr et al. 1993).

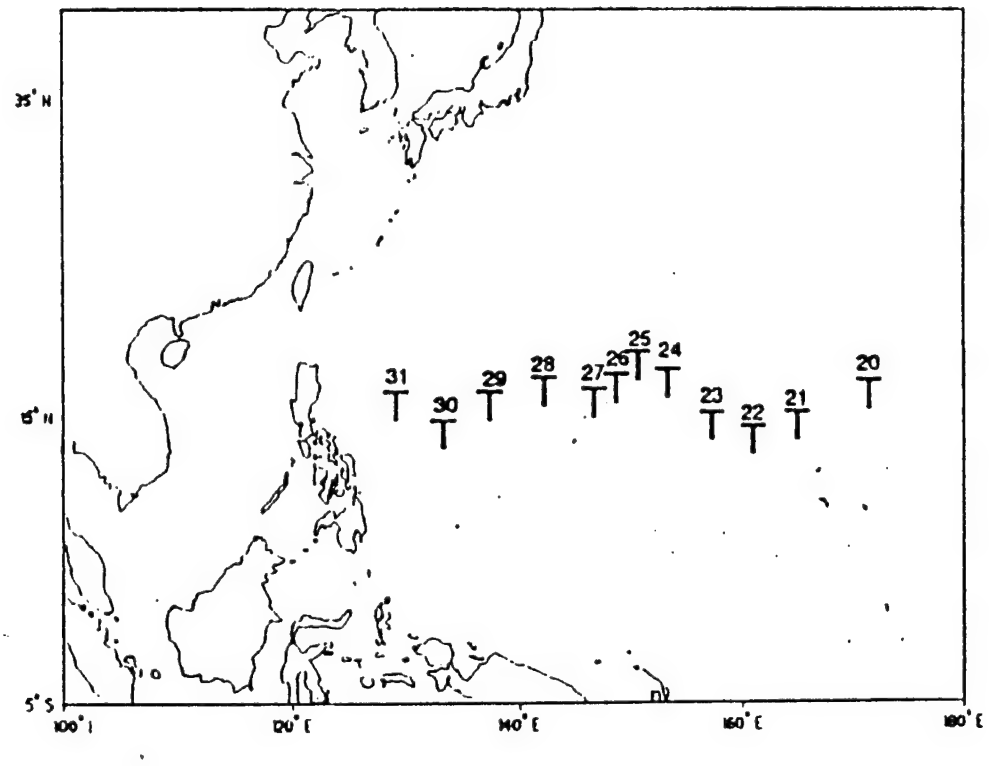


Figure 5. Positions of the center of the 200 mb TUTT cell at 0000 UTC each day between 20 July and 31 July 1993 (Harr et al. 1993).

extension continued to direct the large-scale monsoon flow to the north. Although intense convection continued within the confluent flow between the monsoon gyre and the subtropical anticyclone, convection was severely inhibited to the east within a broad region between the equator-20°N and 130°E-150°E that was dominated by subsidence in the strong subtropical anticyclone and the TUTT cell.

Given the persistent, large-scale evolution of this overall monsoon gyre, subtropical anticyclone, and TUTT cell system, the focus is then on the confluent flow between the subtropical ridge and the monsoon gyre where repeated deep convection occurred. Fortunately, the two AOPs provide mesoscale observations in the target area on the two days prior to the formation of TS Ofelia.

## B. AIRCRAFT OBSERVING PERIOD AOP-1A

The objective of AOP-1A was to investigate the structure of a loosely organized MCS that had been present to the south of TY Nathan for at least two diurnal convection maximum periods (Fig. 6). The MCS structure will be derived from the ODW soundings deployed by the 815th Weather Squadron WC-130. The analyses from NOGAPS and rawinsonde soundings from Guam, Palau, Chuuk, Pohnpei, and Yap (Table 3) will be used to describe the larger scale environment of the detailed observations in the TCM-93 region.

Rawinsonde soundings (not shown) from Palau and Yap three hours prior to the commencement of AOP-1A are moist with southwesterly winds at 10 m $s^{-1}$ in the low to mid-levels attributed to the monsoon gyre. The depth of the westerlies extends from the surface to 600 mb at Palau and from the surface to 450 mb at Yap. The Guam rawinsonde indicates a moist sounding with southerly winds at 10 m $s^{-1}$ from the surface to approximately 400 mb that is associated with the inflow of TY Nathan. The Chuuk and Pohnpei soundings indicate easterly flow from the surface to approximately 400 mb. Below 400 mb, the meeting of the easterly flow and the monsoon southwesterly flow at the longitude of Guam defines the region of confluence and the southerly winds. Thus, the easterly flow is undercutting the southwesterly flow associated with the monsoon gyre, which presumably provides the

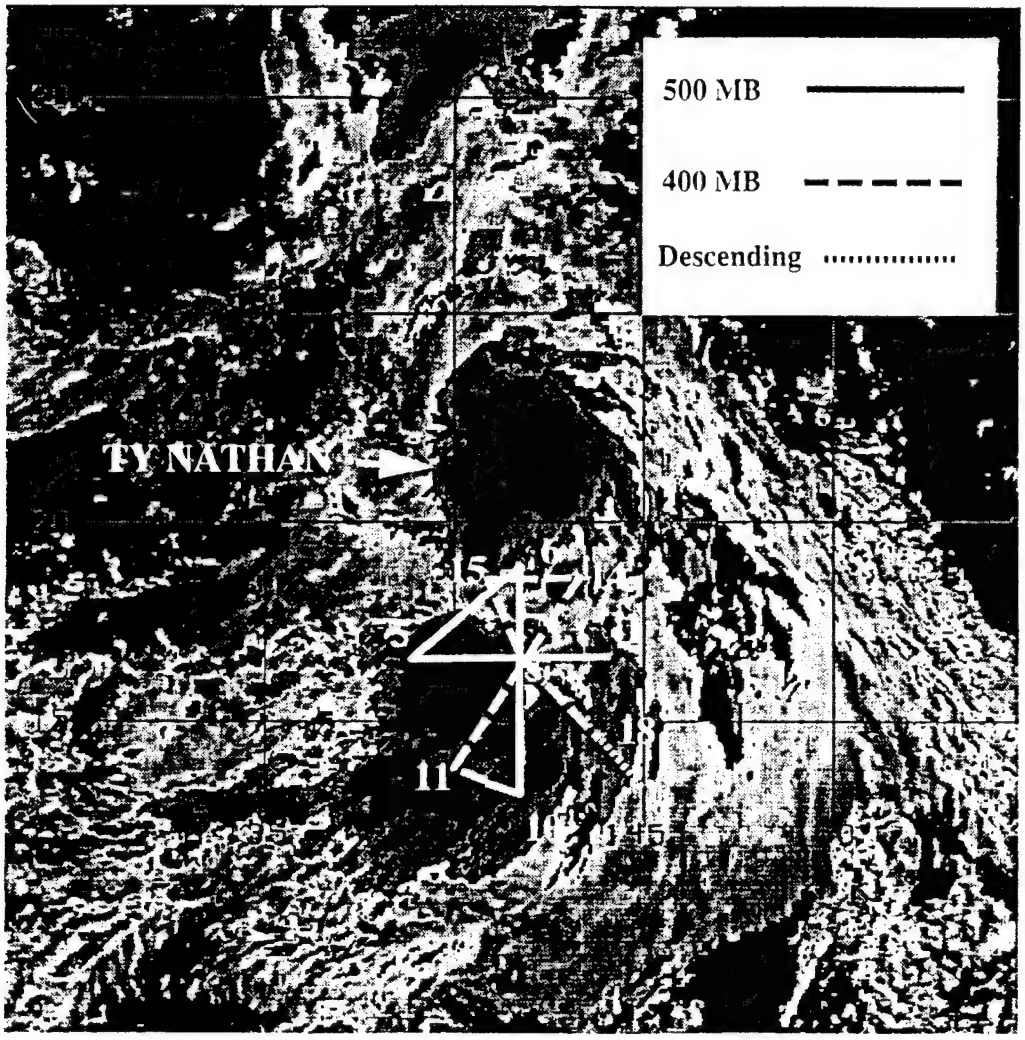


Figure 6. Infrared satellite image at 0030 UTC 23 July 1993 for the region of TCM-93 at the beginning of AOP-1A. The cirrus shield associated with the target MCS is centered near 16°N, 140°E, and TY Nathan is near 21°N, 141°E. The black region near the center of TY Nathan defines temperatures below -80°C, and the adjacent dark gray, gray, and then black regions represent temperature increases in 5°C intervals. A standard gray scale is used for temperatures between -65°C and -30°C, and temperatures warmer than -30°C are set to black.

| Station Name (Number) | Launch Times (UTC/hhmm) | Location (°N, °E) |
|---|---|---|
| Palau (91408) | 0000, 1200 | 7.4, 134.3 |
| Yap (91413) | 0000, 1200 | 9.6, 138.1 |
| Guam (91217) | 0000, 1200 | 13.5, 144.9 |
| Chuuk (91334) | 0000, 1200 | 7.5, 151.9 |
| Pohnpei (91348) | 0000, 1200 | 7.0, 158.1 |

Table 3. Summary of rawinsonde station names, launch times, and geographical locations of stations used to define the large-scale flow for TCM-93.

lifting of the moist monsoon westerlies and results in persistent convection in the confluent area. While westerly winds are present from 350 to 300 mb in the Guam sounding, winds above 300 mb are from the north-northwest associated with flow around the 200 mb TUTT cell system.

Introducing the ODW data at 850 mb from the alpha flight pattern in Fig. 1 into the NOGAPS first-guess field at 850 mb (Fig. 7a) with the multiquadric interpolation technique (Fig. 7b) results in noticeable differences in the large-scale flow. As stated earlier, the multiquadric interpolation technique smoothly analyzes the scales represented by the observations in a particular region of the domain while not producing unrealistic analyses elsewhere. For example, the multiquadric analysis at 850 mb (Fig. 7b) has a stronger area of southerly flow between the monsoon gyre and the large subtropical anticyclone. Such a strong southerly flow is indicated by both the 0000 UTC and the 1200 UTC rawinsondes from Guam as well as soundings from ODWs 1, 2, 17, and 18 (see locations in Fig. 1). The multiquadric analysis also has intensified the flow surrounding the anticyclone extension centered near 8°N, 142°E and has caused the flow to become more elliptical. This change can be attributed to the 0000 UTC and 1200 UTC rawinsondes from Palau and Yap, which indicate strong southwesterly flow associated with the monsoon gyre. The ODW soundings also helped to define the large-scale flow in the region north of Yap and south of 16°N. Soundings from ODWs 9, 10, and 12 in Fig. 1 indicate westerly to southwesterly flow from the surface up to the levels of release, which further strengthens the region of southwesterlies around the monsoon gyre in the multiquadric analysis. The low-level easterly flow indicated by the Chuuk and the Pohnpei rawinsondes strengthened and extended the region of easterly flow southward in the vicinity of 10°N, 155°E. The col in the wind field that was located ESE of Guam in the NOGAPS first-guess field was shifted to the SSW of Guam in the multiquadric analyses.

Whereas significant deep convection associated with the diurnal convective maximum was near the center of the alpha flight pattern at the beginning of AOP-1A (Fig. 6), the satellite image toward the end of AOP-1A (Fig. 8) depicts the dissipation of deep convection characteristic of the diurnal convective minimum. A satellite

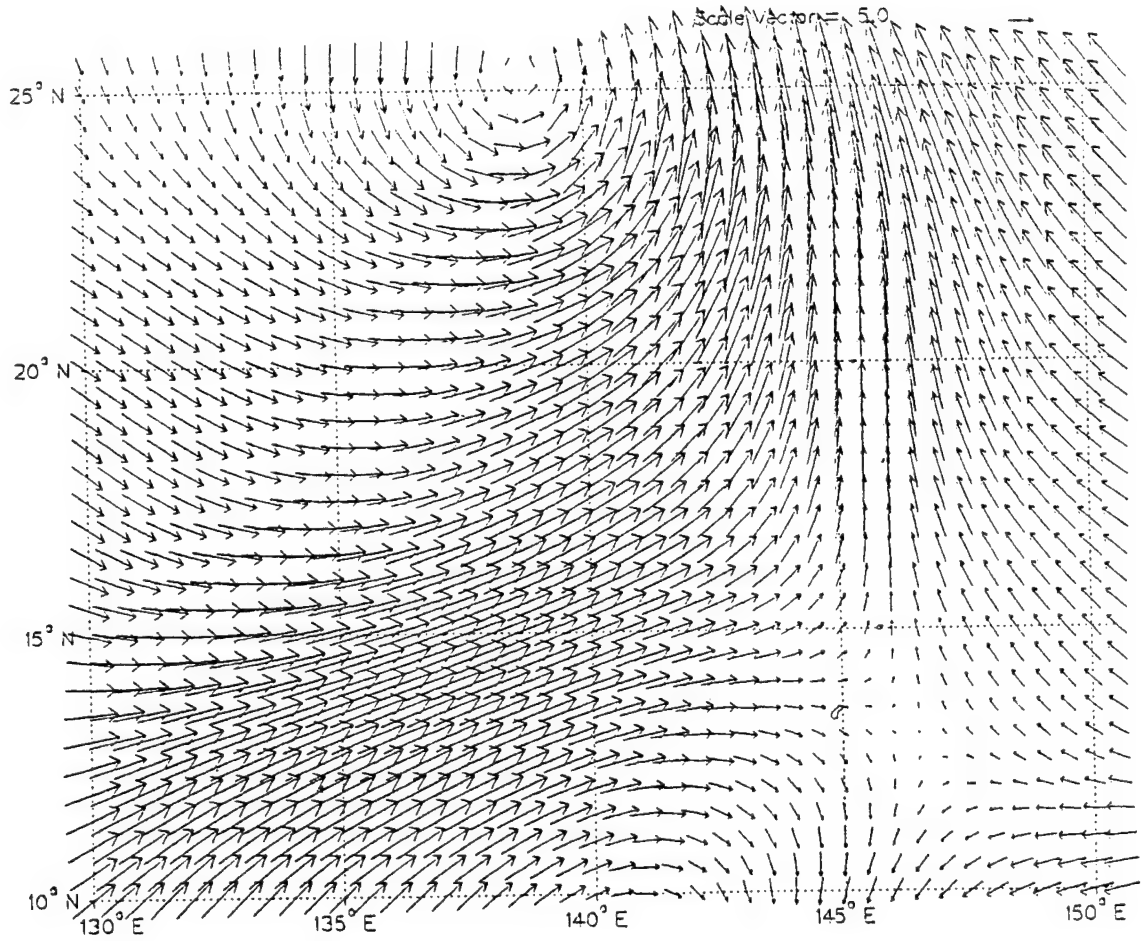


Figure 7a. NOGAPS first-guess field at 850 mb at 0600 UTC 23 July 1993. See scale of wind arrows in m $s^{-1}$ in upper right.

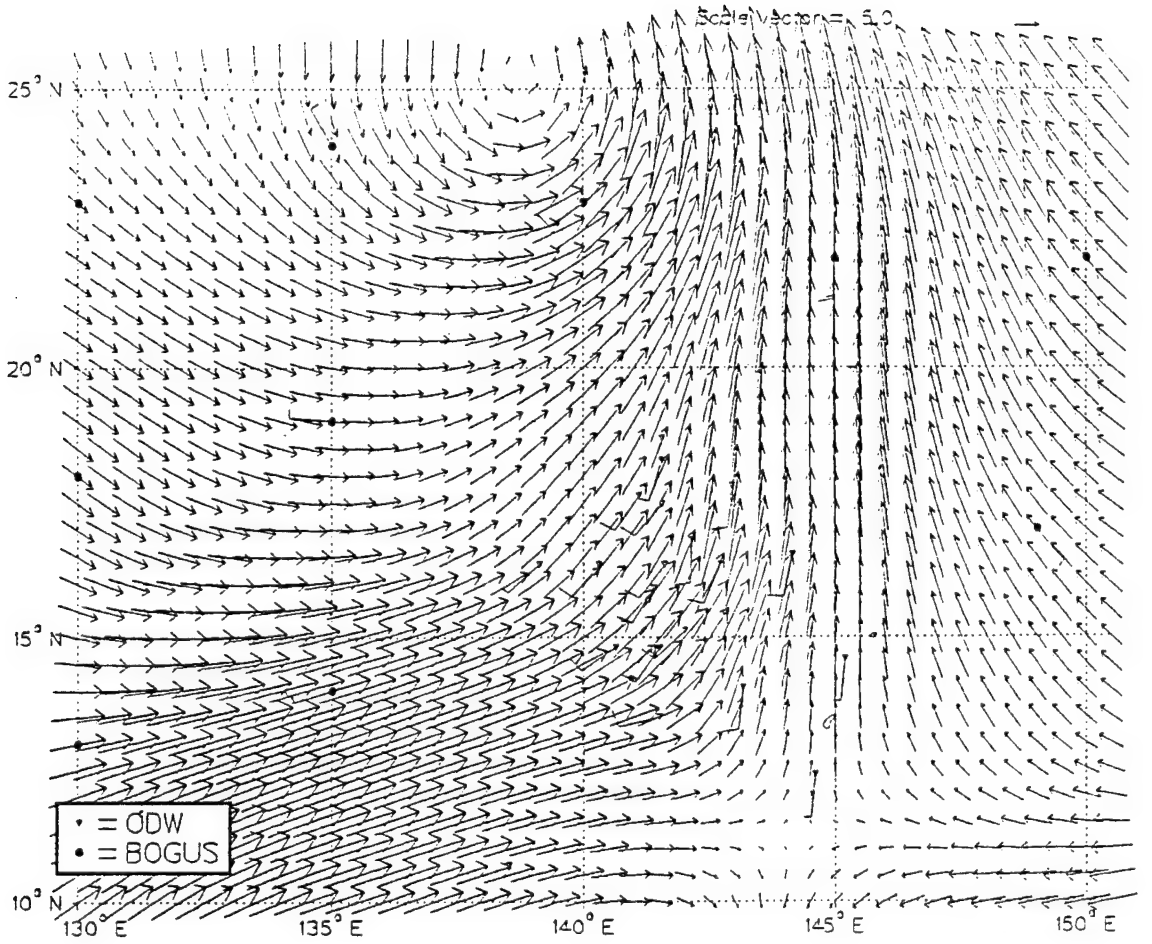


Figure 7b. Multiquadric analysis of 850 mb winds at 0600 UTC 23 July 1993. The TCM-93 observations and zero synthetic wind observations in the data-sparse areas are indicated by the larger wind barbs. See scale of wind arrows in m $s^{-1}$ in upper right.

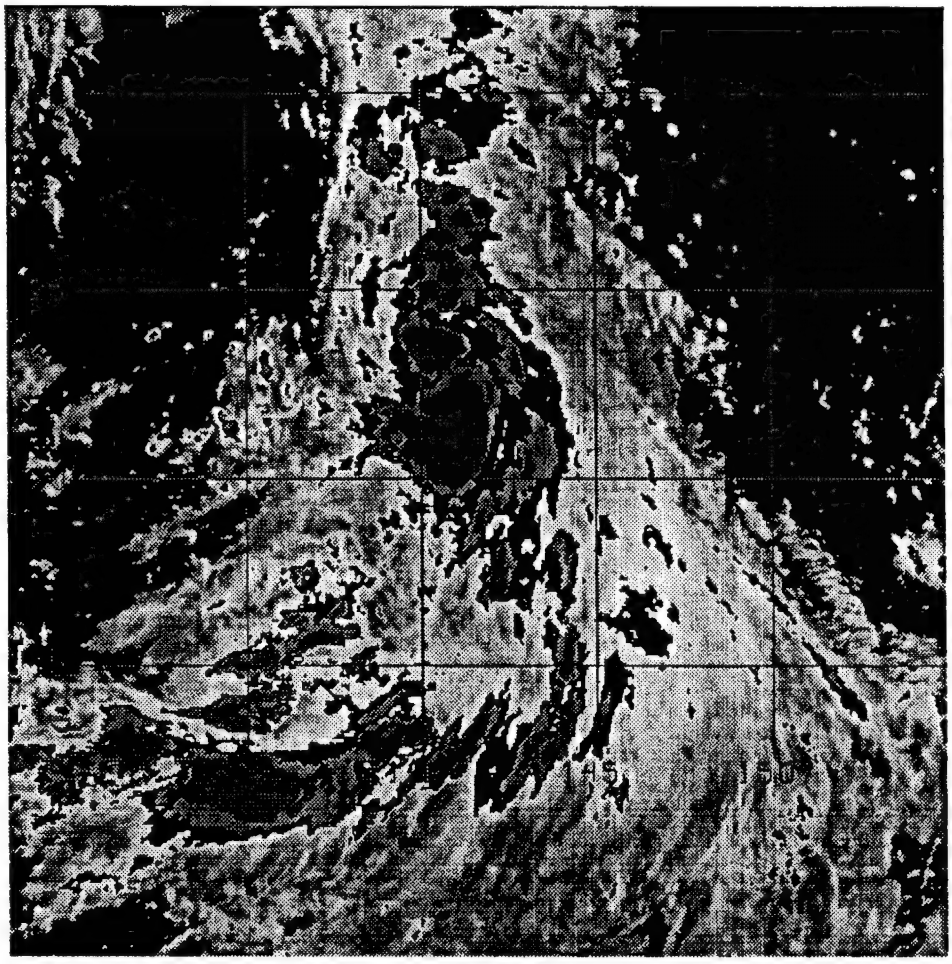

Figure 8. Infrared satellite image as in Fig. 6, except at 0830 UTC 23 July 1993 near the end of AOP-1A.

nephanalysis (Fig. 9) depicts the reduced area of convection in two-hour intervals throughout AOP-1A. During the Tropical Experiment in Mexico (TEXMEX), Emanuel (1993) observed that after the intense convection associated with the tropical MCS dissipated, a stratiform anvil system (similar to that in Figs. 6 and 8) was left behind that continued to precipitate near the axis of the wave trough. Emanuel (1993) proposed that a cold-core mesoscale cyclone in the lower troposphere was driven by the evaporation of precipitation, but this cold core might eventually approach saturation via evaporation from the sea surface. A characteristic of the MCSs observed in TEXMEX was the absence of appreciable positive vorticity near the surface; instead, the largest vorticity amplitude was in the middle troposphere.

The ODW soundings from the WC-130 provided valuable information concerning the three-dimensional structure of the MCS. Flight-level winds during AOP-1A (Figs. 10a, b) indicate the existence of a mid-tropospheric mesoscale cyclonic circulation that was not depicted in the NOGAPS first-guess field or the satellite imagery. Whereas the existence of a mid-tropospheric cyclonic circulation is well-documented by these 500 mb and 400 mb flight-level winds, further details of the mid-level circulation are analyzed through the use of the ODW soundings.

Inserting the ODW soundings from AOP-1A into the NOGAPS first-guess field generally introduces mesoscale phenomena in the region of the alpha flight pattern. However, the multiquadric analysis at 850 mb (Fig. 7b), which is based upon the ODW data, varies little from the NOGAPS first-guess field at 850 mb (Fig. 7a), which indicates that the mesoscale cyclonic circulation is primarily above the 850 mb level. The multiquadric analysis at 650 mb (Fig. 11b) deviates significantly from NOGAPS first-guess field at 650 mb (Fig. 11a). Notice especially the mesoscale cyclonic circulation centered at approximately 16°N, 141°E. The area of weak winds northwest of the mesoscale cyclonic circulation in the multiquadric analysis can be attributed to the northeasterly flow associated with the mesoscale cyclonic circulation opposing the southwesterly flow associated with the monsoon gyre. At 500 mb, the full horizontal extent of the mesoscale cyclonic circulation can be clearly seen in the multiquadric analysis (Fig. 12). An accurate depiction of the mesoscale cyclonic circulation above

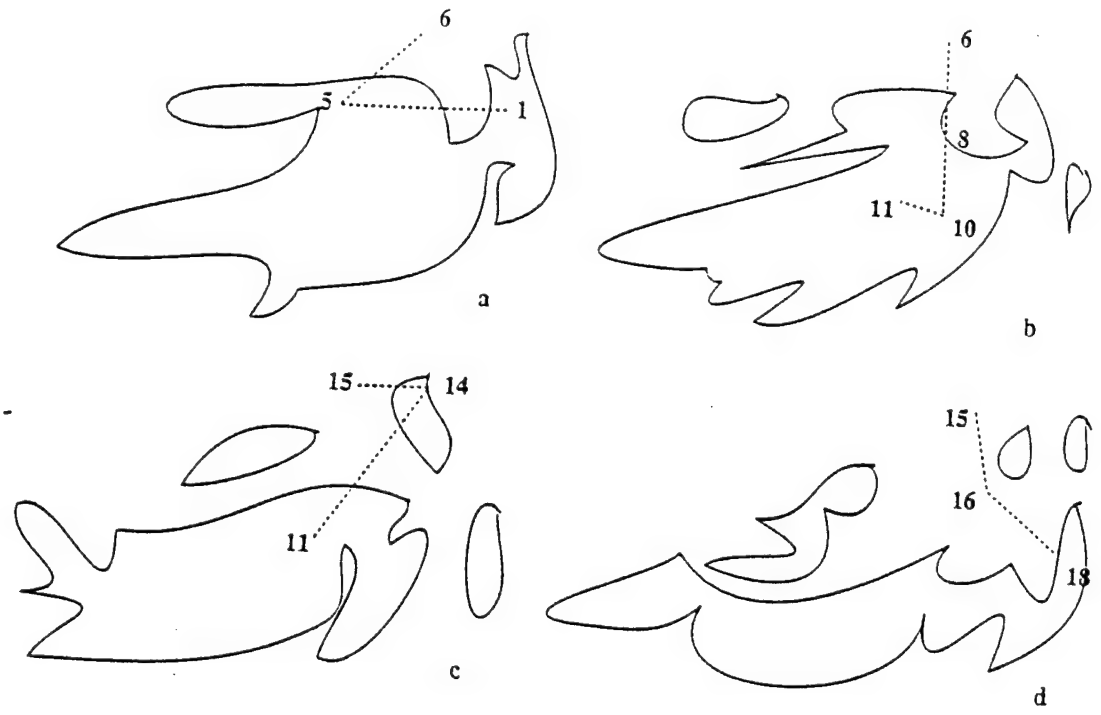


Figure 9. Satellite nephanalysis for AOP-1A showing the regions of deep convection surrounding the alpha flight pattern on 23 July 1993. Times of each nephanalysis are: a) 0230 UTC; b) 0430 UTC; c) 0630 UTC; and d) 0830 UTC, which illustrates the evolution between Figs. 6 and 8. Regions of deep convection with cloud-top temperatures lower than -30°C are depicted by the solid black lines while portions of the alpha flight pattern are depicted by the dashed lines. Numbers adjacent to the alpha flight pattern depict the locations of the individual ODWs with respect to the regions of deep convection. Locations 3 (halfway between 1 and 5), 8, and 16 are nearly at the same position in storm-relative coordinates.

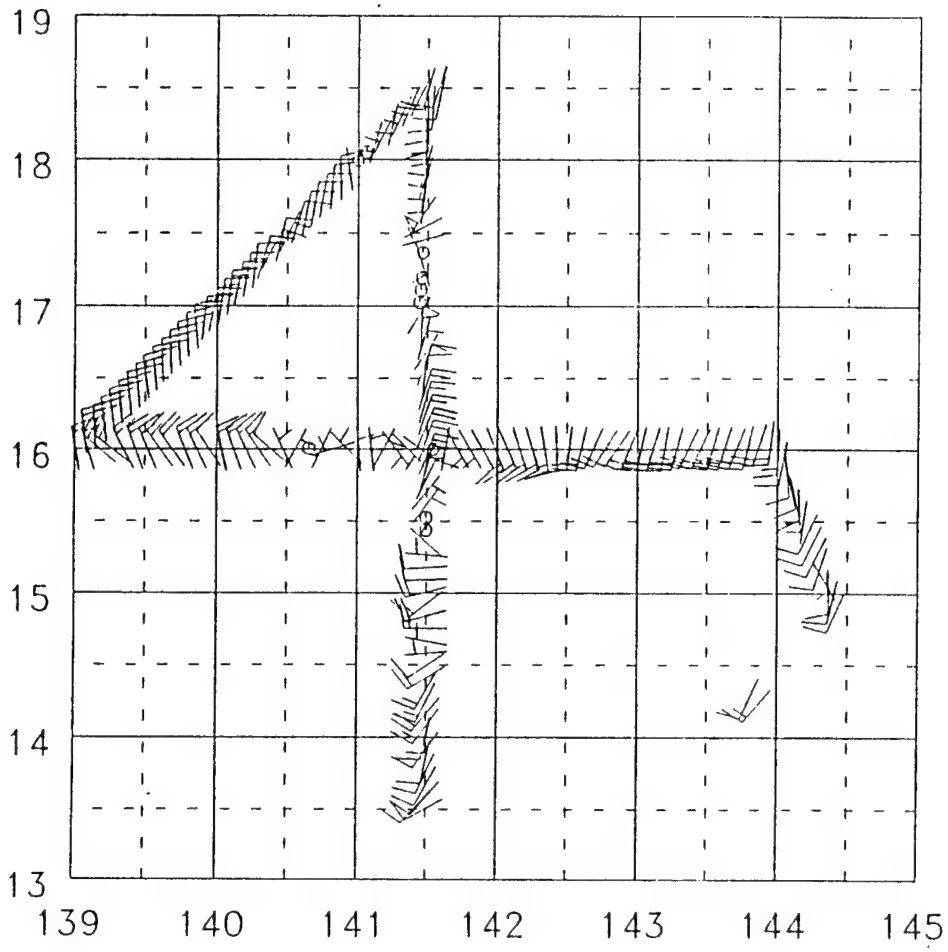


Figure 10a. Flight-level winds (knots) at 500 mb between 0325 and 0605 UTC 23 July 1993 for AOP-1A.

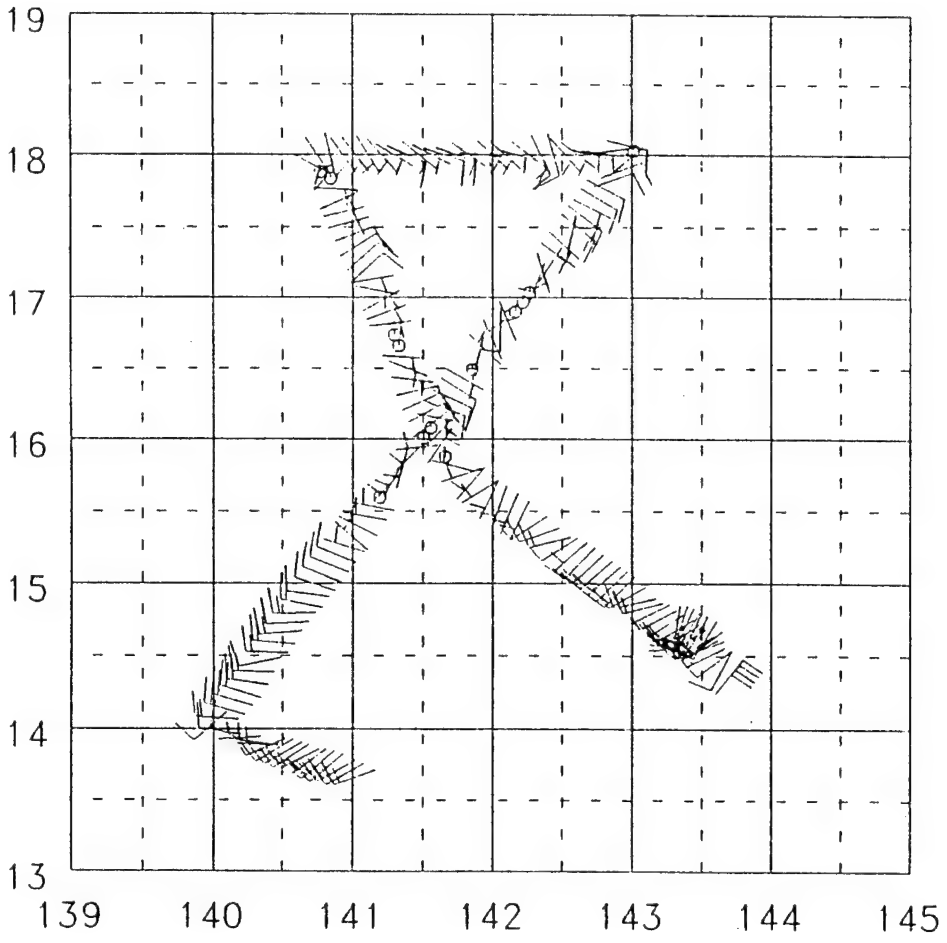


Figure 10b. Flight-level winds (knots) at 400 mb between 0630 and 0857 UTC 23 July 1993 for AOP-1A.

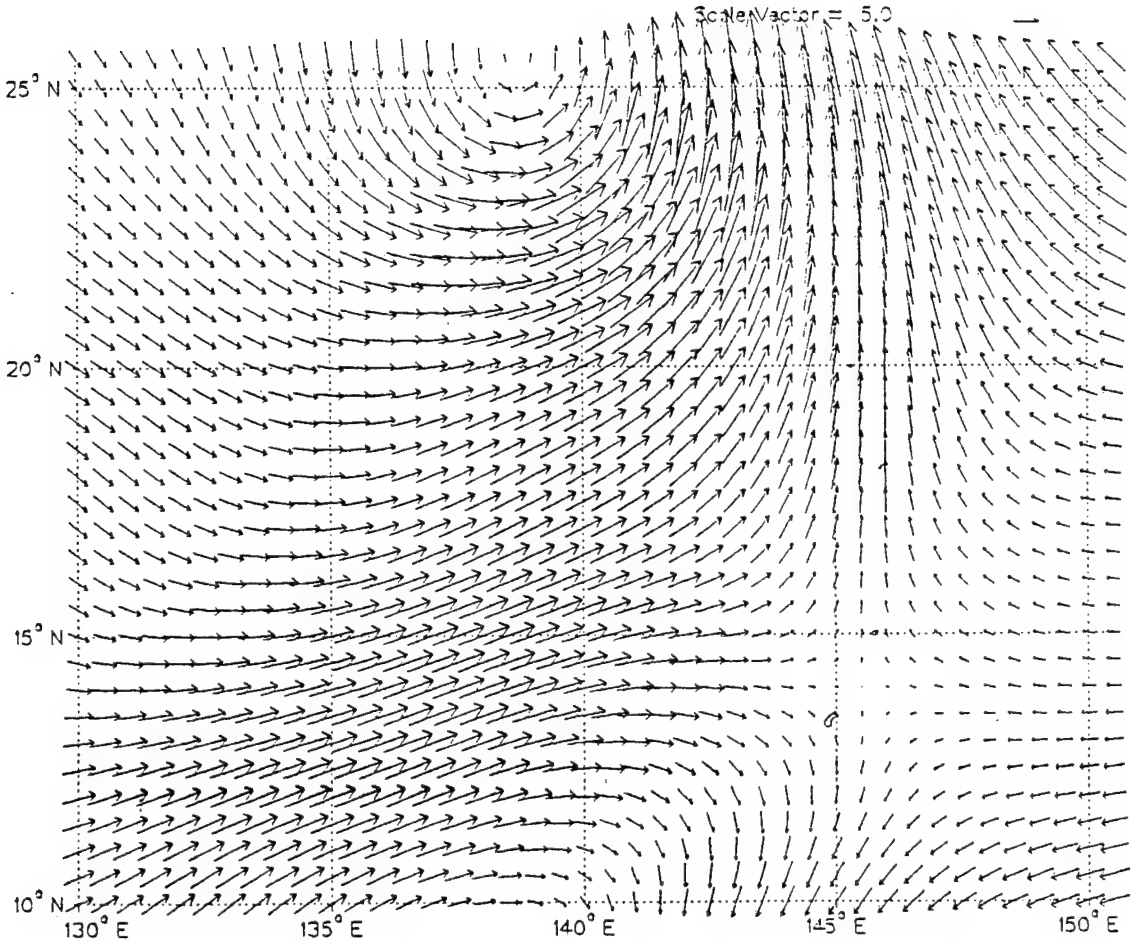


Figure 11a. NOGAPS first-guess field as in Fig. 7a, except at 650 mb.

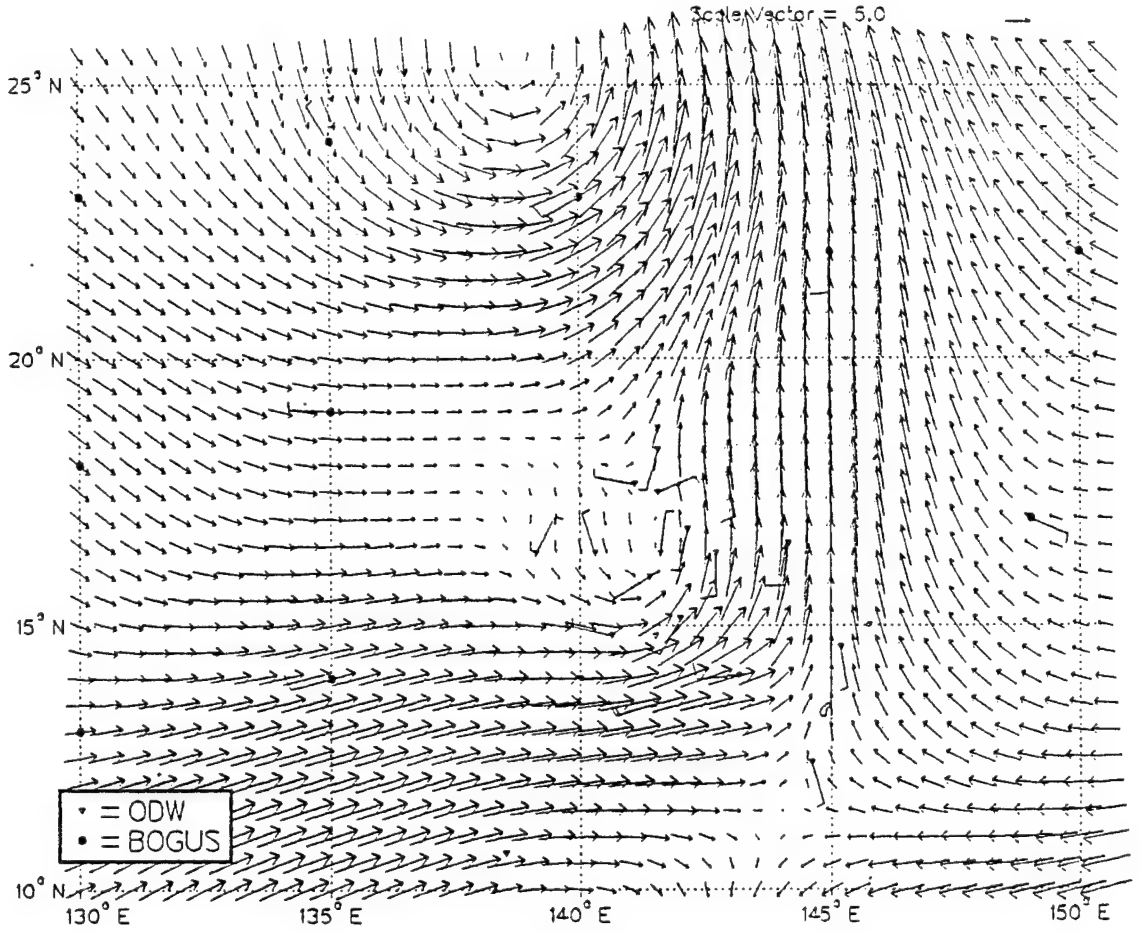


Figure 11b. Multiquadric analysis as in Fig. 7b, except at 650 mb on 0600 UTC 23 July 1993.

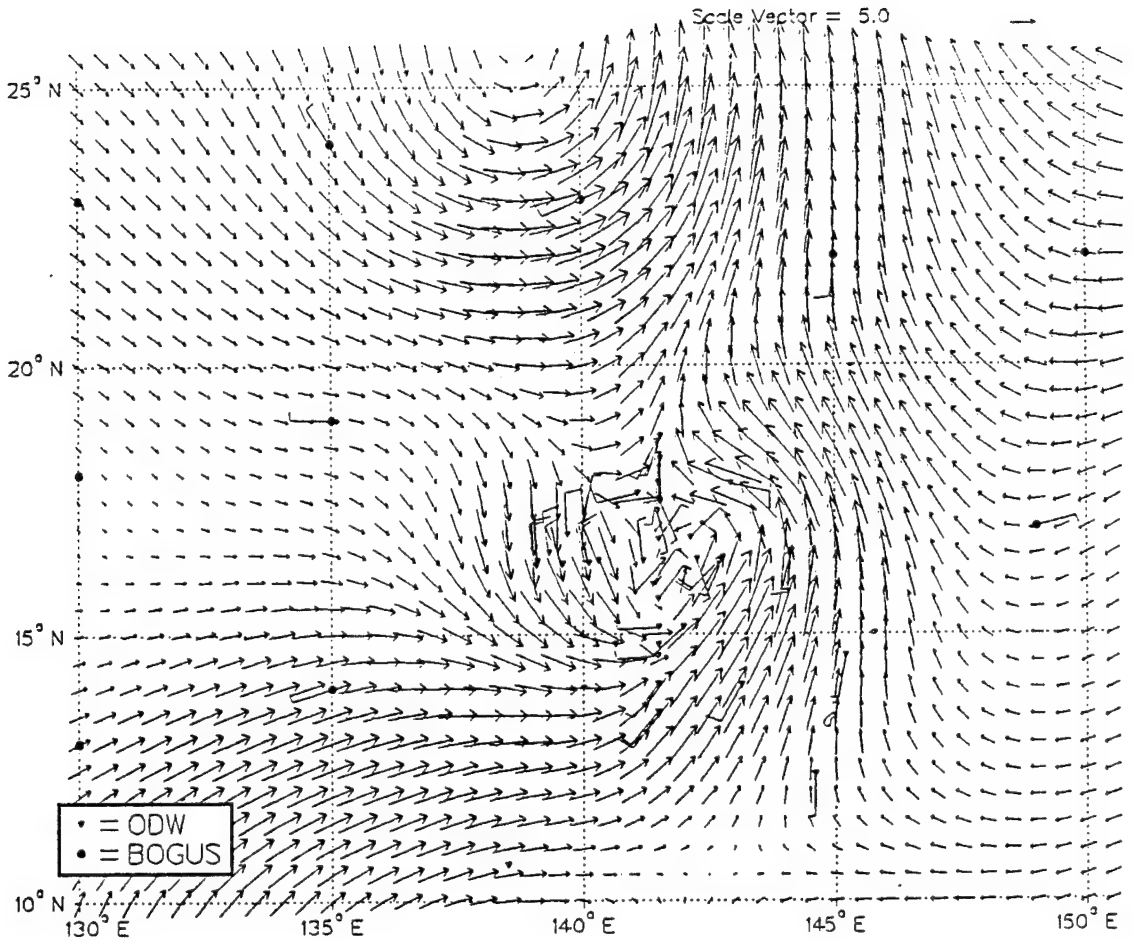


Figure 12. Multiquadric analysis as in Fig. 7b, except at 500 mb on 0600 UTC 23 July 1993.

500 mb could not be obtained due to the limited number of ODW and flight-level winds above 500 mb. Changes between the NOGAPS first-guess field and the multiquadric analyses above 400 mb can be attributed to the island station rawinsonde soundings (Table 3) that help define the vertical structure in the region.

The 500 mb mesoscale cyclonic circulation depicted by the multiquadric analysis that includes the flight-level winds (Fig. 12) is centered at approximately 16°N, 141°E. This places the mesoscale circulation west of the region of persistent, deep convection defined by the rawinsonde sounding from Guam as well as ODWs 1 and 2 (locations given in Table 1 and Fig. 1). The mesoscale circulation is bounded to the north by ODWs 14 and 15. The southern extent of the mesoscale circulation is north of ODWs 9 and 12 and south of ODWs 3 and 4. The horizontal diameter of the southwest-to-northeast oriented mesoscale circulation is thus approximately 390 km.

Potential vorticity as defined by Hoskins et al. (1985) for an isobaric coordinate version of Ertel's theorem for adiabatic, frictionless motion is

$$P = -g(f\mathbf{k} + \nabla_p \times \mathbf{v}) \cdot \nabla_p \theta ,$$

where $P$ is the potential vorticity, $g$ is the gravitational constant, $f$ is the Coriolis parameter, $\mathbf{v}$ is the horizontal wind vector, $\mathbf{k}$ is a unit vertical vector, $\nabla_p$ is the gradient operator on a pressure surface, and $\theta$ is the potential temperature. For a value of $f$ near $10^{-4}$ $s^{-1}$, a convenient unit of $10^{-6}$ $m^2$ $s^{-1}$ K $kg^{-1}$ corresponds approximately to a 10 K change in $\theta$ per 100 mb, and is called the potential vorticity unit. Whereas tropospheric values are typically of the order of 1-2 units, values in the stratosphere are at least an order of magnitude larger (Hoskins et al. 1985). The values of potential vorticity used in this study were calculated from the multiquadric analyses of the winds and the potential temperature.

A vertical cross-section of potential vorticity centered on 16°N, 141°E (Fig. 13) verifies the presence of a mid-level mesoscale vortex between approximately 700 mb and up to at least 400 mb. The diameter of the mid-level vortex in Fig. 13 is approximately 460 km. The major contribution to the positive potential vorticity center is the increase of relative vorticity attributed to mid-level convergence and the associated mid-level vertical stretching of the mesoscale vortex. That is, the static

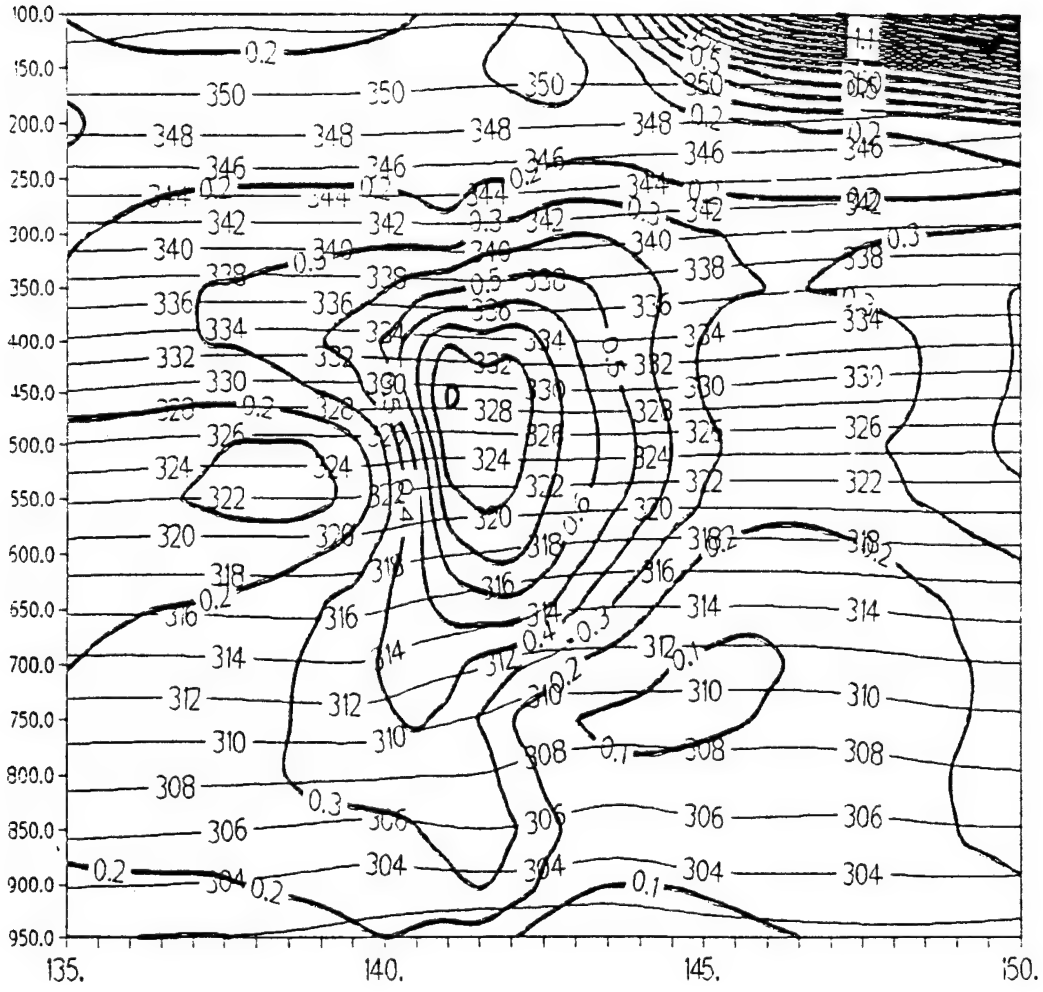


Figure 13. East-west vertical (pressures in mb) cross-section of potential vorticity (units of $10^{-6}$ $m^2$ K $s^{-1}$ $kg^{-1}$) along 16°N at 0600 UTC 23 July 1993.

stability contribution to potential vorticity was small over this region. The analysis of the cyclonic circulation above 400 mb is less certain due to the lack of ODW or flight-level data above this level. As in the TEXMEX case (Emanuel 1993), the vortex did not penetrate to the surface, so that this mesoscale circulation system could not tap into the ocean heat and moisture source via surface fluxes.

Thermodynamic aspects of the MCS structure were derived from the individual ODWs (see the times and the locations in Table 1). The dry mid-level ODW soundings in the vicinity of the mesoscale vortex circulation correlate well with the clear area near 17° N, 142°E in the 0531 UTC 23 July 1993 GMS visible satellite image (Fig. 14). This clear area is attributed to a strong region of subsidence due to the proximity of TY Nathan to the north, the strong MCS to the south, and regions of less intense convection to the east and west. ODWs 3 and 4 (Fig. 15a, b) near the center of the mid-tropospheric vortex circulation indicate that warm, dry layers exist between 550-900 mb and 600-825 mb respectively. The different elevations of the dry layers in the soundings indicate that the mid-level circulation may have had a slight upward tilt from west-to-east due to the strong convection and uplifting east of the mesoscale circulation. The ODW 8 (Fig. 16a) and ODW 16 (Fig. 16b) soundings, which were dropped near the location of ODW 3 after a delay of approximately 1.5 h and 4.5 h respectively, seem to indicate considerable moistening of the dry layer that appears in ODW 3. In addition to the time delay (Table 1), some of this change may be due to a slight misplacement when the soundings are plotted in the storm-relative coordinate system. ODWs 9 and 12 (not shown) are saturated above 650 mb and 775 mb respectively, and have deep dry layers below these levels to near the surface. Although ODWs 9 and 12 are located in the large-scale southwesterly flow associated with the monsoon gyre, the dry layers are attributed to the strong subsidence beneath the stratiform precipitation area of the MCS that had maximum amplitude prior to AOP-1A.

Some of the problems with the ODW soundings made analysis of the mesoscale vertical and horizontal structure difficult. In the north-to-south leg of the alpha flight pattern (Fig. 1), ODW 6 failed at 868 mb and ODW 9 had a layer of

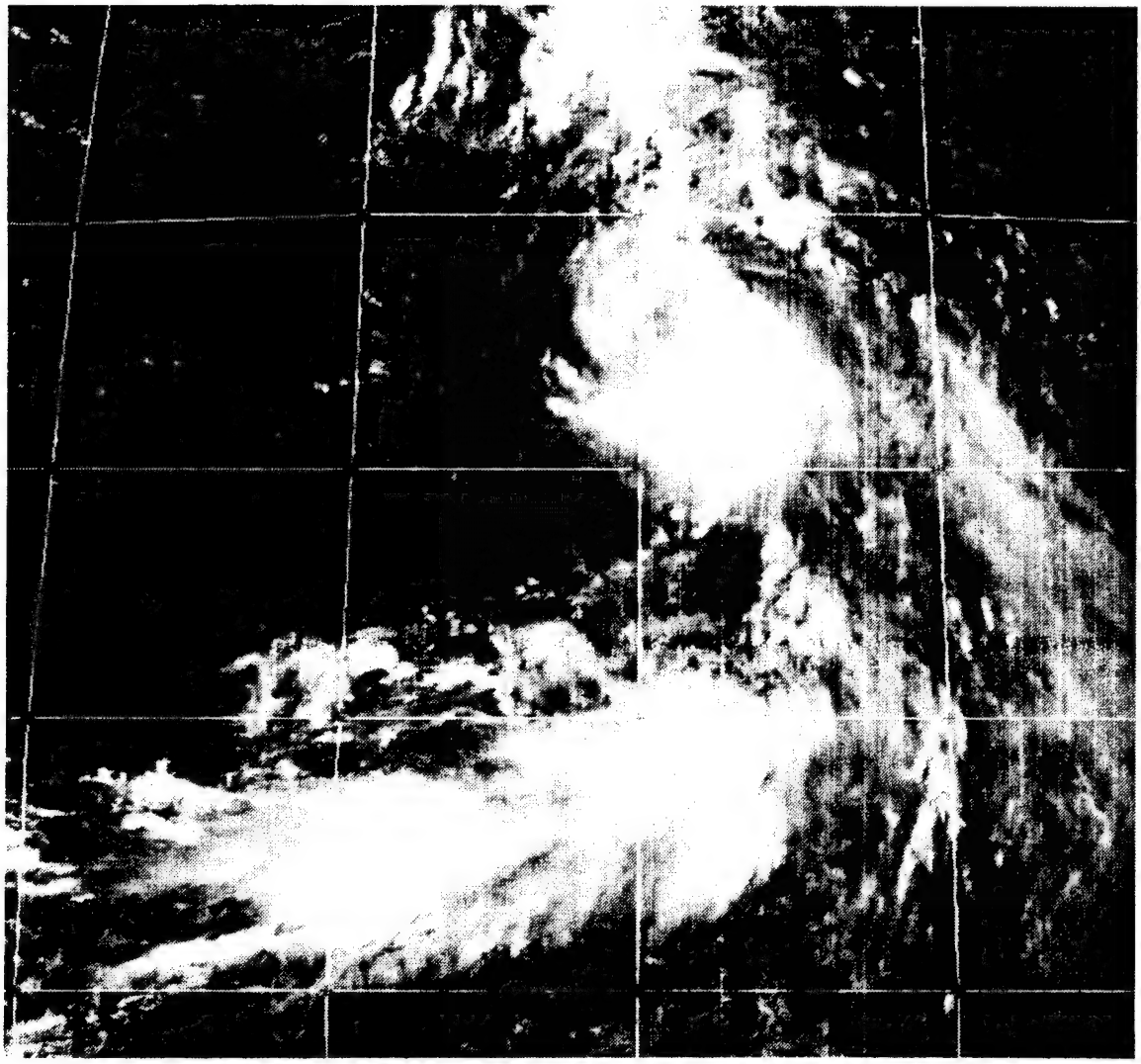

Figure 14. GMS visible satellite image at 0531 UTC 23 July 1993. The coordinate intersection near the center of the image is at 20°N, 140°E, and the intervals are 5 deg.

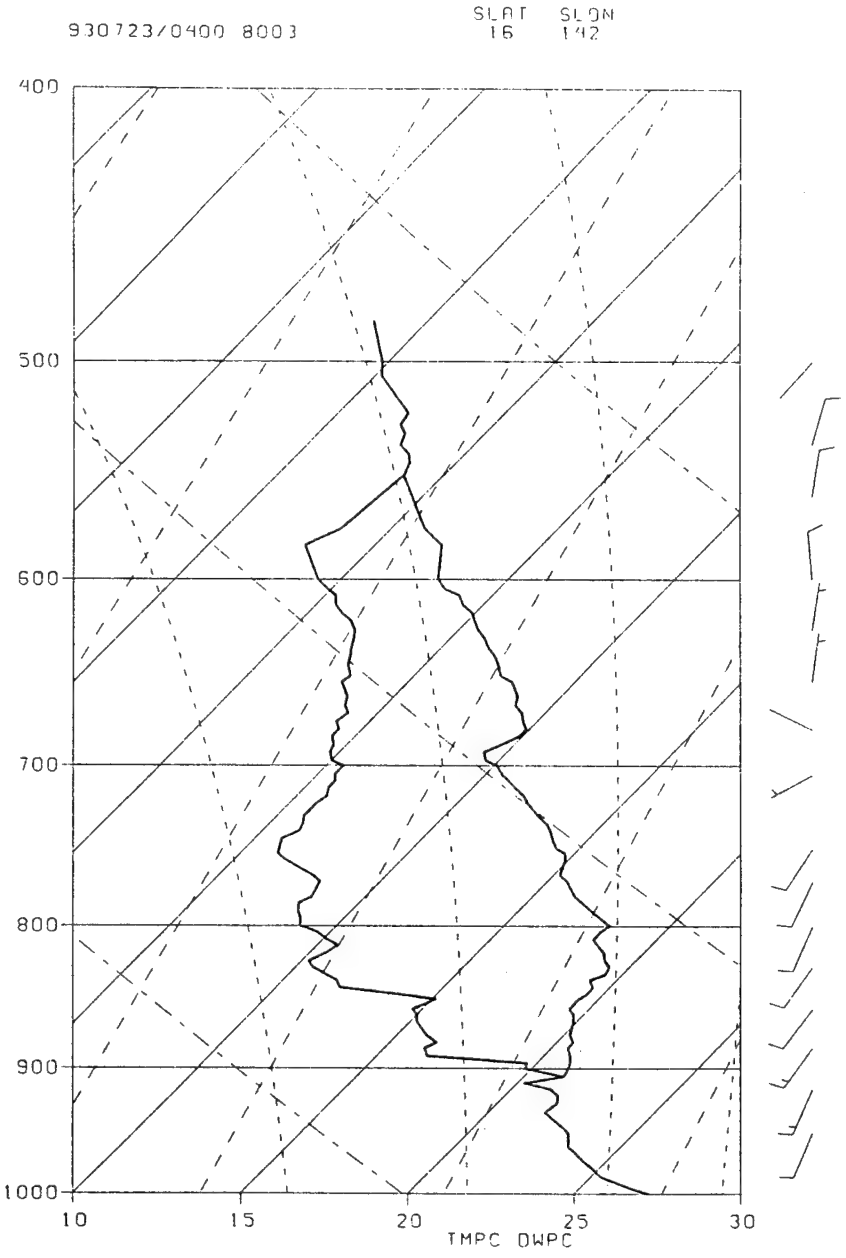


Figure 15a. ODW sounding at location 3 (see Table 1 and Fig. 1) deployed at 0354 UTC 23 July 1993. Temperatures and dew point temperatures are displayed on a skew-T-ln p diagram and wind barbs (m $s^{-1}$) are shown on the right.

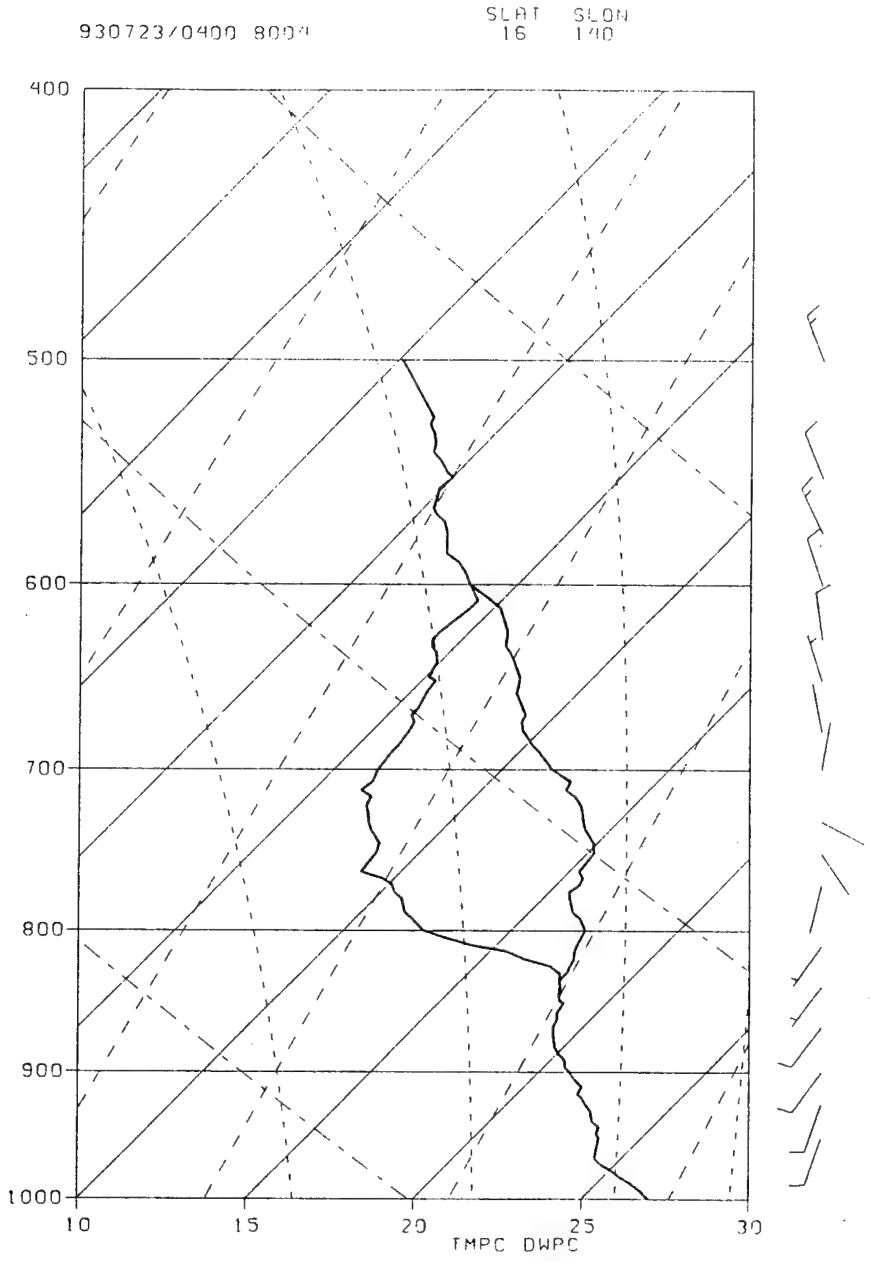


Figure 15b. ODW sounding as in Fig. 15a, except at location 4 deployed at 0409 UTC 23 July 1993.

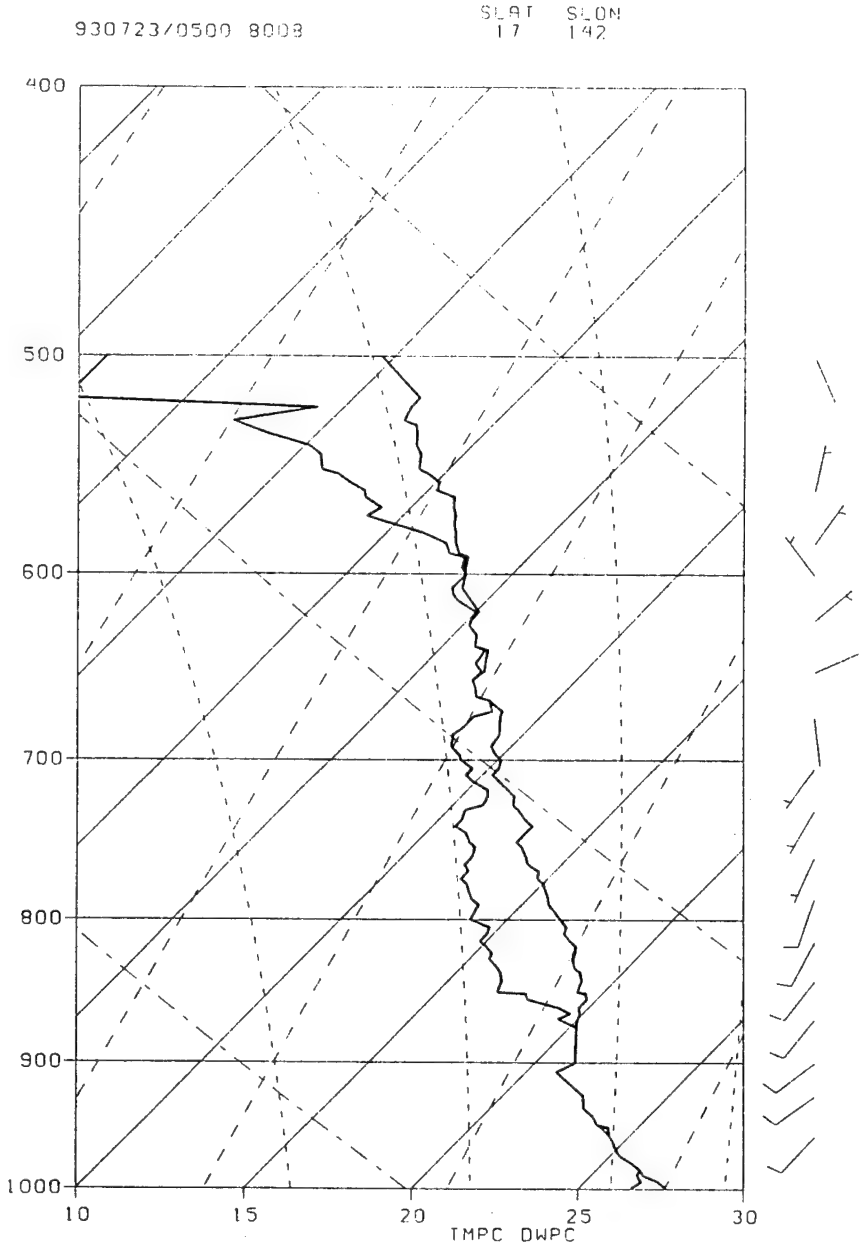


Figure 16a. ODW 8 sounding as in Fig. 15a, except deployed at 0522 UTC 23 July 1993.

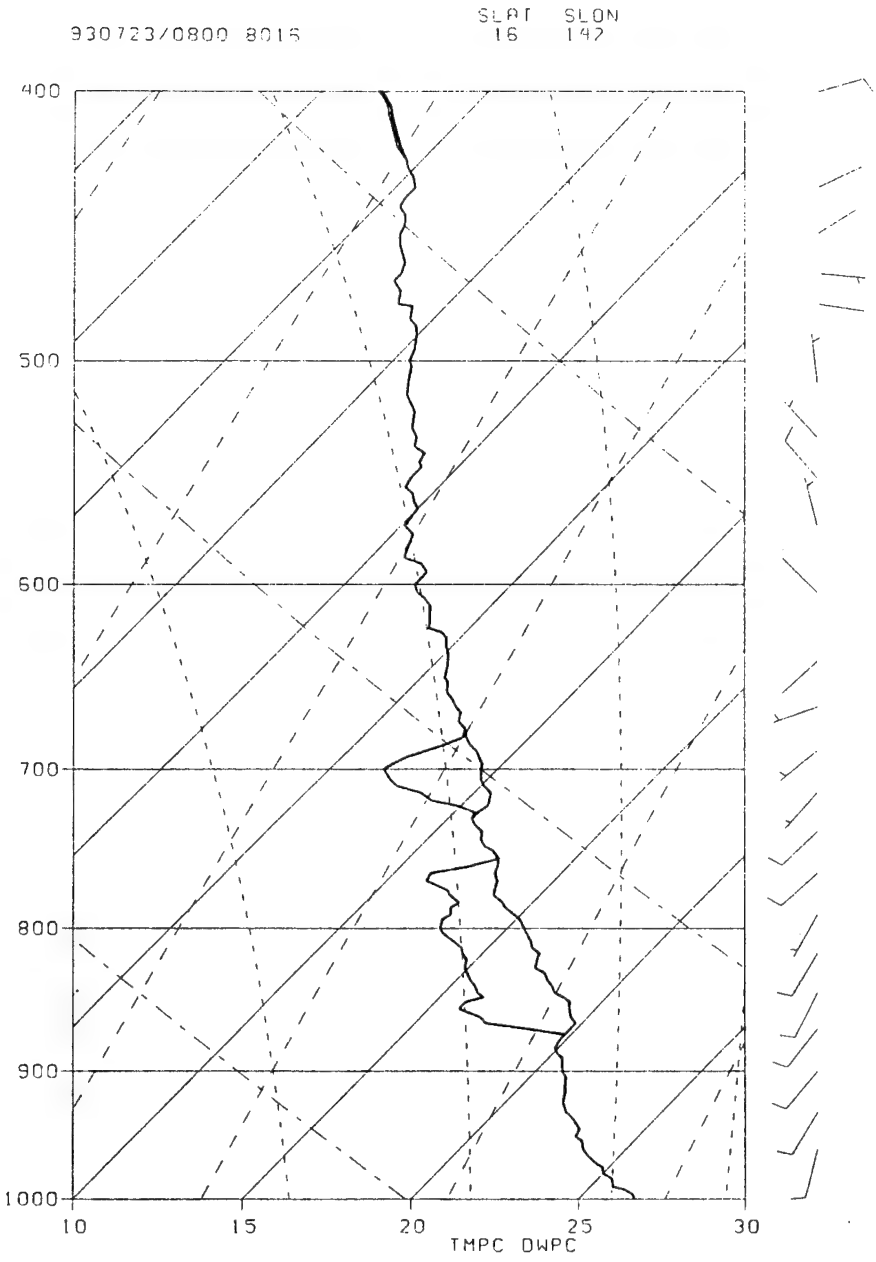


Figure 16b. ODW 16 sounding as in Fig. 15a, except deployed at 0818 UTC 23 July 1993.

easterly winds above 650 mb that were excluded from the multiquadric analysis (see Appendix). Some of the differences in the vertical soundings in the areas of deep convection may be associated with diurnal effects or with mesoscale phenomena that exist on scales not resolvable by the ODW spacing in the alpha flight pattern.

In summary, the significant deep convection that was present at the beginning of AOP-1A dissipated toward the end of AOP-1A due to diurnal effects. The ODWs deployed by the WC-130 during AOP-1A provide critical information concerning the three-dimensional structure of the MCS. Utilizing the ODW soundings, the multiquadric interpolation technique with the operational NOGAPS analysis as a first-guess field introduces mesoscale phenomena in the region of the alpha flight pattern that depict the existence of a mid-tropospheric mesoscale cyclonic circulation. This mid-level mesoscale vortex, which extends between approximately 700 mb and up to at least 400 mb, is west of the region of persistent, deep convection. The horizontal diameter of the mid-level mesoscale cyclonic circulation as determined from the multiquadric analyses and a cross-section of potential vorticity is approximately 460 km. ODW soundings taken near the center of the mid-level mesoscale cyclonic circulation have deep dry layers below the mid-level vortex. The different elevations of the dry layers indicate that the mid-level circulation may have had a slight upward tilt from west-to-east due to the strong convection and uplifting east of the mesoscale circulation. Thus, the AOP-1A observations indicate a mid-tropospheric cyclonic vortex as has been documented in the midlatitude MCSs and in some tropical MCSs. Subsequent observations in this region and the relationship to the development of TS Ofelia will be discussed in the following sections.

## C. AIRCRAFT OBSERVING PERIOD AOP-1B

The objective of AOP-1B was to determine whether the mid-level mesoscale cyclonic circulation that was detected during AOP-1A persisted between AOP-1A and AOP-1B. Based on the location of the mid-level mesoscale cyclonic circulation center relative to the satellite imagery on the previous day, the alpha flight pattern for AOP-1B had been centered at 17°N, 141°E on a persistent area of convection within the

main confluent monsoon flow south of TY Nathan. The structure of the MCS will be derived from the ODW soundings deployed by the 815th Weather Squadron WC-130. The analyses from NOGAPS and rawinsonde soundings from Guam, Palau, Chuuk, Pohnpei, and Yap (Table 3) will be used to provide the larger scale environment of the detailed observations in the TCM-93 region.

The GMS satellite imagery and the rawinsonde soundings from the island stations indicate that the entire system of TUTT cell, subtropical ridge, and monsoon gyre have moved westward between the end of AOP-1A and the beginning of AOP-1B. Two hours prior to the commencement of AOP-1B, the rawinsonde soundings (not shown) from Palau and Yap (station locations are given in Table 3) are moist with southwesterly winds from 5 to 10 m $s^{-1}$ in the low- to mid-troposphere attributed to flow around the monsoon gyre. The depth of the southwesterlies extends from the surface to 600 mb at Palau and from the surface to 500 mb at Yap. The Guam rawinsonde indicates a moist sounding with southerly winds of 10 m $s^{-1}$ from the surface to approximately 500 mb attributed to the flow around the eastern edge of the monsoon gyre. The Pohnpei sounding indicates easterly flow from the surface to approximately 500 mb. No sounding was available from Chuuk. Below 500 mb, the meeting of the easterly flow and the monsoon southwesterly flow west of Guam and east of Yap defines the region of confluence and the southerly winds. Based on these soundings and the satellite imagery, the easterly flow is continuing to undercut the southwesterly flow associated with the monsoon gyre, which presumably provides the lifting of the moist monsoon westerlies and results in persistent convection in the formation area. In the Guam sounding, winds above 400 mb are from the north-northwest associated with the flow around the TUTT cell system.

Introducing the ODW data at 850 mb from the alpha flight pattern in Fig. 2 into the NOGAPS first-guess field at 850 mb (Fig. 17a) with the multiquadric interpolation technique (Fig. 17b) results in noticeable differences in the large-scale flow. The NOGAPS first-guess field at 850 mb depicts southwesterly flow throughout the AOP-1B observing area with a region of north-oriented confluent flow near 19°N, 144°E. The multiquadric analyses at 850 mb (Fig. 17b) depicts a region of north-

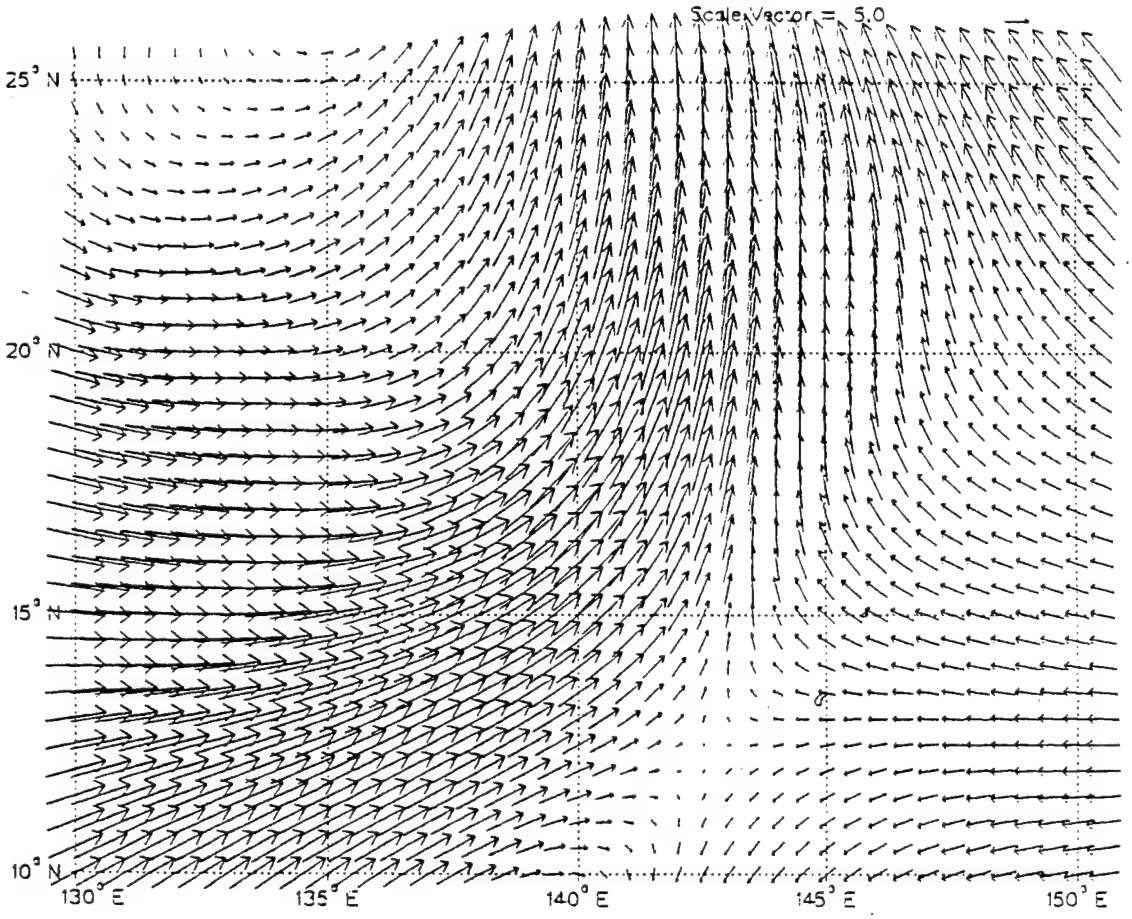


Figure 17a. NOGAPS first-guess field at 850 mb at 0800 UTC 24 July 1993. See scale of wind arrows in m $s^{-1}$ in upper right.

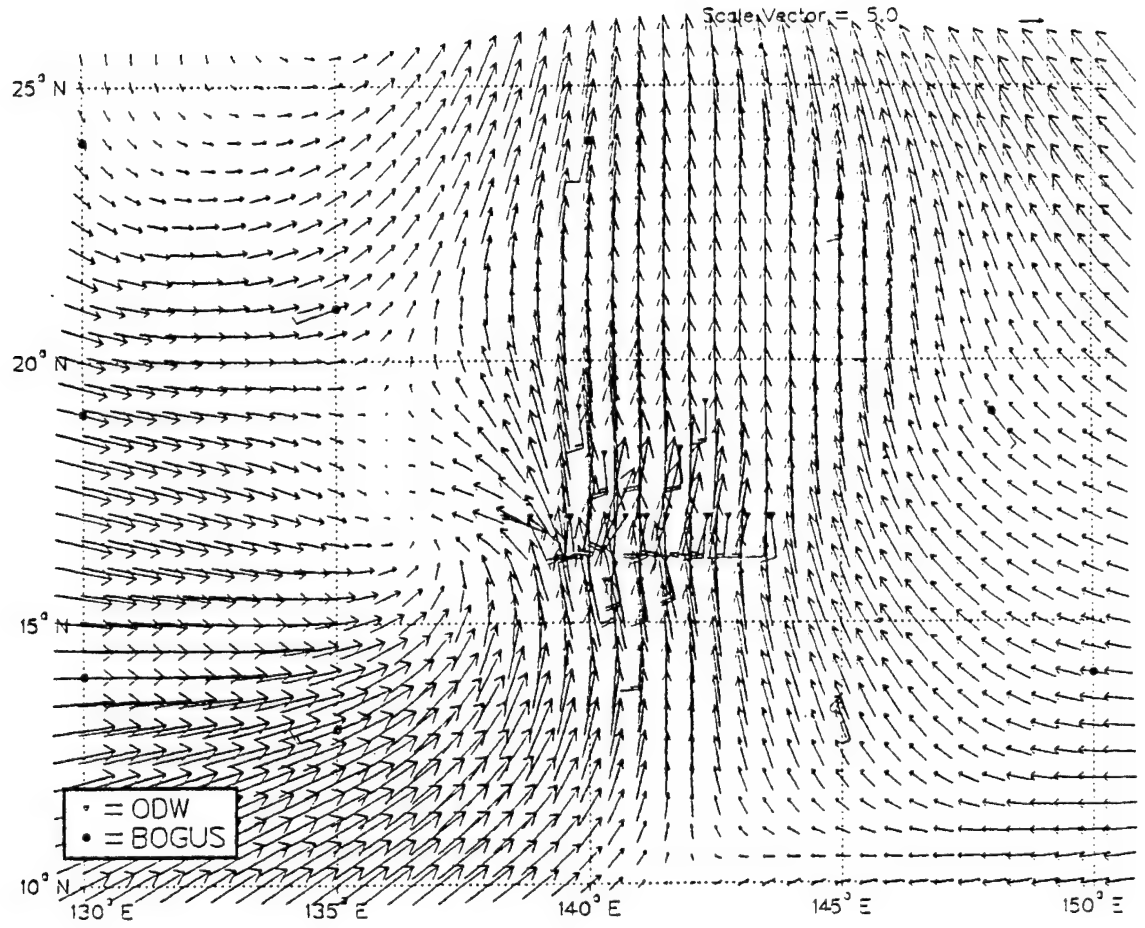


Figure 17b. Multiquadric analysis of 850 mb winds at 0800 UTC 24 July 1993. The TCM-93 observations and zero synthetic wind observations in the data-sparse areas are indicated by the larger wind barbs. See scale of wind arrows in m $s^{-1}$ in upper right.

oriented confluent flow near 17°N, 141°E. The difference between the positioning of the north-oriented confluent flow in the NOGAPS first-guess field at 850 mb and the multiquadric analysis at 850 mb can be attributed to the 0000 UTC 24 July 1993 rawinsonde soundings (not shown) from Guam and Yap as well as soundings from ODWs 2, 3, 4, 5, 8, 9, 10, and 11 (see locations in Fig. 2) that depict low-level southerly flow. The multiquadric analysis at 850 mb also depicts southeasterly flow to the west-northwest of the north-oriented confluent flow that can be attributed to the flow around the monsoon gyre. The col that was centered near 13°N, 143°E in the NOGAPS first-guess field at 850 mb was moved southward in the multiquadric analysis at 850 mb.

As in AOP-1A, the deep convection associated with the diurnal convective maximum observed in the enhanced IR satellite imagery at the beginning of AOP-1B (Fig. 18) dissipated toward the end of AOP-1B (Fig. 19) due to the diurnal convective minimum. A satellite nephanalysis (Fig. 20) depicts the dissipation of the deep convection in two-hour intervals throughout AOP-1B.

The flight-level winds in AOP-1B (Figs. 21a, b, c) provided some evidence of two mid-level mesoscale cyclonic circulations that were not detected in the NOGAPS first-guess field or the satellite imagery. Whereas the center of the alpha flight pattern coincided with the center of the mid-level mesoscale cyclonic circulation defined by the flight-level winds in AOP-1A, the positions of the two mesoscale circulations were not as clearly defined by the flight-level winds in AOP-1B. The flight-level winds near the western end of the east-to-west flight path at 850 mb (Fig. 21a) only indicate a cyclonic turning of the winds. However, the flight-level winds near the western end of the west-to-east flight path at 700 mb (Fig. 21b) indicate the existence of a mid-level mesoscale cyclonic circulation in the vicinity of ODW 1 and ODW 2 (see Fig. 2) for AOP-1B. The flight-level winds at 500 mb (Fig. 21c) indicate the existence of a separate mid-level mesoscale cyclonic circulation in the vicinity of ODW 14 and ODW 15 near the northwestern corner of the alpha flight pattern for AOP-1B. Whereas the mesoscale circulation detected by the 850 mb and the 700 mb flight-level winds appears to be located on the cyclonic shear side of the monsoon gyre, the

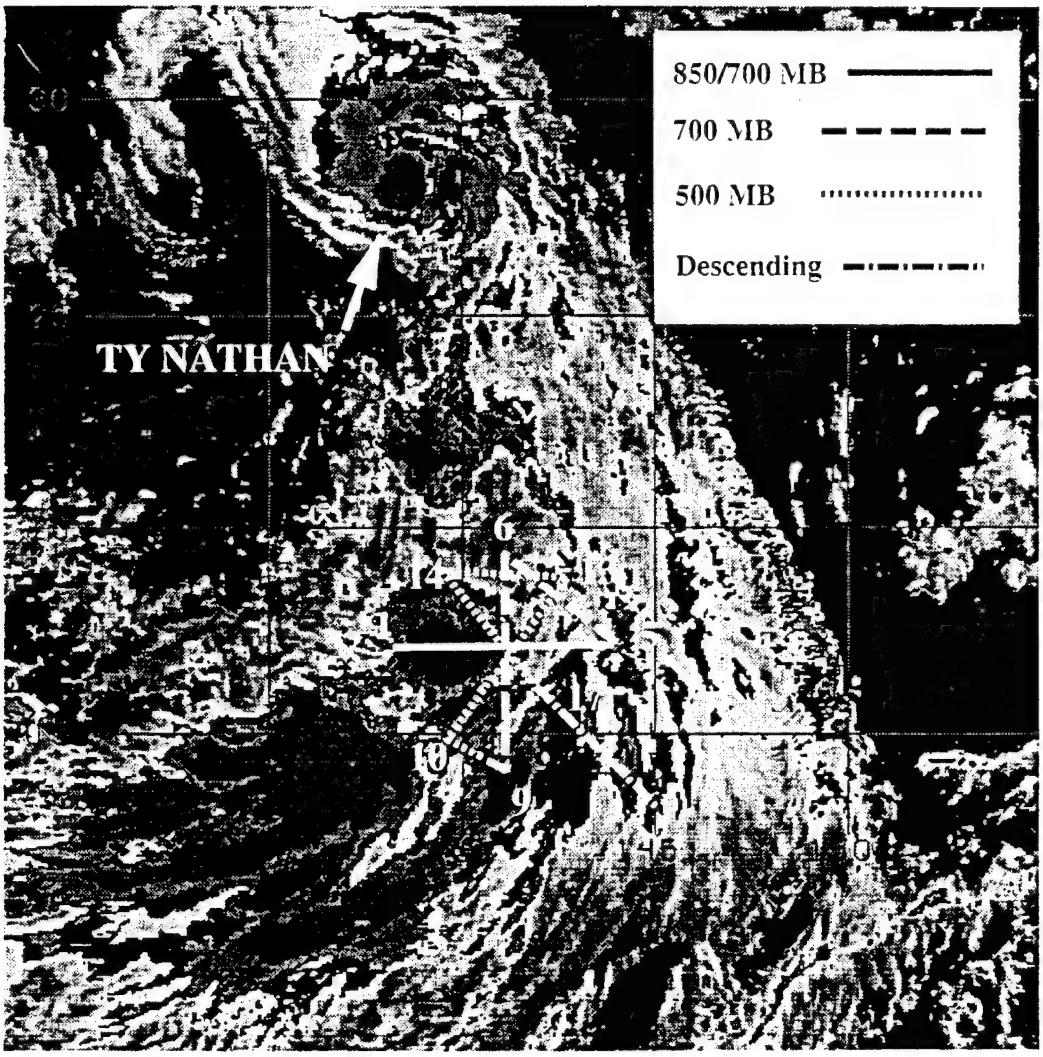


Figure 18. Infrared satellite image as in Fig. 6, except at 0130 UTC 24 July 1993 at the beginning of AOP-1B.

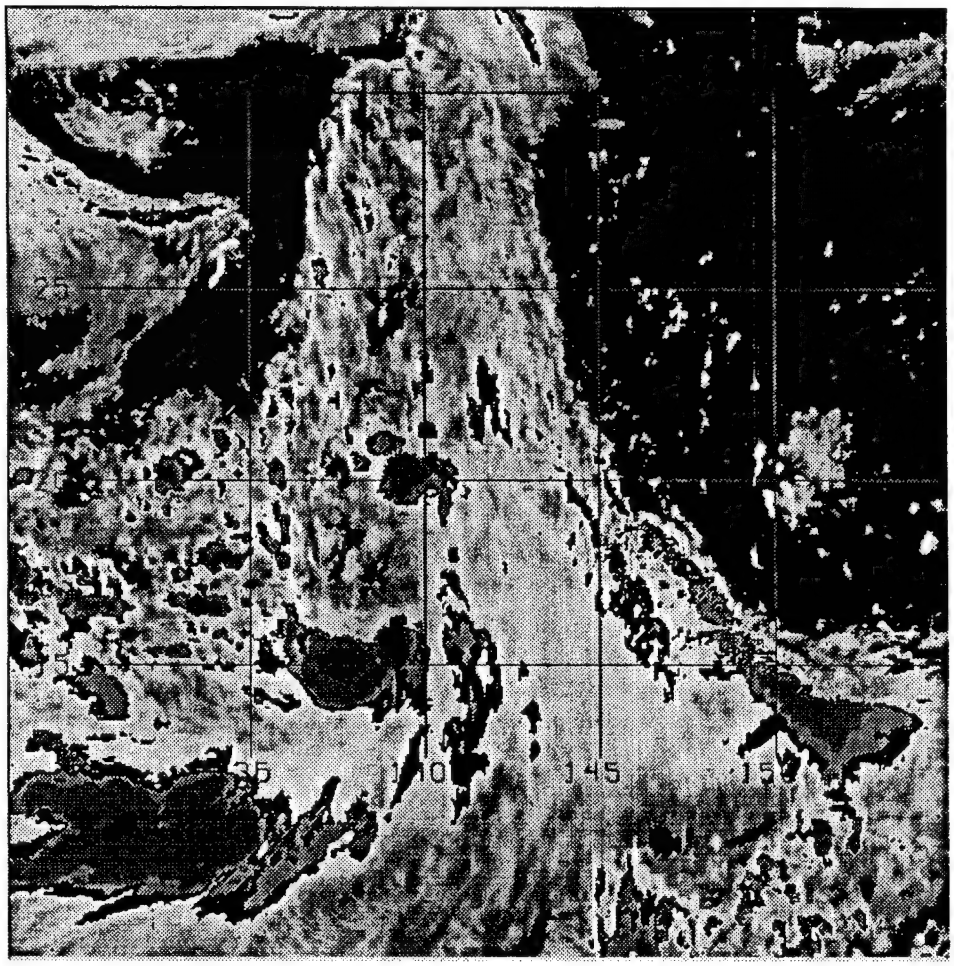


Figure 19. Infrared satellite image as in Fig. 6, except at 1130 UTC 24 July 1993 near the end of AOP-1B.


Figure 20. Satellite nephanalysis as in Fig. 9 except for AOP-1B on 24 July 1993. Times of each nephanalysis for AOP-1B are: a) 0130 UTC; b) 0330 UTC; c) 0530 UTC; d) 0730 UTC; e) 0930 UTC; and f) 1130 UTC, which illustrate the evolution of the cloud patterns between Figs. 18 and 19. The portions of the flight path and ODW positions (see complete pattern in Fig. 18) during the intervals between satellite images are indicated by the dotted lines and the numbers respectively.

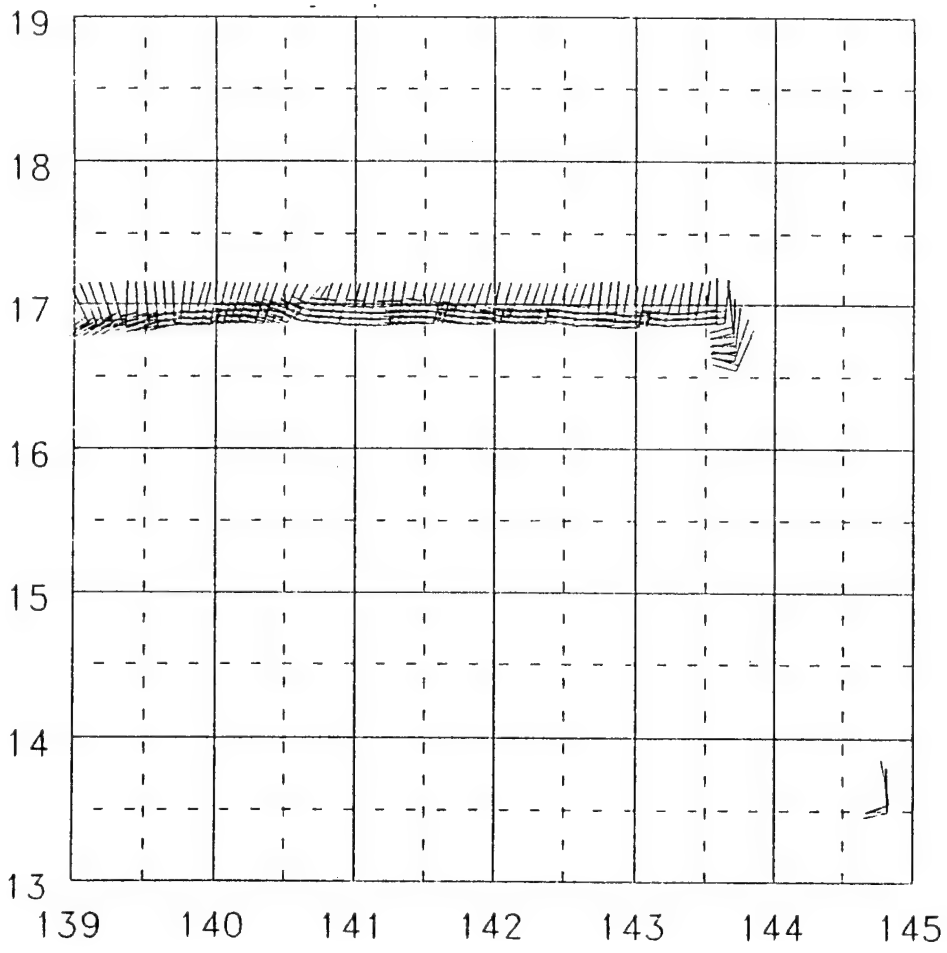


Figure 21a. Flight-level winds (knots) at 850 mb between 0225 and 0425 UTC 24 July 1993 for AOP-1B. The complete flight track is in Fig. 2. The winds in the lower right are observations as the WC-130 ascended through 850 mb after takeoff from Guam.

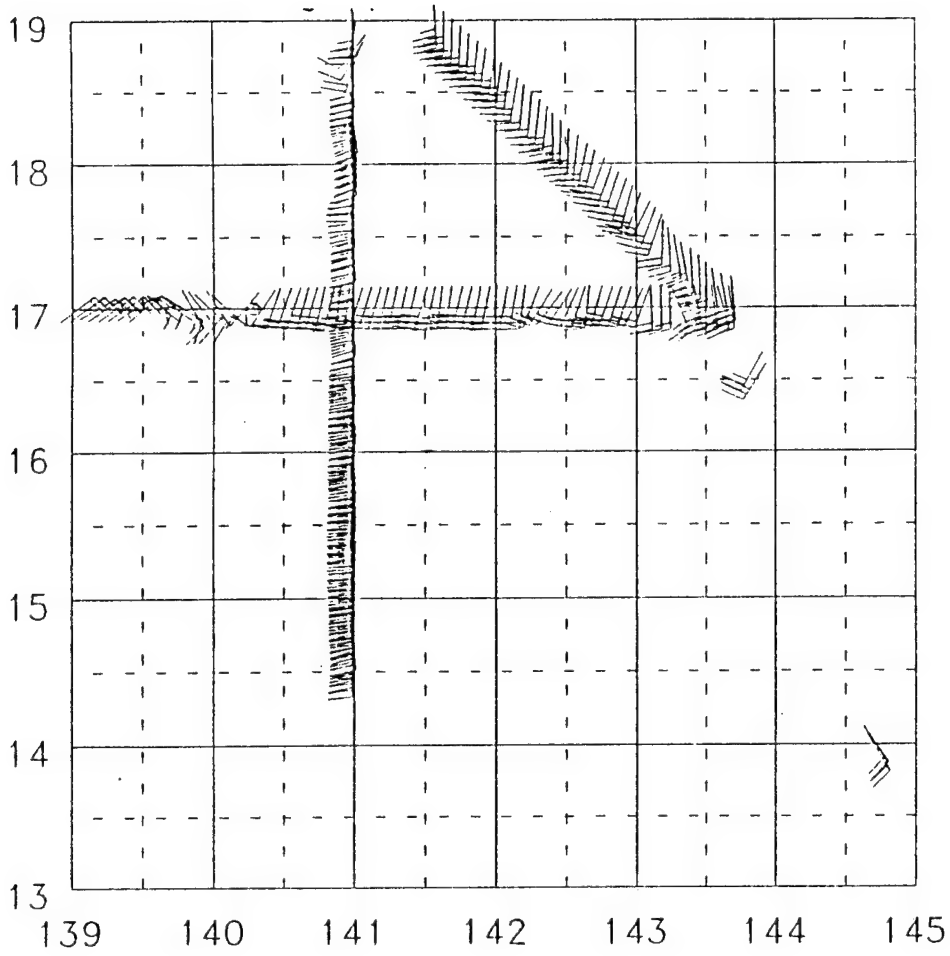


Figure 21b. Flight-level winds (knots) at 700 mb between 0442 and 0822 UTC 24 July 1993 for AOP-1B. The winds in the lower right are observations as the WC-130 ascended through 700 mb after takeoff from Guam.

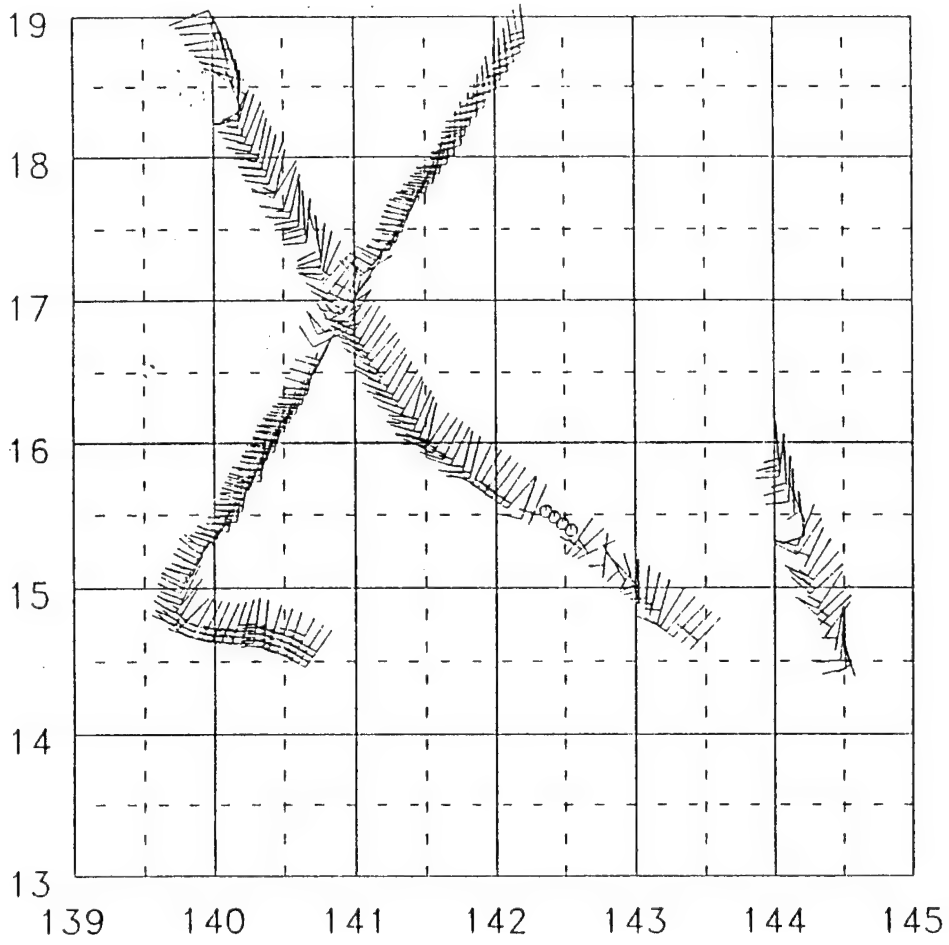


Figure 21c. Flight-level winds (knots) at 500 mb between 0842 and 1118 UTC 24 July 1993 for AOP-1B.

mesoscale circulation detected by the 500 mb flight-level winds appears to be located in the cyclonic shear on the northern edge of the monsoon gyre.

Although the multiquadric analysis at 850 mb (Fig. 17b) indicates a cyclonic circulation centered near 17°N, 136°E, it is difficult to determine whether the cyclonic circulation is attributed to the monsoon gyre or the mid-level mesoscale cyclonic circulation detected by the 850 mb flight-level winds in Fig. 21a. No indication of the northern mid-level mesoscale cyclonic circulation is found in the multiquadric analysis at 850 mb. Since ODW soundings 14 and 15 provided 850 mb winds in that region, the absence of the northern mesoscale cyclonic circulation at 850 mb must mean that this circulation was confined to the mid-troposphere, which may indicate that it was recently generated. The multiquadric analysis at 700 mb (Fig. 22) depicts a mid-level mesoscale cyclonic circulation centered near 16°N, 138°E, and a weaker cyclonic circulation near 18°N, 139°E. Due to the limited ODW data in the vicinity of the two mesoscale circulations, only the eastern quadrants of these circulations are well resolved by the multiquadric analyses at 700 mb. The key north-northeasterly wind observations between the two mesoscale circulation centers are from ODW 1 and ODW 2. The multiquadric analysis at 500 mb (Fig. 23) only indicates the existence of the northern mid-level mesoscale cyclonic circulation centered near 18°N, 139°E. The reason the 500 mb multiquadric analysis does not indicate the southern mesoscale cyclonic circulation is the absence of any ODW observations above the 700 mb flight leg in that region (see Fig. 21b and Fig. 2). Although the key ODW 1 and ODW 2 soundings (deployed from just above 700 mb) were able to resolve the western part of the southern mesoscale circulation, none of the western half is resolved even at 500 mb for the northern mesoscale circulation. As in the multiquadric analysis at 700 mb, the multiquadric analysis at 500 mb is only able to resolve the eastern half of the mesoscale cyclonic circulation.

Further details of the two mid-level mesoscale cyclonic circulations are analyzed through the use of the ODW soundings. Thermodynamic aspects of the MCS structure were derived from the individual ODWs (see the times and the locations in Table 2). The satellite nephanalysis for AOP-1B (Fig. 20) shows the

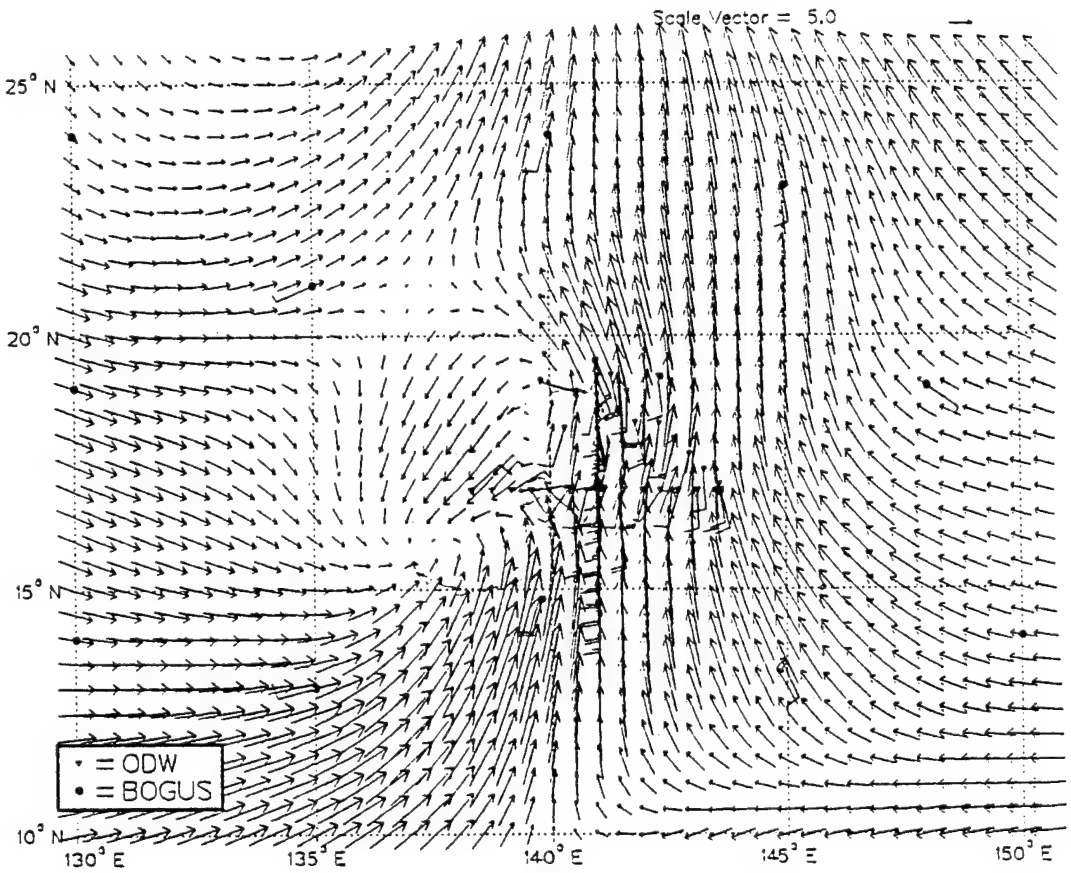


Figure 22. Multiquadric analysis as in Fig. 17b, except at 700 mb at 0800 UTC 24 July 1993.

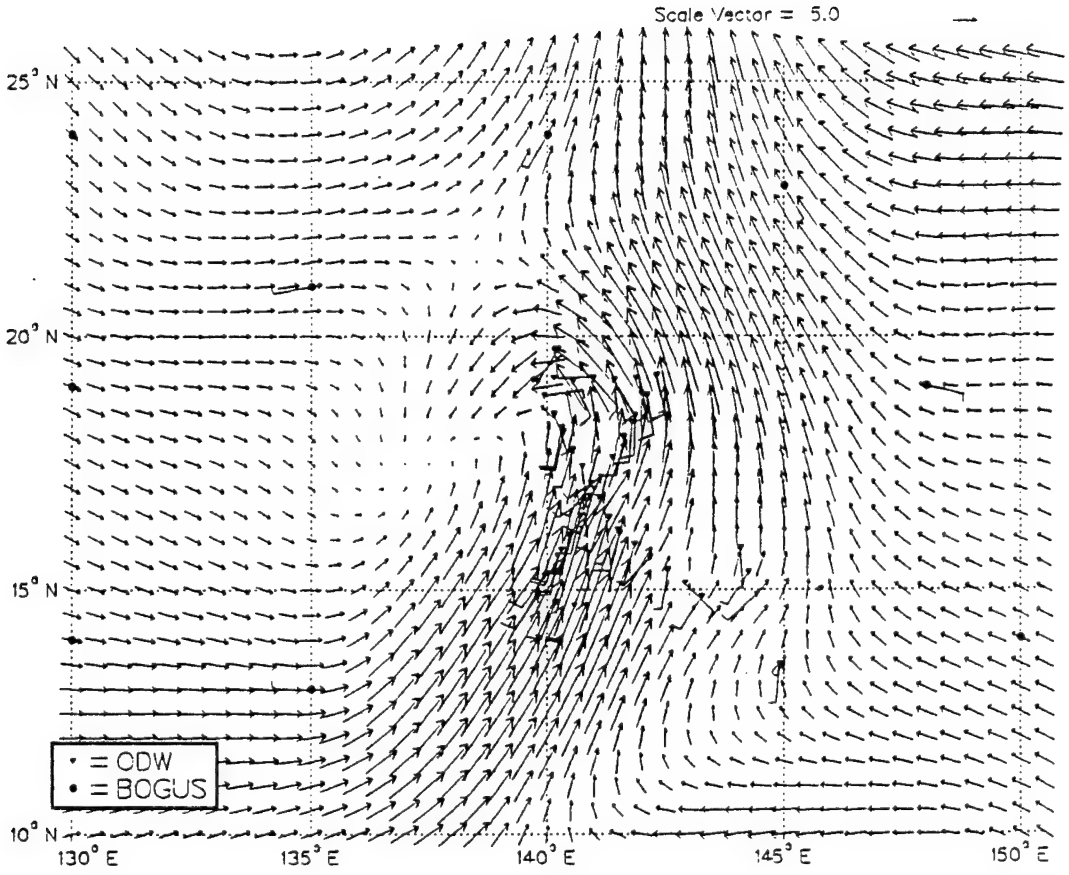


Figure 23. Multiquadric analysis as in Fig. 17b, except at 500 mb at 0800 UTC 24 July 1993.

regions of deep convection relative to the locations of the ODWs. ODW 1 and ODW 2 were deployed in the vicinity of the southern mesoscale cyclonic circulation depicted by the flight-level winds at 700 mb (Fig. 21b) and the multiquadric analysis at 700 mb (Fig. 22). The sounding from ODW 1 (Fig. 24a) has a warm, dry layer between 875-725 mb with southeasterly to easterly winds from the surface up to 700 mb. This vertical structure is similar to the soundings on the eastern edge of the mesoscale cyclonic vortex in AOP-1A. However, the ODW 2 sounding (Fig. 24b) is saturated from the surface up to 775 mb and becomes warm and dry only above 775 mb. The vertical extent of the warm, dry layer is unknown due to the lack of ODW data above 700 mb. Notice the southerly to southeasterly winds from the surface up to 700 mb, which suggest a region of confluence between the easterly flow and the monsoon southwesterly flow at the longitude of ODW 2. As in AOP-1A, the southern mesoscale cyclonic circulation appears to be located to the west of this north-oriented confluent flow.

ODW 14 and ODW 15 were deployed in the vicinity of the northern mesoscale cyclonic circulation depicted by the flight-level winds at 500 mb (Fig. 21c) and the multiquadric analysis at 500 mb (Fig. 23). ODW 14 (Fig. 25a), which was located north of the northern mesoscale cyclonic circulation, is saturated from the surface up to 500 mb. Southerly winds are found from the surface up to 725 mb, and then the wind backs from easterlies at 700 mb to northerlies at 500 mb. The saturated sounding from ODW 14 is attributed to its location in an organized convective cell (Fig. 20e) that will be discussed later in this section. The sounding from ODW 15 (Fig. 25b), which was located southeast of the northern mesoscale circulation, has a warm, dry layer from 975-810 mb with southerly winds from the surface up to 500 mb. The southerly winds are attributed to ODW 15 being located more in the north-oriented confluent flow. Although the thermodynamic structure of ODW 15 is similar to ODW 1 in the southern mesoscale circulation (Fig. 24a), the warm, dry layer in ODW 15 appears to be closer to the surface.

Vertical cross-sections of divergence and potential vorticity may provide additional information on the two mesoscale circulations. The vertical cross-section of

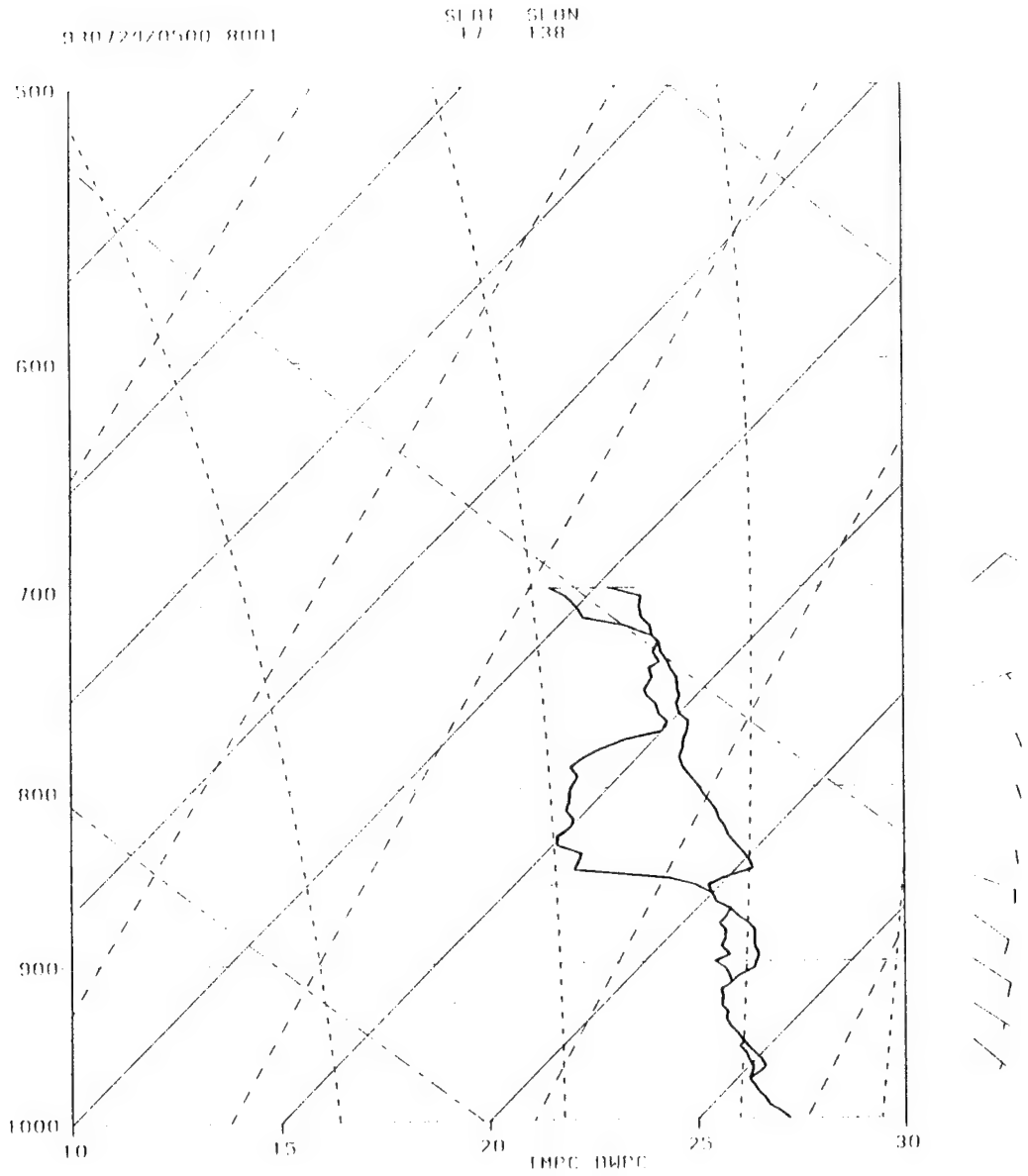


Figure 24a. ODW 1 sounding as in Fig. 15a, except deployed at 0442 UTC 24 July 1993.

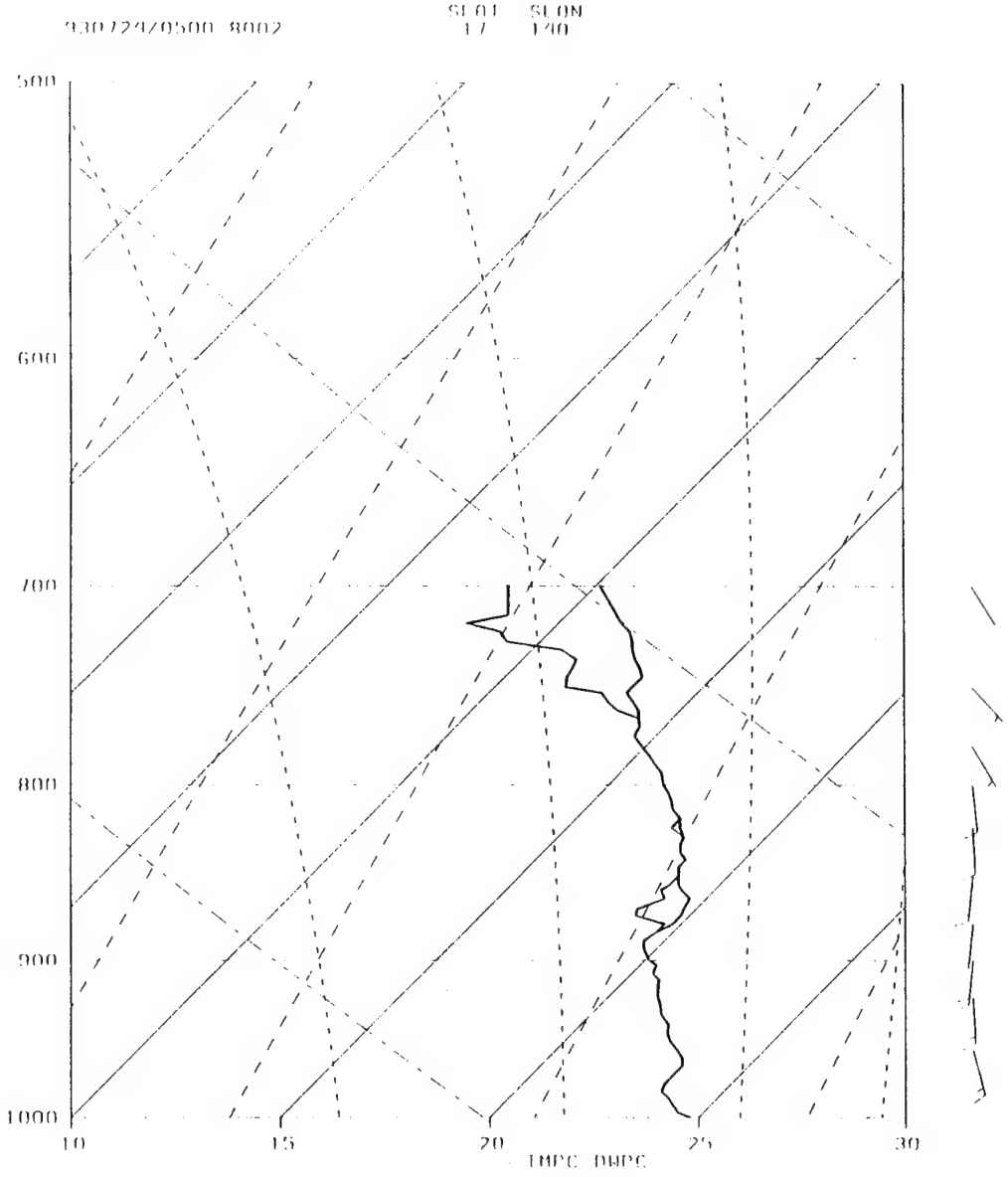


Figure 24b. ODW 2 sounding as in Fig. 15a, except deployed at 0502 UTC 24 July 1993 during AOP-1B. The complete flight track with all ODW locations is given in Fig. 2.

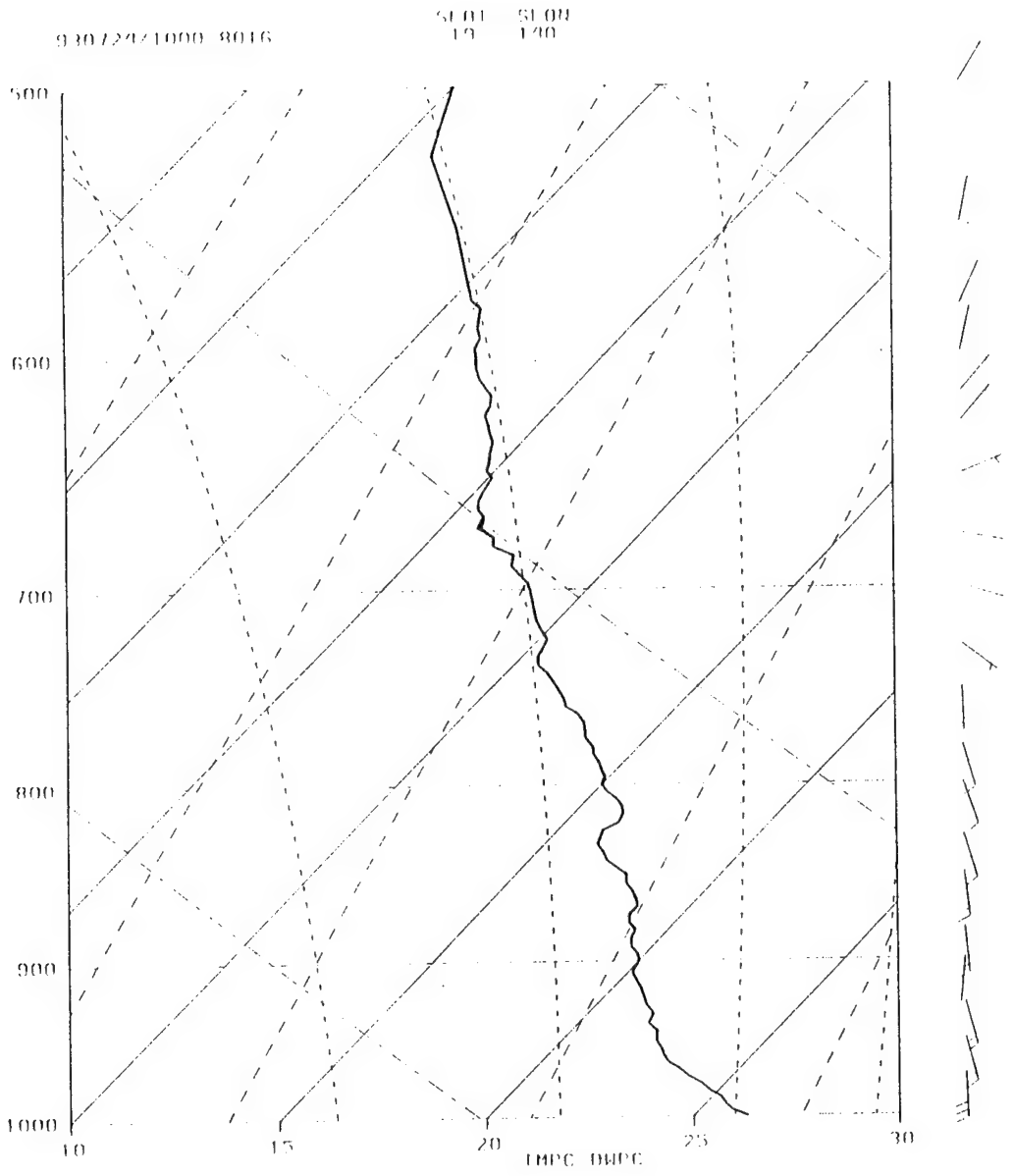


Figure 25a. ODW 14 sounding as in Fig. 15a, except deployed at 1023 UTC 24 July 1993.

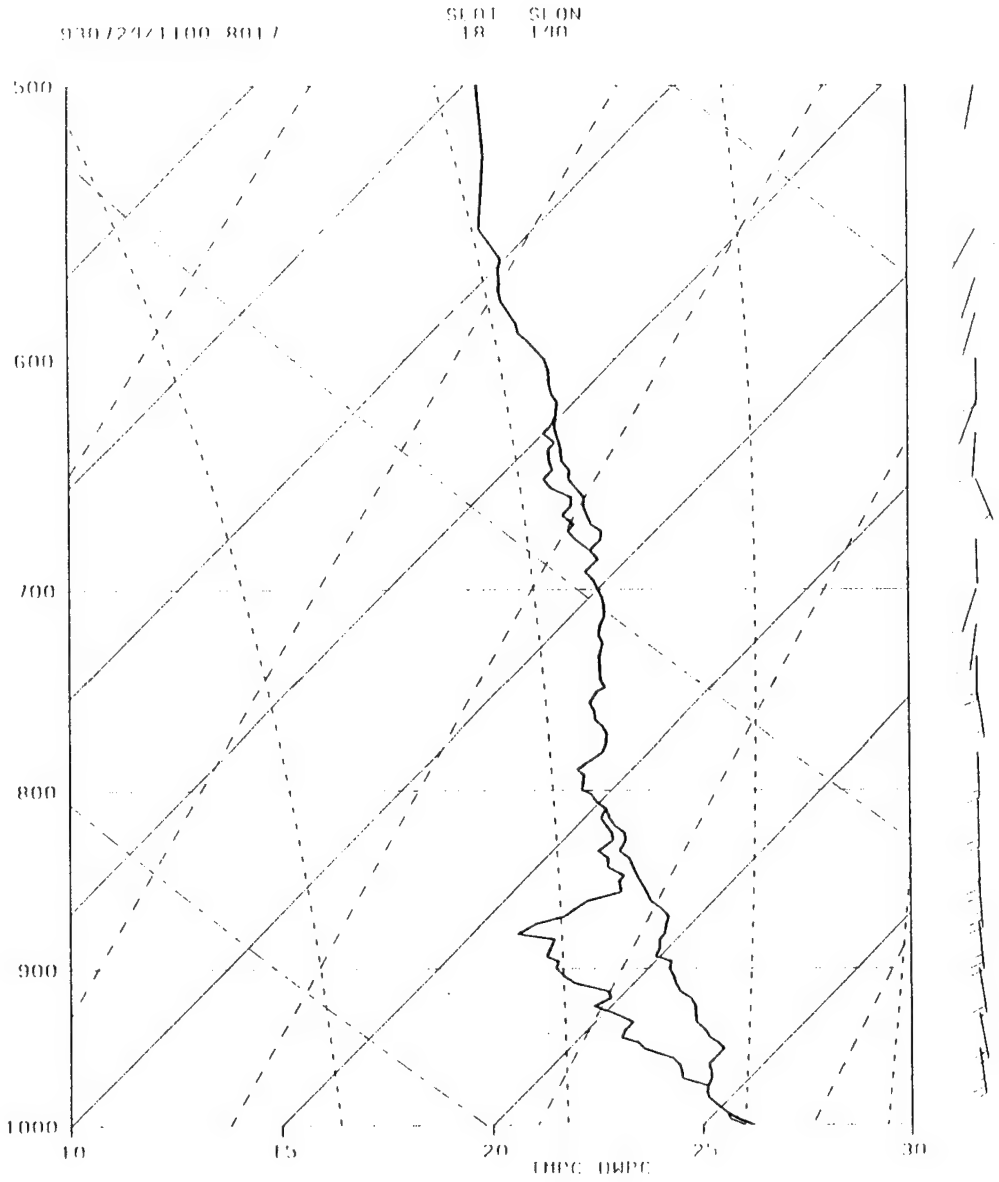


Figure 25b. ODW 15 sounding as in Fig. 15a, except deployed at 1043 UTC 24 July 1993.

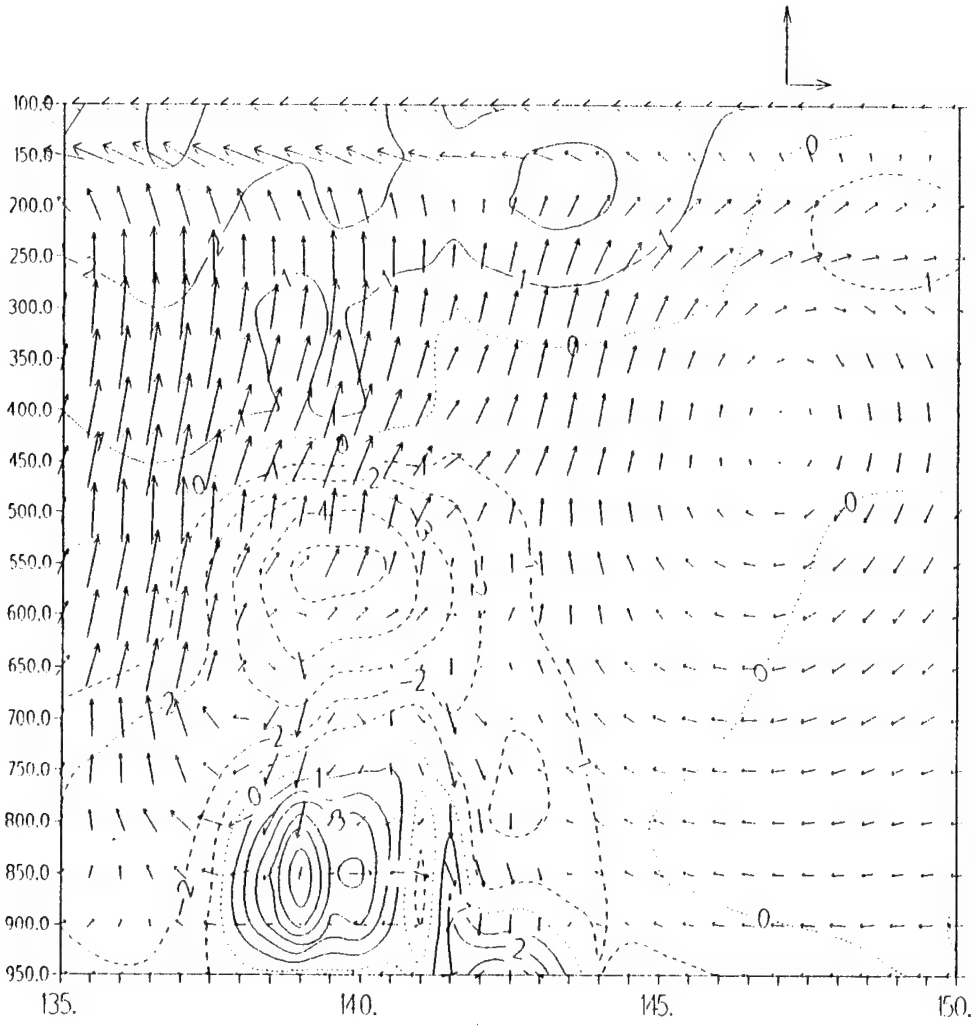


Figure 26. Vertical cross-section of divergence ($10^{-5}$ $s^{-1}$) and vectors of vertical wind (cm $s^{-1}$) and horizontal wind (m $s^{-1}$) along 17°N. Regions of divergence are depicted by the solid lines while regions of convergence are depicted by the dashed lines.

divergence along 17°N near the southern mesoscale circulation (Fig. 26) computed from the multiquadric analyses has a region of convergence at 550 mb overlying a region of divergence at 850 mb near 17°N, 139°E. Upward motion is found above the region of convergence and downward motion is above the region of divergence. The divergent layer extends from the surface to approximately 750 mb while the convergent layer extends from 750 mb to approximately 500 mb. This vertical cross-section of divergence and vertical motion supports the stretching of columns expected to generate a mid-level mesoscale cyclonic circulation. Similar regions of convergence and divergence were found in the mesoscale circulation detected in AOP-1A. Whereas the base of the divergent layer was at 850 mb in AOP-1A, the base of the divergent layer extended downward to the surface in AOP-1B.

The vertical cross-section of potential vorticity (Fig. 27) computed from the multiquadric analyses does indeed have a narrow band of positive potential vorticity extending down to the surface in the vicinity of the mid-level mesoscale cyclonic circulation near 17°N, 139°E. By contrast, the positive values of potential vorticity in AOP-1A (Fig. 13) remained well above the ocean surface. Because positive values of potential vorticity are extending down to the surface near the center of the mid-level mesoscale cyclonic circulation in AOP-1B, the surface fluxes from the warm ocean surface may be expected to contribute to the further growth of the mesoscale circulation.

The flight-level winds at 850 mb and 700 mb (Figs. 21a, b) and the soundings from ODW 1 and ODW 2 (Figs. 24a, b) enable the multiquadric analyses to depict crudely the southern mesoscale cyclonic circulation near 17°N, 139°E. The lack of ODW data and flight-level winds to the west of ODW 1 prevents an accurate depiction of the western extent of the mesoscale circulation. Due to the lack of ODW data and flight-level winds above 700 mb in the vicinity of the southern mesoscale cyclonic circulation, the vertical extent of the mesoscale circulation above 700 mb is unknown. Indeed, the vertical cross-sections of potential vorticity and divergence computed from the multiquadric analyses above 700 mb are a result of the blend with the horizontal and the vertical specifications of the NOGAPS first-guess field. Below

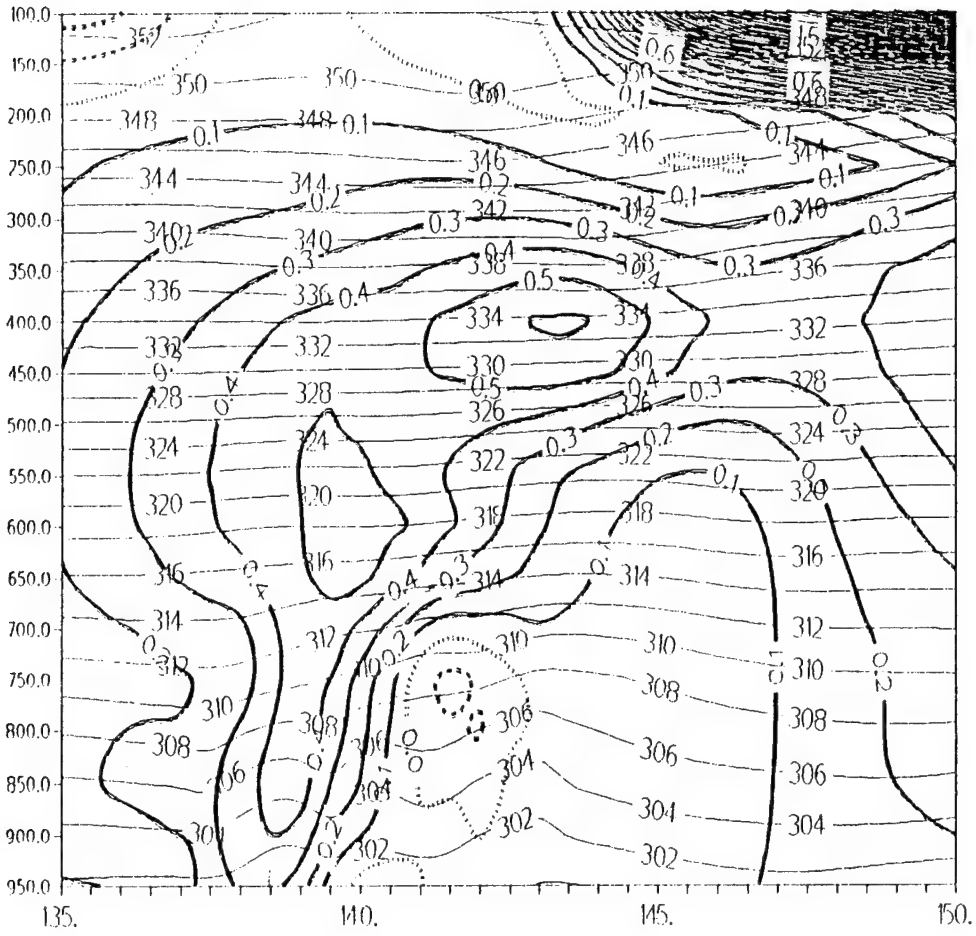


Figure 27. East-west vertical (pressures in mb) cross-section of potential vorticity (units of $10^{-6}$ $m^2$ K $s^{-1}$ $kg^{-1}$) as in Fig. 13, except along 17°N at 0800 UTC 24 July 1993.

700 mb, the vertical and the horizontal structure of the mesoscale cyclonic circulation is loosely defined by the vertical cross-section of potential vorticity (Fig. 27) due to the availability of data from ODW 1 and ODW 2.

Based on the westward movement of the large-scale features between AOP-1A and AOP-1B and the associated westward movement of the mesoscale cyclonic circulation on the cyclonic shear side of the monsoon gyre, it is believed that the southern mesoscale cyclonic circulation detected by the multiquadric analysis at 700 mb in AOP-1B is the same mesoscale cyclonic circulation documented in AOP-1A. If this is true, then the mesoscale cyclonic circulation would have had a west-northwest track with a speed of translation of 3 m $s^{-1}$ between 0600 UTC 23 July 1993 and 0800 UTC 24 July 1993, which is certainly a reasonable translation. Because positive values of potential vorticity are extending down to the surface near the center of the mid-level mesoscale cyclonic circulation in AOP-1B, the surface fluxes from the warm ocean surface may be expected to contribute to the further growth and intensification of the mesoscale circulation. Based on the multiquadric analysis at 500 mb (Fig. 12) and the vertical cross-section of potential vorticity (Fig. 13) in AOP-1A, the mid-level mesoscale cyclonic circulation had a horizontal diameter of approximately 460 km. However, the narrow band of positive potential vorticity extending downward to the surface near 17°N, 139°E in AOP-1B has a horizontal diameter of approximately 225 km, which suggests some intensification.

Animation of the enhanced IR satellite imagery at the end of AOP-1B (Fig. 19) indicates rotation about an organized convective cell near 20°N, 139°E. The northern mid-level mesoscale cyclonic circulation detected by the flight-level winds at 500 mb in Fig. 21c is attributed to this organized convective cell. In the hours following AOP-1B, this convective cell follows a west-northwesterly track at 5 m $s^{-1}$ along the northern edge of the monsoon gyre and dissipates (Fig. 28a, b, c, d). Therefore, the mid-level mesoscale cyclonic circulation detected by the flight-level winds at 500 mb in the northwest corner of the alpha flight pattern is not related to the eventual formation of TS Ofelia.

In summary, the vertical and horizontal extent of the two mid-level mesoscale

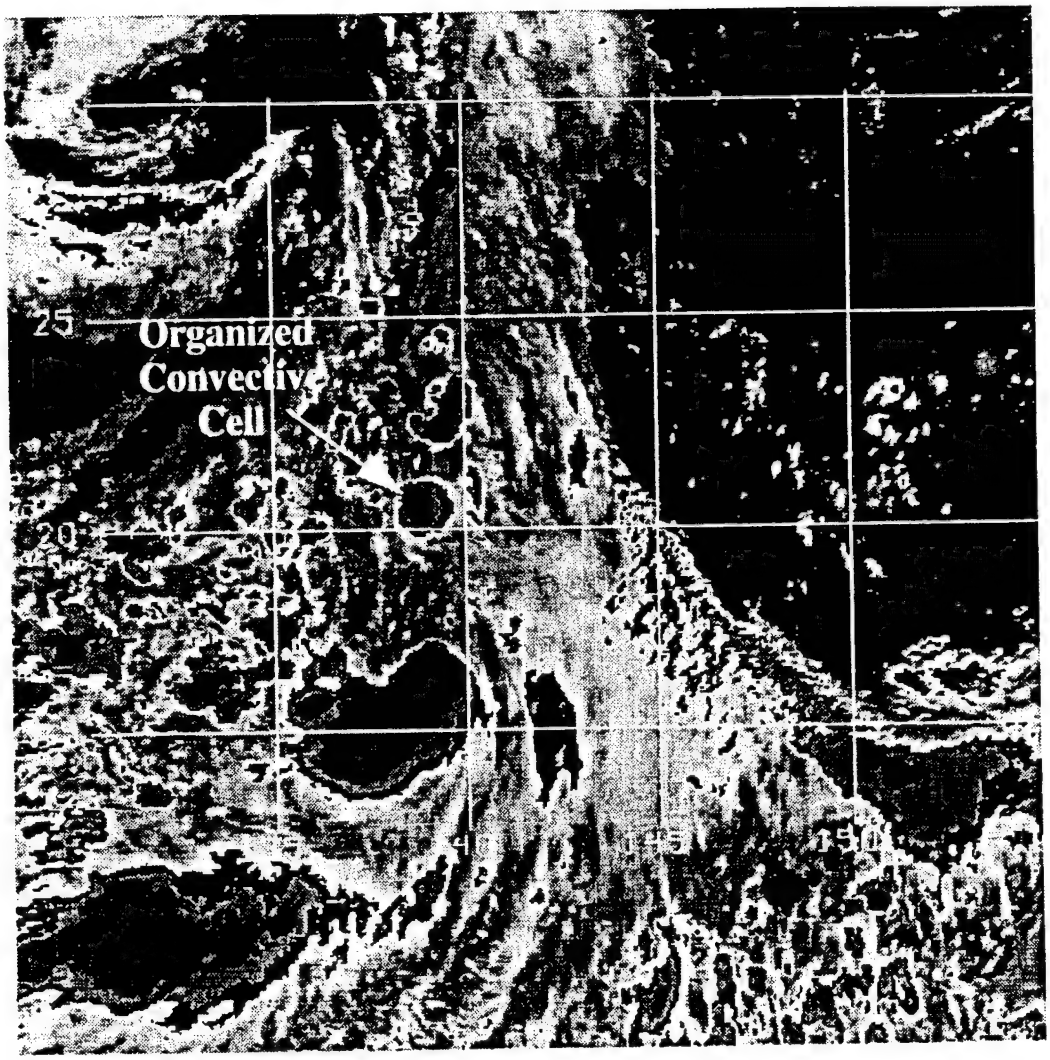


Figure 28a. Infrared satellite image as in Fig. 6, except at 1430 UTC 24 July 1993 after the completion of AOP-1B. Notice in this image the circular convective element near 20°N, 139°E that moves west-northwest in Figs. 28b and 28c, and dissipates prior to Fig. 28d.

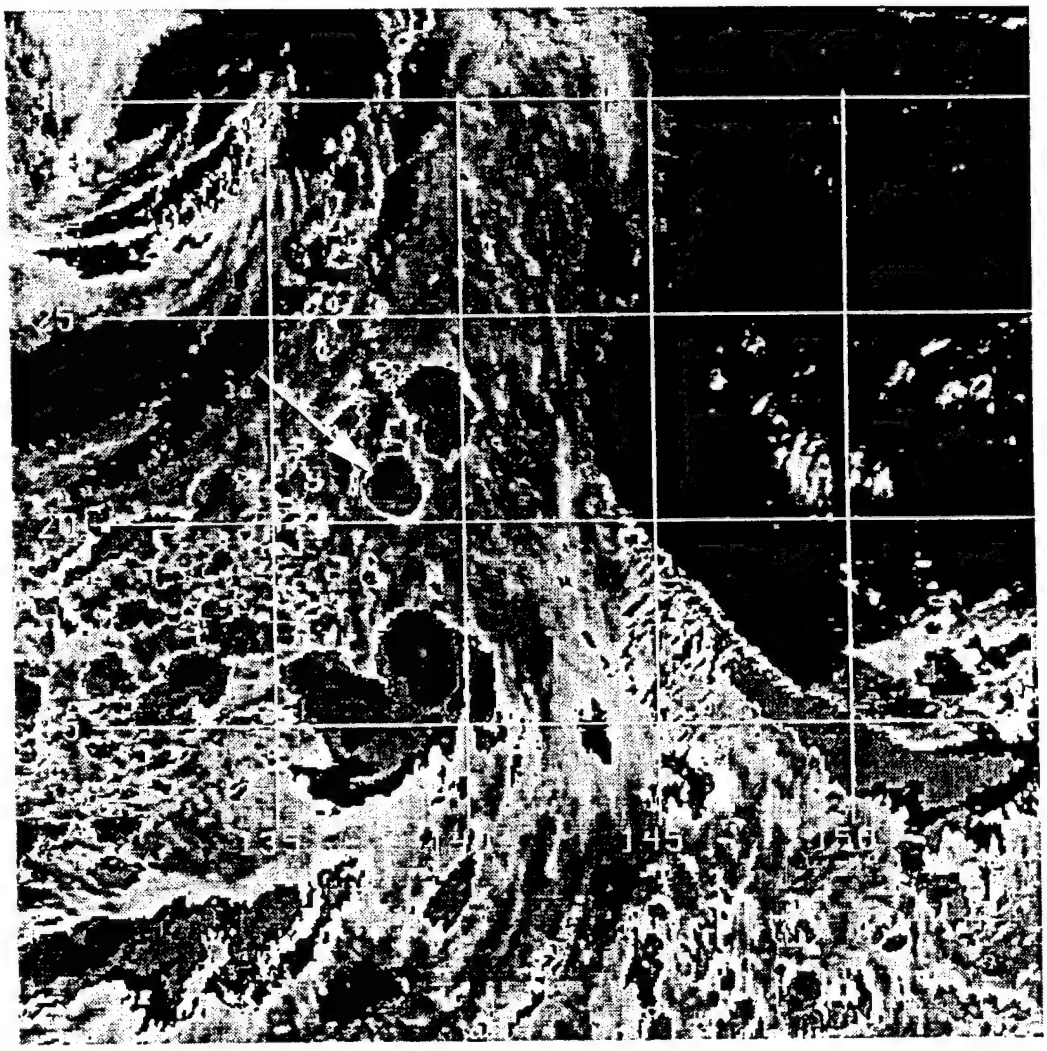

Figure 28b. Infrared satellite image as in Fig. 28a, except at 1730 UTC 24 July 1993.

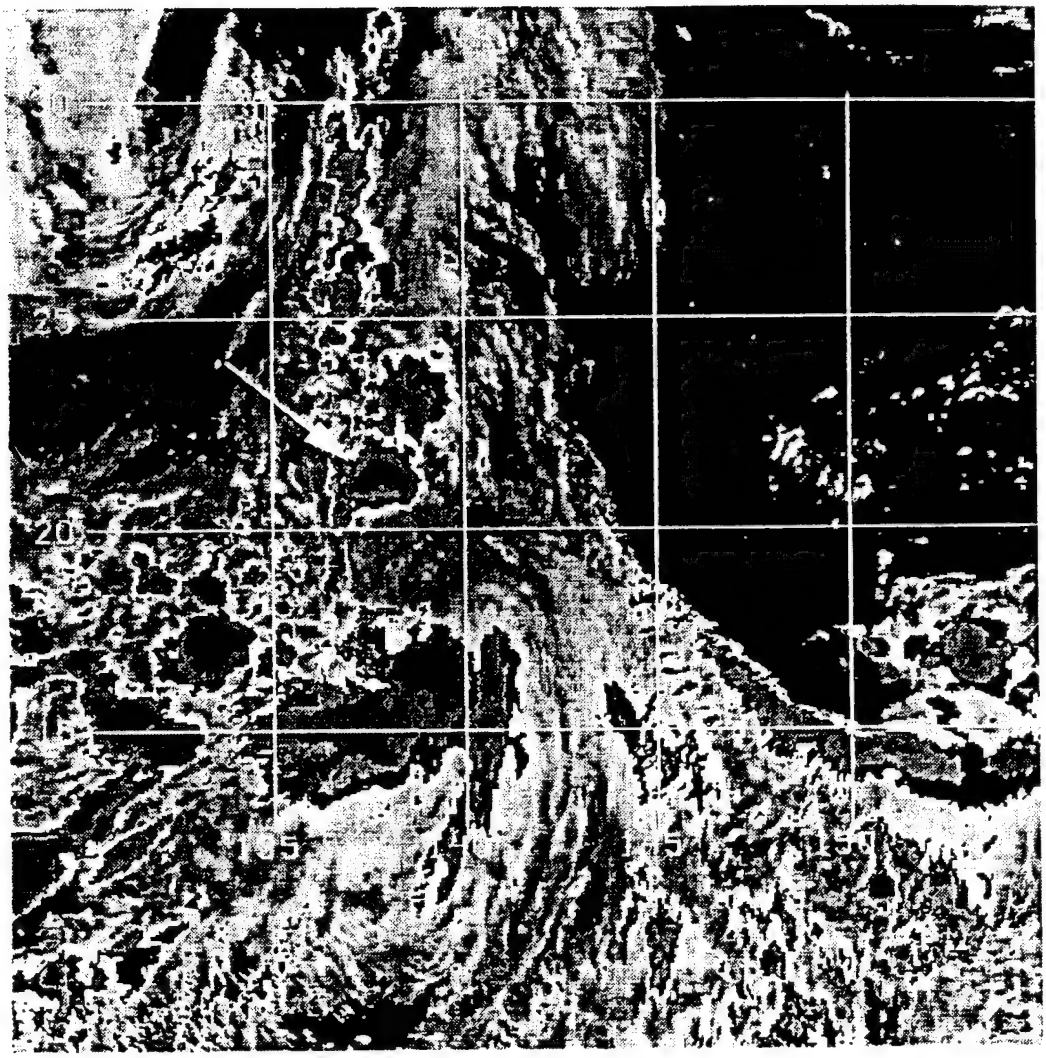


Figure 28c. Infrared satellite image as in Fig. 28a, except at 2030 UTC 24 July 1993.

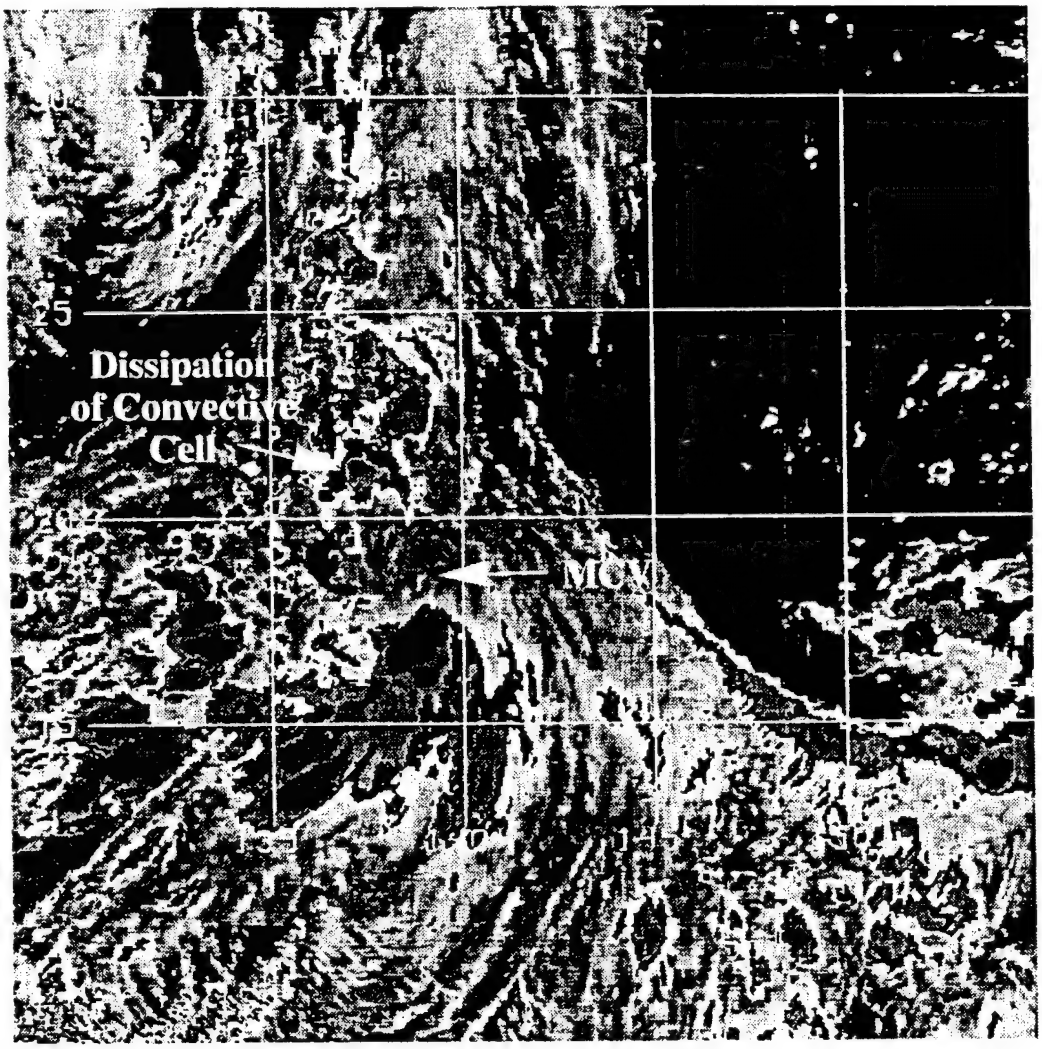


Figure 28d. Infrared satellite image as in Fig. 28a, except at 2230 UTC 24 July 1993. Notice the circular convective element in Figs. 28a-c has dissipated, but a circulation about an apparent center near 18°N, 139°E has developed.

cyclonic circulations was unable to be determined accurately from the multiquadric analyses in AOP-1B due to the limited amount of ODW data in the vicinity of the two mesoscale circulations. The lack of ODW soundings to the west of the centers prevented a confident size estimate for each mesoscale circulation in the multiquadric analyses. The multiquadric analyses at 700 mb and 500 mb do depict two mid-level mesoscale cyclonic circulations that were not detected in the NOGAPS first-guess field. The southern mesoscale cyclonic circulation depicted by the multiquadric analysis at 700 mb appears to be located more in the cyclonic shear of the monsoon gyre while the northern mesoscale cyclonic circulation depicted by the multiquadric analysis at 500 mb is located in the cyclonic shear on the northern edge of the monsoon gyre. The vertical cross-sections of potential vorticity and divergence indicate the southern mesoscale cyclonic circulation centered near 17°N, 139°E did extend down to the surface. The extension of the mid-tropospheric vortex down to the surface may be expected to contribute to the growth and the intensification of the mesoscale circulation.

Based on the westward movement of the entire system of TUTT cell, subtropical ridge, and monsoon gyre, it is concluded that the mid-level mesoscale cyclonic circulation depicted by the multiquadric analyses at 700 mb and 500 mb near 17°N, 139°E is the same mesoscale circulation detected on the cyclonic shear side of the monsoon gyre in AOP-1A. The association of this mid-level mesoscale cyclonic circulation with the formation of TS Ofelia will be examined in the next section. By contrast, the second mid-level mesoscale cyclonic circulation detected by the flight-level winds at 500 mb appears to be linked to an organized convective cell centered near 20°N, 139°E in the GMS enhanced IR satellite imagery that tracked west-northwest following AOP-1B. This mesoscale circulation is not related to the formation of TS Ofelia.

## D. THE FORMATION OF TROPICAL STORM OFELIA

Ten hours after the completion of AOP-1B, a mesoscale cyclonic circulation was clearly revealed by curved cumulus bands in the 2230 UTC 24 July 1993 GMS

visible imagery (Fig. 29). The corresponding GMS enhanced IR image at 2230 UTC 24 July 1993 in Fig. 28d also has an indication of low-level curved bands. The vortex was exposed due to the encroaching upper-level winds associated with the TUTT cell to the northeast of the mesoscale cyclonic circulation. Two extended bands of convection to the northwest and the southeast of the vortex center demonstrate the organization and the development of the mesoscale cyclonic circulation. Based on the GMS visible imagery at 2230 UTC 24 July 1993 (Fig. 29), the inner bands of the mesoscale cyclonic circulation have a horizontal diameter of approximately 55 km. The remnants of the organized convective cell associated with the northern mesoscale cyclonic circulation in AOP-1B followed a west-northwest track at 5 m $s^{-1}$ (Figs. 28a, b, c, d) and eventually became a part of the convective band located to the northwest of the vortex center (Fig. 29). Because of the well-documented movement of the organized convective cell in Figs. 28a-d and the location of this convective cell with respect to the mesoscale vortex in Fig. 29, it is clear that two separate and distinct mesoscale cyclonic circulations existed during AOP-1B. If the southern mesoscale cyclonic circulation detected in AOP-1B is the same mesoscale cyclonic circulation detected by the GMS visible imagery in Fig. 29, the mesoscale cyclonic circulation would have had a north-northwest track with a speed of translation of 3.7 m $s^{-1}$ between 0800 UTC 24 July 1993 and 2230 UTC 24 July 1993. Again, this very reasonable translation speed is the basis for concluding that this vortex in the visible imagery is indeed the southern vortex during AOP-1B, and the continuation of the vortex from AOP-1A.

Following the initial detection of the exposed mesoscale vortex at 2230 UTC 24 July 1993 (Fig. 29), the mid-level mesoscale cyclonic circulation was able to be tracked hourly with the GMS visible imagery (Figs. 30a, b, c, d). Based on the GMS visible imagery, the inner bands of the mesoscale vortex in Fig. 30a have a horizontal diameter of approximately 24 km, which suggests contraction and further intensification of the mesoscale cyclonic circulation.

Six hours after the initial detection of the mid-level mesoscale vortex in the GMS visible imagery, the first outbreak of deep convection that would lead to the

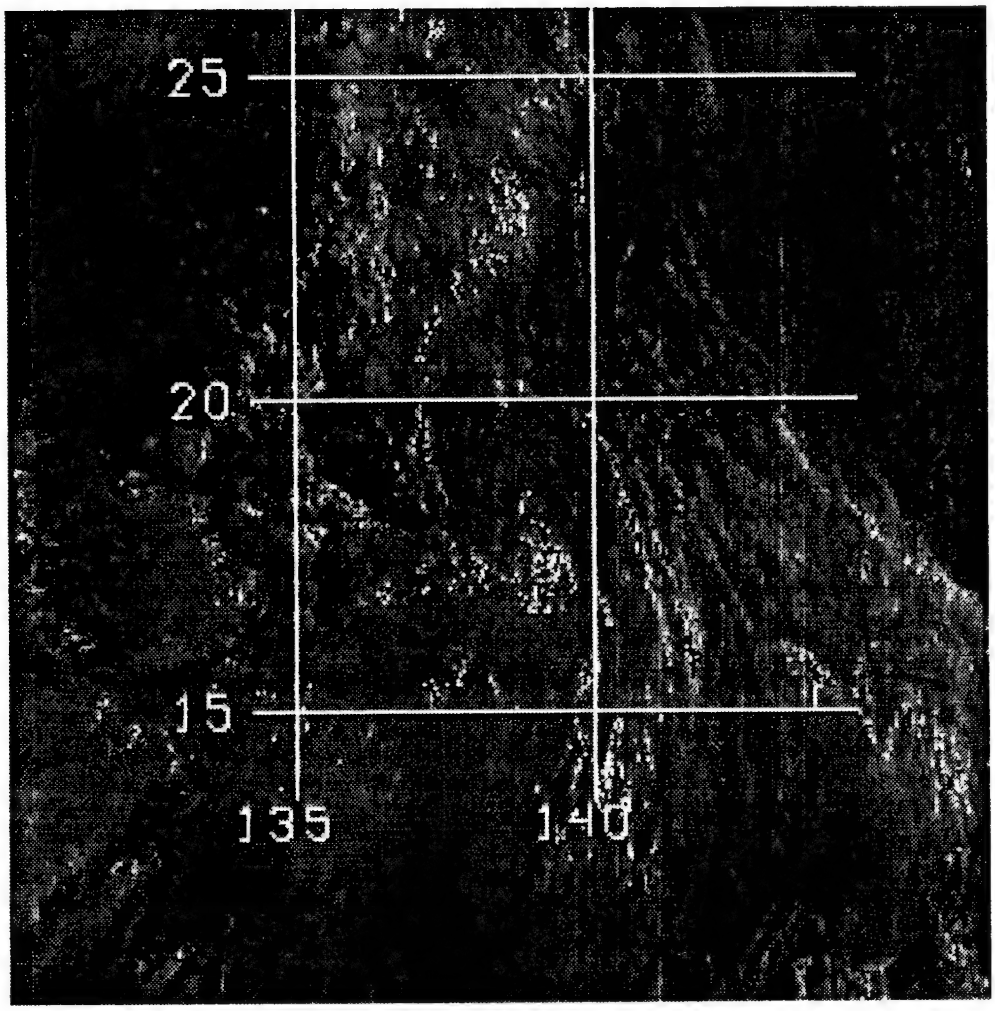


Figure 29. Visible satellite image at 2230 UTC 24 July 1993, which is the first discernible daylight imagery following AOP-1B. Notice the curved cumulus cloud lines that clearly define a circulation center near 18°N, 138°E, and the elongated bands of convection located to the northwest and to the southeast of the mesoscale vortex that appear to spiral into the circulation center.

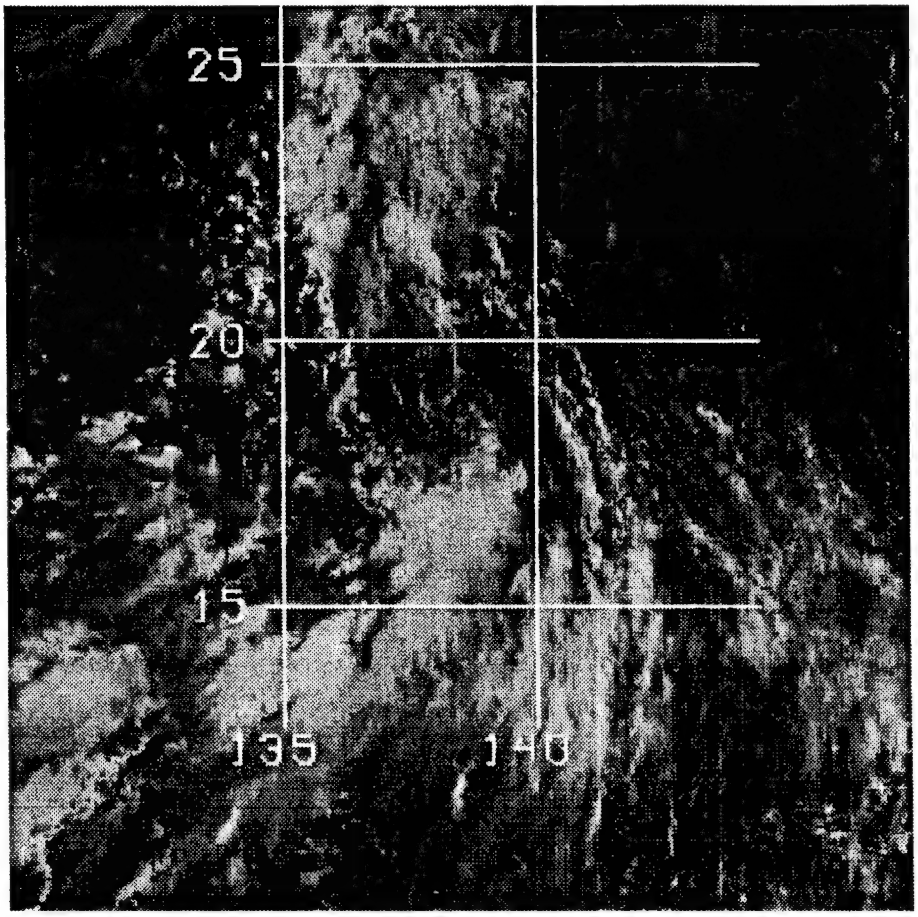


Figure 30a. Visible satellite image as in Fig. 29, except at 0030 UTC 25 July 1993 . Notice in this image the evolution of the curved bands in Fig. 29. As the mesoscale vortex moves to the north-northwest in Figs. 30b-d, the first outbreak of deep convection, and the development of a central dense overcast that would later become TS Ofelia are shown.

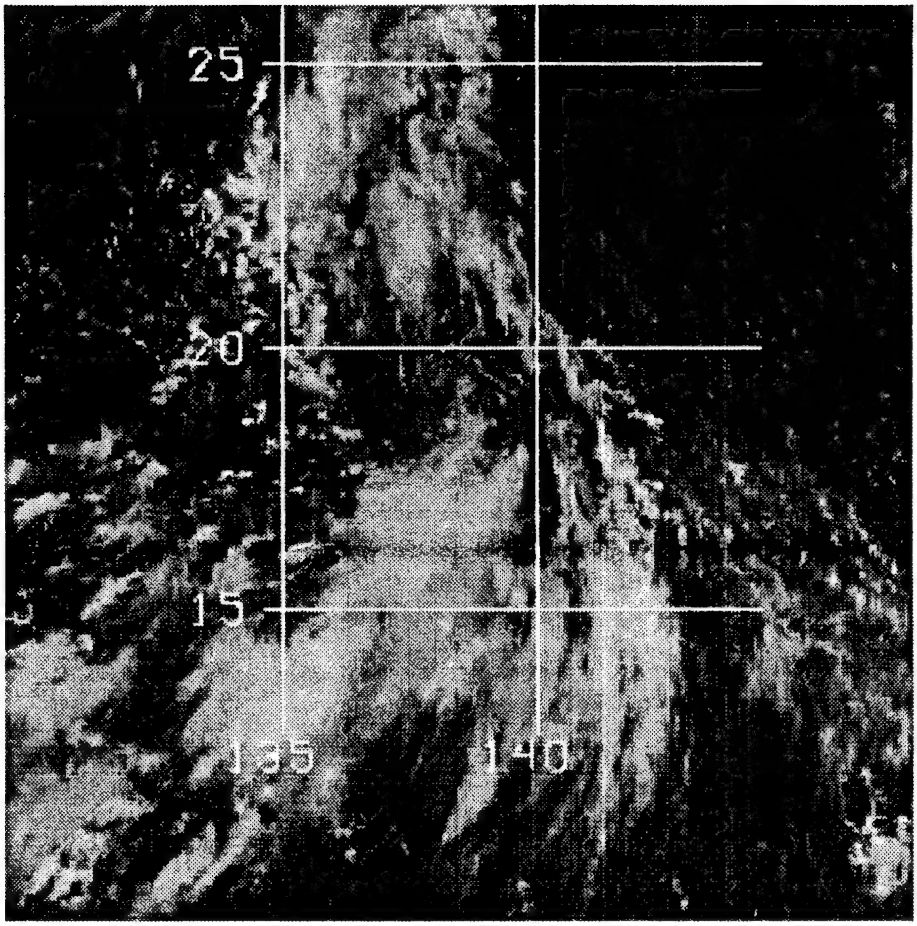


Figure 30b. Visible satellite image as in Fig. 29, except at 0230 UTC 25 July 1993.

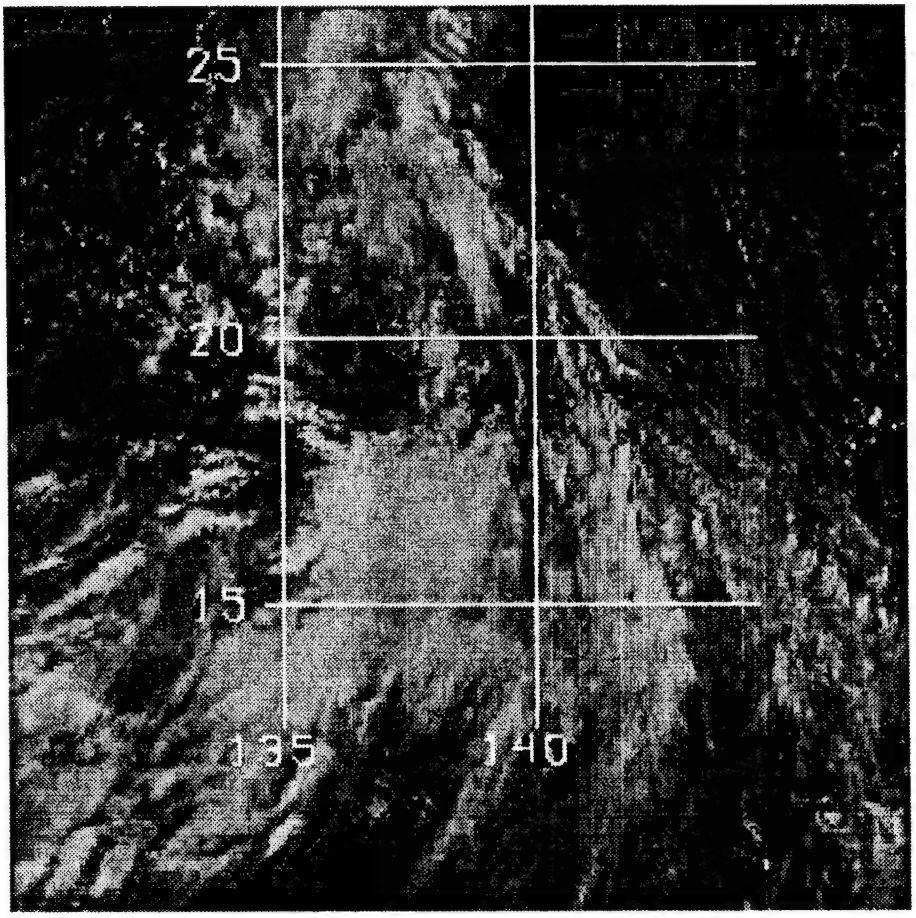


Figure 30c. Visible satellite image as in Fig. 29, except at 0430 UTC 25 July 1993. Note the first outbreak of deep convection near 20°N, 138°E associated with the formation of TS Ofelia.

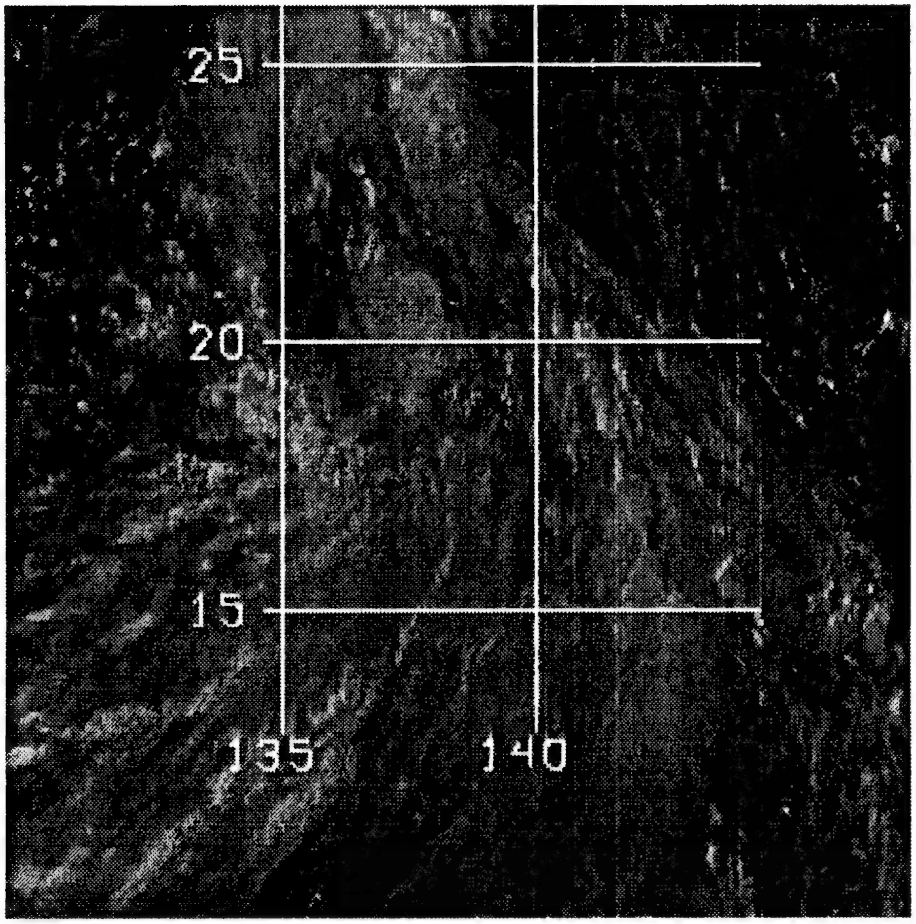


Figure 30d. Visible satellite image as in Fig. 29, except at 0630 UTC 25 July 1993. Note the development of a central dense overcast that would later become TS Ofelia near 21°N, 137°E.

formation of TS Ofelia was first detected near 20°N, 138°E along the north-northwest track of the mesoscale cyclonic circulation (Fig. 31). The speed of translation from where the vortex was first revealed in the visible imagery at 2230 UTC 24 July 1993 (Fig. 29) and the position where deep convection erupted at 0430 UTC 25 July 1993 (Fig. 31) was 8.8 m $s^{-1}$ toward the north-northwest. The accelerated translation of the mesoscale cyclonic circulation is believed to be due to its location in the cyclonic shear of the monsoon gyre. With the subsequent organization and continued development of the deep convection around the mesoscale vortex, a deeper layer of southerly environmental flow may have contributed to the accelerated translation. The favored development of the deep convection on the northern side of the vortex may have contributed a northward propagation component to the total translation as well.

In summary, the outbreak of deep convection eventually leading to the formation of TS Ofelia is well documented in the visible imagery. This convection develops in association with a mesoscale vortex that is clearly depicted in the visible imagery beginning at 2230 UTC (0830 local) 24 July 1993. Based on the implied translation speed from the end of AOP-1B until this first visible image (Fig. 29) on 24 July 1993, it is concluded that the southern mesoscale vortex during AOP-1B is the same vortex in the visible image. Thus, the environmental structure of the mesoscale vortex first detected in AOP-1A, and measured less completely in AOP-1B, is considered to be the pre-existing structure in which TS Ofelia eventually developed. This is considered to be the best available data set of the environmental structure in which a "midget" typhoon forms.

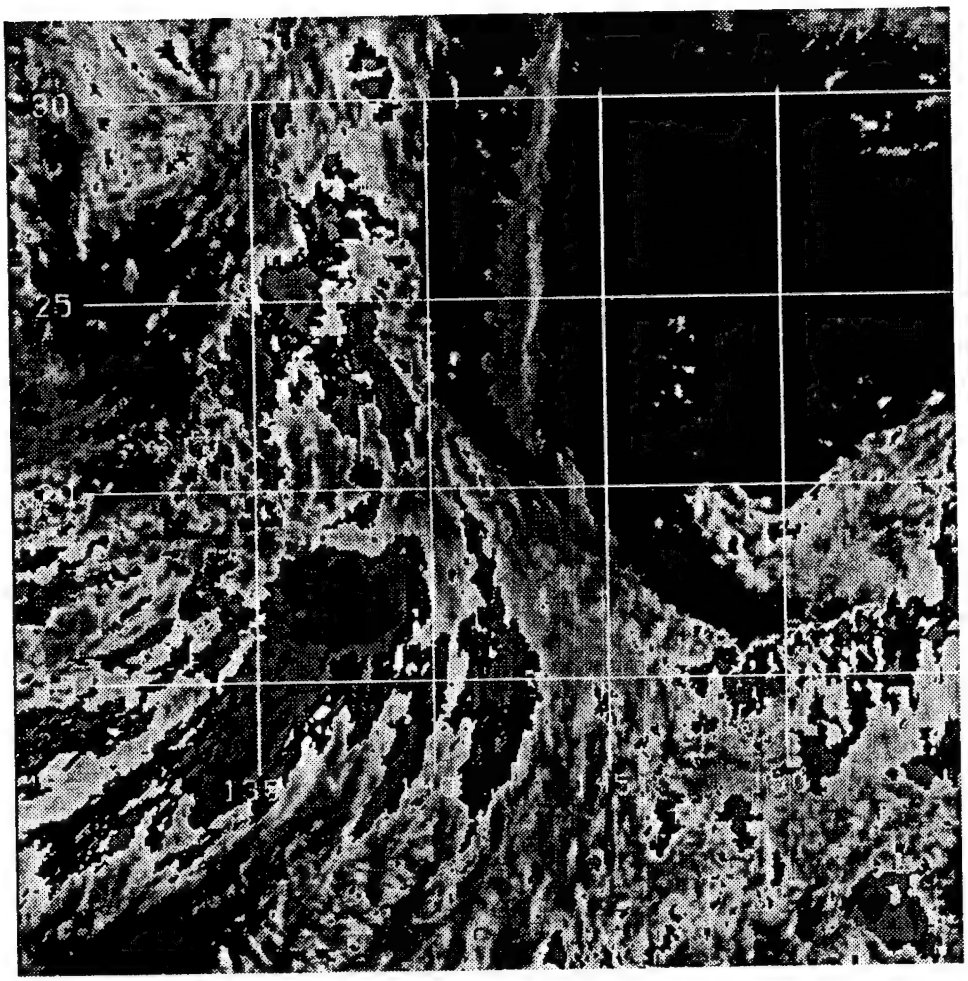


Figure 31. Infrared satellite image as in Fig. 6, except at 0430 UTC 25 July 1993 showing the cloud shield associated with the formation of TS Ofelia.

# IV. SUMMARY AND CONCLUSIONS

The specific objectives of this study were: (i) to examine the structure of circulations that contributed to the forcing of the persistent convection along the eastern edge of the monsoon gyre; and (ii) to describe the mesoscale circulation structure in the region of deep convection that subsequently resulted in the formation of TS Ofelia. Rawinsonde observations from Guam, Palau, Chuuk, Pohnpei, and Yap helped to define the structure of the large-scale flow during AOP-1A and AOP-1B. The rawinsonde observations showed that the moist southwesterly flow around the southern portion of the monsoon gyre was subjected to large-scale lifting as it was undercut by the easterly winds along the southern portion of the subtropical ridge. The strength of the subtropical anticyclone extension to the southwest increased as it moved westward, which displaced the monsoon gyre westward. Thus, the axis of the north-oriented confluent flow between the monsoon gyre and the expanding subtropical ridge was steadily shifted westward. Given the persistent, large-scale, westward evolution of this overall monsoon gyre, subtropical anticyclone, and TUTT cell system, the focus of AOP-1A and AOP-1B became the north-oriented confluent flow between the subtropical ridge and the monsoon gyre where repeated deep convection occurred. The two AOPs provided flight-level winds and ODW data in the confluence area on the two days prior to the formation of TS Ofelia to help define the mesoscale structure of the circulation.

A multiquadric interpolation technique was used to blend the ODW data and aircraft flight-level winds from AOP-1A and AOP-1B into background fields from archived Fleet Numerical Meteorology and Oceanography Center (FNMOC) global analyses. These ODWs were an essential component in documenting the three-dimensional structure of the MCS. Thermodynamic and dynamic structures were analyzed directly from the ODWs as well as from gridded analysis fields.

In AOP-1A, the significant deep convection that was present at the beginning of AOP-1A dissipated toward the end of AOP-1A as expected during the diurnal

convective minimum period. Utilizing the ODW soundings, the multiquadric interpolation technique with the operational NOGAPS analysis as a first-guess field introduced mesoscale circulations in the region, and especially documented a mid-tropospheric mesoscale cyclonic circulation. This mesoscale vortex, which extended vertically from approximately 700 mb up to at least 400 mb, was west of the region of persistent, deep convection. The horizontal diameter of the mid-level mesoscale cyclonic circulation was approximately 460 km as determined from the multiquadric analyses at 500 mb (Fig. 12) and a cross-section of potential vorticity (Fig. 13). ODW soundings near the center of the mid-level mesoscale cyclonic circulation have deep dry layers below the mid-level vortex. The different elevations of the dry layers indicate that the mid-level mesoscale cyclonic circulation may have had a slight upward tilt from west-to-east due to the strong convection and uplifting east of the mesoscale circulation. Thus, the AOP-1A observations suggested the presence of a mid-tropospheric cyclonic vortex as has been previously documented in midlatitude MCSs and in some tropical MCSs.

In AOP-1B, the flight-level winds (Figs. 21a, b, c) provided some evidence of two mid-level mesoscale cyclonic circulations that were not detected in the NOGAPS first-guess field or the satellite imagery. Whereas the center of the alpha flight pattern coincided with the center of the mid-level mesoscale cyclonic circulation defined by the flight-level winds in AOP-1A, the positions of the two mesoscale circulations were not as clearly defined by the flight-level winds in AOP-1B. The vertical and horizontal extents of the two mid-level mesoscale cyclonic circulations were not able to be determined accurately from the multiquadric analyses in AOP-1B due to the limited amount of ODW data in the vicinity of the two mesoscale circulations.

The southern mesoscale cyclonic circulation depicted by the multiquadric analysis at 700 mb (Fig. 22) appears to be located more in the cyclonic shear of the monsoon gyre while the northern mesoscale cyclonic circulation depicted by the multiquadric analysis at 500 mb (Fig. 23) is located in the cyclonic shear on the northern edge of the monsoon gyre. The northern mid-level mesoscale cyclonic circulation detected by the flight-level winds at 500 mb in Fig. 21c was linked to an

organized convective cell near 20°N, 139°E that followed a west-northwesterly track at 5 m $s^{-1}$ along the northern edge of the monsoon gyre and dissipated (Fig. 28a, b, c, d). Therefore, the mid-level mesoscale cyclonic circulation detected by the flight-level winds at 500 mb in the northwest corner of the alpha flight pattern is not related to the eventual formation of TS Ofelia. However, the vertical cross-sections of divergence (Fig. 26) and potential vorticity (Fig. 27) indicate the southern mesoscale cyclonic circulation centered near 17°N, 139°E extended downward to the surface. The extension of the mid-tropospheric vortex down to the surface may be expected to contribute to the growth and the intensification of the southern mesoscale cyclonic circulation.

Further analysis of the cross-section of potential vorticity from AOP-1A (Fig. 13) gives a hint that the narrow band of positive potential vorticity depicted by the vertical cross-section of potential vorticity in AOP-1B may have started its downward descent to the surface during AOP-1A. Based on the westward movement of the entire system of TUTT cell, subtropical ridge, and monsoon gyre and the implied westward 3 m $s^{-1}$ movement of the southern mesoscale circulation between AOP-1A and AOP-1B , it is concluded that the mid-level mesoscale cyclonic circulation depicted by the multiquadric analyses at 700 mb and 500 mb near 17°N, 139°E in AOP-1B is the same mesoscale circulation documented in AOP-1A.

Ten hours after the completion of AOP-1B, the mid-level mesoscale cyclonic circulation detected in AOP-1A and AOP-1B was detected in the 2230 UTC 24 July 1993 GMS visible imagery (Fig. 29). The vortex was exposed due to the encroaching upper-level winds associated with the TUTT cell located to the northeast of the mesoscale cyclonic circulation. Two extended bands of convection to the northwest and the southeast of the vortex center demonstrate the organization and the development of the mesoscale cyclonic circulation. This mesoscale cyclonic circulation was able to be tracked hourly with the GMS visible imagery. Six hours after the initial detection of the mesoscale vortex in the GMS visible imagery, the first outbreak of deep convection near 20°N, 138°E that would lead to the formation of TS Ofelia was detected along the north-northwest track of the mesoscale cyclonic

circulation (Fig. 31). Based on the satellite imagery and the Joint Typhoon Warning Center (JTWC) best tracks, TS Ofelia followed a north-northwest track at approximately 18 kt (9 m $s^{-1}$) until it reached the southern tip of Japan where the tropical storm accelerated and followed a northerly track at approximately 25 kt (12 m $s^{-1}$). The maximum surface winds associated with TS Ofelia were approximately 45 kt (22 m $s^{-1}$) with a minimum sea-level pressure of approximately 991 mb. At 0000 UTC 28 July 1993, the final tropical storm warning was issued by JTWC as TS Ofelia dissipated over the Sea of Japan.

In conclusion, the environmental structure of the mesoscale vortex first detected in AOP-1A, and measured less completely in AOP-1B, is considered to be the pre-existing structure in which TS Ofelia eventually developed. This is considered to be the best available data set of the environmental structure in which a "midget" typhoon forms.

As TS Ofelia moved off to the north and dissipated, the entire system of TUTT cell, subtropical ridge, and monsoon gyre continued to move westward over the subtropical western North Pacific. TY Percy was the third significant tropical cyclone that formed in association with the entire system of TUTT cell, subtropical ridge, and monsoon gyre. The first tropical storm alert associated with TY Percy was issued at 1800 UTC 27 July 1993. Percy was upgraded to a tropical storm at 0600 UTC 28 July 1993 and was upgraded to a typhoon at 1200 UTC 29 July 1993. The maximum surface winds associated with TY Percy were 65 kt (33 m $s^{-1}$) with a minimum sea-level pressure of 976 mb. At 1200 UTC 30 July 1993, the final tropical storm warning was issued on Percy as it dissipated over the Sea of Japan. Based on the satellite imagery, TY Percy had formation characteristics similar to those of TY Nathan and TS Ofelia. Because the formation area of TY Percy was beyond the range of the Air Force WC-130, the mesoscale structure of TY Percy was not able to be observed during TCM-93. Similar to TS Ofelia, TY Percy followed a north-oriented track at approximately 11 kt (5 m $s^{-1}$) until it approached the southern coast of Japan where the tropical cyclone accelerated and followed a north-northeast track at approximately 25 kt (12 m $s^{-1}$). Because of the similarities in formations as depicted

on satellite imagery relative to the persistent circulations, and the common north-oriented tracks, these three storms appear to be an example of repetitive tropical cyclone formation.

Although the formation and the evolution of TS Ofelia were fairly well-documented, many questions remain concerning the dynamic principles linking mesoscale cyclonic circulations to tropical storm formation. The environmental structure of the mesoscale circulations detected in AOP-1A and AOP-1B are considered to be the pre-existing environmental structure in which TS Ofelia eventually developed. In AOP-1A, the mesoscale cyclonic circulation was documented from 700 mb up to at least 400 mb. In AOP-1B, the mesoscale cyclonic circulation extended downward to the surface and was located within the cyclonic shear of the monsoon gyre. The physical mechanisms linking the mesoscale circulations to the monsoon gyre and the specific process by which the downward evolution of the mesoscale circulations occurs need further study. Perhaps simulations with high resolution numerical models may help explain the dynamics of the vertical and the horizontal motions associated with the mesoscale cyclonic circulations detected during AOP-1A and AOP-1B and their relationship to tropical cyclone formation.

# APPENDIX. DATA MANAGEMENT TECHNIQUES

Because the multiquadric interpolation technique is designed to draw closely to the data, the accuracy of the mesoscale circulations depicted by the multiquadric analyses depends critically on the accuracy of the ODW data. In this study, each ODW sounding was first examined using the pre-analysis objective Quality Control (QC) technique currently used by the Fleet Numerical Meteorology and Oceanography Center (FNMOC) for rawinsondes (Baker 1991). The ODWs were subjected to extensive vertical consistency checks that included tests for unlikely lapse rates and tests for unrealistic wind speeds and directional shears.

In the lapse rate portion of the QC, the vertical temperature profile in the ODW sounding is checked for unreasonable lapse rates, by scanning layer by layer from the surface to the highest level. Although the lapse rate was allowed to be slightly superadiabatic, extreme inversions were not permitted. If an unlikely lapse rate was detected, an attempt was made to determine which temperature was in error by examining the adjacent layers. If the error was able to be isolated, a change of sign for that temperature was tested and a substitution provided if appropriate. This test is valuable for detecting and correcting sign errors (Baker 1991).

In addition, vertical wind shear QC checks were applied to the wind data at standard pressure levels using two methods: (i) checking the wind speed shear; and (ii) checking a combination of the directional shear and the sum of the wind speeds. For the check of one standard pressure level wind, one more adjacent standard pressure level wind was needed (Baker 1991).

Certain problems are commonly encountered in the retrieval of thermodynamic data with an ODW (Franklin 1987). One of the problems involves the short time period needed for the ODW thermistor and carbon hygristor to reach ambient conditions after deployment from the aircraft. Although the thermistor equalibrates in just a few seconds, humidity estimates for about the first 30 s of fall (~20 mb) may be in error. During TCM-93, the data retrieved from the ODW during the first 100 s of

flight were analyzed closely to determine whether this problem occurred. A second problem may occur when an ODW falls out of a cloud into the drier air below, and water on or near the thermistor evaporates. In this case, temperature errors of up to 8°C may develop at the interface of the cloud and the dry air below (Franklin 1987).

Measurements of the signal phase from the eight world-wide Omega transmitters are collected every 10 s. Receipt of three or more of these signals allows the motion of the ODW (the wind) to be computed (Franklin 1987). During TCM-93, wind estimates were computed every 30 s in real-time and stored as part of the TCM-93 data base. Although Franklin (1987) showed that recomputing the wind from the Omega data as part of the post-processing has significant advantages, the WC-130 aircraft used for the TCM-93 missions did not have the capability to archive raw Omega signals during TCM-93.

Certain problems are sometimes encountered when computing wind with ODWs. The presence of noise in the Omega data requires that the signals be smoothed before they can be used in the wind-finding equations. The airborne ODW system uses a quadratic least-squares fitting algorithm, and this procedure is susceptible to noise in the Omega data. Franklin (1987) found that a scale-controlled cubic-spline technique developed by Ooyama gives better results. Despite the corrections found in all wind-finding algorithms to account for the sequential nature of the Omega transmissions, accelerations of the aircraft (turns) adversely affect the wind estimates (Franklin 1987). During TCM-93, flight missions were conducted to avoid sudden turns or accelerations after an ODW was deployed.

The ODW soundings from AOP-1A and AOP-1B were subjected to all of the vertical checks described above. In addition to these vertical checks, the ODWs were subjected to horizontal QC checks by comparing the ODW winds in a storm-relative coordinate system at individual pressure levels. In AOP-1A, the winds from ODW 9 created inconsistencies in the multiquadric analyses below 400 mb (Fig. 32) that led to a convoluted vertical structure of the MCS. ODW 9 has a layer of easterly winds from 650-500 mb that did not correlate with the winds from ODW 12 and ODW 17 (see locations in Fig. 1). While ODW 12 has southwesterly to westerly winds from

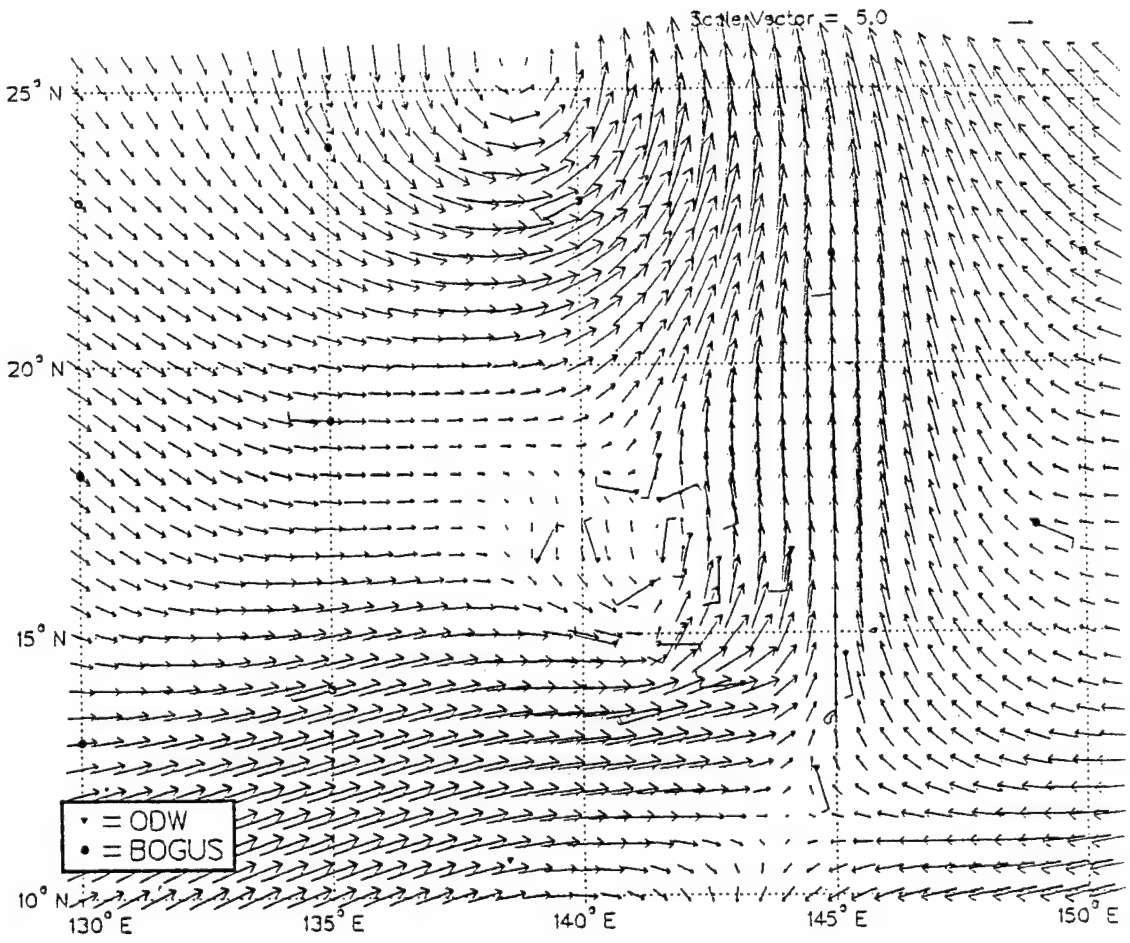


Figure 32. Multiquadric analysis at 650 mb for 0600 UTC 23 July 1993, except using the winds from ODW 9 near 15°N, 141.5°E. This analysis should be compared with Fig. 11b in which the ODW 9 wind was omitted.

the surface up to 400 mb, ODW 17 has southwesterly winds from the surface up to 400 mb. It is possible that the ODW 9 sounding implies the presence of a mesoscale feature that was not able to be resolved from the 100 km average spacing between the ODWs in AOP-1A. However, the layer of easterly winds from ODW 9 were discarded due to the failure of these winds to pass the horizontal QC checks.

## REFERENCES


Baker, N. L., 1991: Quality control of meteorological observations for the Fleet Numerical Oceanography Center operational atmospheric database. NOARL Tech. Note 124. Prediction Systems Division Atmospheric Directorate, Monterey, CA 93943-5006, 59 pp.

Barnes, S. L., 1973: Mesoscale objective analysis using weighted time-series observations. NOAA Tech. Memo. ERL NSSL-62, National Severe Storms Laboratory, Norman, OK, 60 pp. [NTIS COM-73-10781].

Cressman, G. P., 1959: An operational objective analysis system. *Mon. Wea. Rev.*, **87**, 367-374.

Elsberry, R. L., G. M. Dunnavan, and E. J. McKinley, 1992: Operations plan for the Tropical Cyclone Motion (TCM-92) mini-field experiment. Tech. Rep. NPS-MR-92-002, Naval Postgraduate School, Monterey, CA 93943, 46 pp.

Emanuel, K. A., 1993: The physics of tropical cyclogenesis over the eastern Pacific. In *Tropical Cyclone Disasters*, J. Lighthill, Z. Zhemin, G. Holland, and K. Emanuel, Eds., Peking University Press, 136-142.

Frank, W. M., 1987: Tropical cyclone formation. Chap. 3 in *A Global View of Tropical Cyclones*, Office of Naval Research, Arlington, VA 22217, 53-90.

Frank, W. M., and S. -Y. Chen, 1991: Simulations of vortex formation in convective weather systems. *Preprints, 19th Conference on Hurricanes and Tropical Cyclones*, Miami, FL, American Meteorological Society, Boston, MA 02108, 241-244.

Frank, W. M., 1992: Tropical cyclone formation. Colorado State University, Department of Atmospheric Sciences, 30th Anniversary Symposium, 5-6 May.

Franke, R., 1982: Scattered data interpolation: Tests of some methods. *Math. Comput.*, **38**, 181-200.

Franklin, J. L., 1987: Reduction of errors in omega dropwinsonde data through postprocessing. NOAA Tech. Memo. ERL AOML-65, Atlantic Oceanographic and Meteorological Laboratory, Miami, FL 33149, 22 pp.

Fritsch, J. M., J. D. Murphy, and J. S. Kain, 1994: Warm core vortex amplification over land. *J. Atmos. Sci.*, **51**, 1780-1807.

Harr, P. A., R. L. Elsberry, E. A. Ritchie, H. E. Willoughby, M. A. Boothe, L. E. Carr III, and R. A. Jeffries, 1993: Tropical Cyclone Motion (TCM-93) Field Experiment Summary. Tech. Rep. NPS-MR-93-004, Naval Postgraduate School, Monterey, CA 93943, 120 pp.

Harr, P. A., and R. L. Elsberry, 1995: Structure of a mesoscale convective system embedded in Typhoon Robyn during TCM-93. Submitted to *Mon. Wea. Rev.*

Hertenstein, R. F. A., and W. H. Schubert, 1991: Potential vorticity anomalies associated with squall lines. *Mon. Wea. Rev.*, **119**, 1663-1672.

Hoskins, B. J., M. E. McIntyre, and A. W. Robertson, 1985: On the use and significance of isentropic potential vorticity maps. *Quart. J. Roy. Meteor. Soc.*, **111**, 877-946.

Houze, R. A., 1977: Structure and dynamics of a tropical squall-line system. *Mon. Wea. Rev.*, **105**, 1540-1567.

Lander, M. A., 1994: Description of a monsoon gyre and its effects on the tropical cyclones in the western North Pacific during August 1991. *Weather and Forecasting*, **9**, 640-654.

Miller, D. T., and J. M. Fritsch, 1991: Mesoscale convective complexes in the western Pacific Region. *Mon. Wea. Rev.*, **119**, 2978-2991.

Nuss, W. A., and D. W. Titley, 1994: Use of multiquadric interpolation for meteorological objective analysis. *Mon. Wea. Rev.*, **122**, 1611-1631.

Raymond, D. J., and H. Jiang, 1990: A theory for long-lived mesoscale convective systems. *J. Atmos. Sci.*, **47**, 3067-3077.

Smull, B. F., and R. A. Houze, Jr., 1985: A midlatitude squall line with a trailing region of stratiform rain: Radar and satellite observations. *Mon. Wea. Rev.*, **113**, 117-133.

Zehr, R. M., 1992: Tropical cyclogenesis in the western North Pacific. NOAA Tech. Rep. NESDIS 61, U. S. Dept. of Commerce, Washington, D. C., 181 pp.

Zipser, E. J., 1977: Mesoscale and convective-scale downdrafts as distinct components of squall-line structure. *Mon. Wea. Rev.*, **105**, 1568-1589.

## INITIAL DISTRIBUTION LIST

| | | No. Copies |
|---|---|---|
| 1. | Defense Technical Information Center<br>Cameron Station<br>Alexandria VA 22304-6145 | 2 |
| 2. | Librarian<br>Code 52<br>Naval Postgraduate School<br>411 Dyer Rd Rm 104<br>Monterey CA 93943-5101 | 2 |
| 3. | Oceanography Department<br>Code OC/BF<br>Naval Postgraduate School<br>833 Dyer Rd Rm 311<br>Monterey CA 93943-5122 | 1 |
| 4. | Meteorology Department<br>Code MR/HY<br>Naval Postgraduate School<br>589 Dyer Rd Rm 252<br>Monterey CA 93943-5114 | 1 |
| 5. | Dr. R. L. Elsberry<br>Code MR/Es<br>Naval Postgraduate School<br>589 Dyer Rd Rm 252<br>Monterey CA 93943-5114 | 2 |
| 6. | Dr. P. A. Harr<br>Code MR/Hr<br>Naval Postgraduate School<br>589 Dyer Rd Rm 252<br>Monterey CA 93943-5114 | 1 |
| 7. | LT Michael S. Kalafsky<br>Naval Pacific Meteorology and Oceanography Center West/JTWC<br>PSC 489 Box 12<br>FPO AP 96540-0051 | 2 |

8. Commanding Officer 1
Fleet Numerical Meteorology and Oceanography Center
7 Grace Hopper Ave Stop 4
Monterey CA 93943-0120

9. Chief of Naval Research 1
800 N. Quincy Street
Arlington VA 22217

10. Commanding Officer 1
Naval Pacific Meteorology and Oceanography Center
COMNAVMARIANAS Box 12
FPO AP 96540-0051

11. C. P. Guard 1
University of Guam/ONR
223 Papato Lane
Sinajana, Guam 96926-4646